

2018

# Environmental Links To Ectopic Kidney Diseases

Firas Alhasson

*University of South Carolina*

Follow this and additional works at: <https://scholarcommons.sc.edu/etd>

 Part of the [Environmental Studies Commons](#), [Life Sciences Commons](#), and the [Occupational and Environmental Health Nursing Commons](#)

---

## Recommended Citation

Alhasson, F.(2018). *Environmental Links To Ectopic Kidney Diseases*. (Doctoral dissertation). Retrieved from <https://scholarcommons.sc.edu/etd/4576>

This Open Access Dissertation is brought to you by Scholar Commons. It has been accepted for inclusion in Theses and Dissertations by an authorized administrator of Scholar Commons. For more information, please contact [dillarda@mailbox.sc.edu](mailto:dillarda@mailbox.sc.edu).

# ENVIRONMENTAL LINKS TO ECTOPIC KIDNEY DISEASES

by

Firas Alhasson

Bachelor of Veterinary Medicine and Surgery  
University of Basra, 2003

Master of Science  
University of Basra, 2009

---

Submitted in Partial Fulfillment of the Requirements

For the Degree of Doctor of Philosophy in

Environmental Health Sciences

The Norman J. Arnold School of Public Health.

University of South Carolina

2018

Accepted by:

Saurabh Chatterjee, Major Professor

Samir S. Raychoudhury, Committee Member

Geoff Scott, Committee Member

Dwayne Porter, Committee Member

Cheryl L. Addy, Vice Provost and Dean of the Graduate School

© Copyright by Firas Alhasson, 2018.  
All Rights Reserved

## DEDICATION

My humble effort I dedicate to my previous mother and siblings, my sweet and loving wife Aqila, and my adorable daughters Riyam and Nora whose affection, love, encouragement, and prays of day and night make me able to get such success and honor.

## ACKNOWLEDGEMENTS

Firstly, I would like to express my sincere gratitude to my advisor Dr. Saurabh Chatterjee for the continuous support of my Ph.D. study and related research, for his patience, motivation, and immense knowledge. His guidance helped me in all the time of research and writing of this thesis. I could not have imagined having a better advisor and mentor for my Ph.D. study.

I would also like to thank my other PhD committee members: Dr. Geoff Scott, Dr. Dwayne Porter, and Dr. Samir Raychoudhury for their insightful comments and encouragement which incited me to widen my research from various perspectives.

I am grateful to all of those with whom I have had the pleasure to work during this and other related projects. I thank my fellow lab mates in for the stimulating discussions and for all the fun we have had in during my Ph.D career. Especial thanks to Dr. Ratanesh Seth and Dr. Suvarthi Das for their helps and guides during my first year in the lab.

Last but not the least, I would like to thank my family: my parents and to my brothers and sister for supporting me spiritually throughout writing this thesis and my my life in general.

## ABSTRACT

Nonalcoholic fatty liver disease (NAFLD) is the most common liver disease in the western culture and worldwide. Its morbidity has been raising and it has become a burden on the public health. NAFLD is associated with other metabolic diseases such as Diabetic Mellitus and hypertension. NAFLD is a wide spectrum of symptoms, from an accumulation of fat in the liver (cirrhosis) to production of scar tissue (Fibrosis). The liver along with other distal organs such as the kidney and cardiovascular system can be damaged as ectopic manifestations of NAFLD. Contamination of drinking water with Cyanobacterium toxin (Microcystin) and water disinfection byproduct like trihalomethane (like Bromodichloromethane) play a critical role in progressing NAFLD. Here, I have examined the molecular mechanism of BDCM and microcystin in induce glomerular toxicity and renal inflammation when NAFLD was present. I found that BDCM can induce glomerular inflammation when NAFLD is present. BDCM caused renal immunotoxicity and impacted glomerular function through high mobility group box-1 (HMGB1) and mesangial cell activation. Mesangial cell activation can be caused by increasing leptin level after BDCM exposure. High leptin level upregulated mesangial cell NOX2 and increased miR-21 expression which in turn released TGF- $\beta$  and caused tubular inflammation. In-vitro, mesangial cells proliferated and increased alpha smooth muscle actin ( $\alpha$ SMA) expression after they were treated with leptin. Leptin caused mesangial cell NOX2 subunits Gp91 and P47 phox to colocalize via JAK/ STAT pathway dependence which in turn increased peroxynitrite releasing, miR21 activation,

and TGF $\beta$  expression. Furthermore, mesangial cells NOX2 activation by leptin exposure attenuated after Apocynin treatment. Comparing with tubular cells kept on cell culture media only, tubular cells incubated with leptin- treated mesangial cell supernatant showed increases in inflammatory marker expressions like IL-1 $\beta$ , TNF- $\alpha$ , and interferon- $\gamma$ . Microcystin is another example of a toxin that could increase the severity of glomerulonephritis caused by NAFLD. Here I found that microcystin can accelerate NAFLD toxicity in the kidney. High expression of  $\alpha$ SMA found in NAFLD mice treated with microcystin compared with NAFLD mice alone and mice treated with microcystin but did not have NAFLD. Renal tissue surrounding the glomeruli had increased NOX2 activation as shown by increased colocalization of NOX2 subunits, GP91 and P47 Phox. Mice lacking miR21 gene and mesangial cell line treated with miR21 inhibitor shown significant decreased in mesangial cell activations and renal immunotoxicity. Thus, microcystin exposure increased the severity of NAFLD caused glomerulonephritis via the NOX2- miR21 axis.

## TABLE OF CONTENTS

DEDICATION.....	iii
ACKNOWLEDGEMENTS.....	iv
ABSTRACT.....	v
LIST OF FIGURES.....	ix
LIST OF TABLES.....	xi
CHAPTER 1: INTRODUCTION.....	1
CHAPTER 2: NKT CELL MODULATES NAFLD POTENTIATION OF METABOLIC OXIDATIVE STRESS-INDUCED MESANGIAL CELL ACTIVATION AND PROXIMAL TUBULAR TOXICITY.....	7
2.1 INTRODUCTION.....	9
2.2 MATERIALS AND METHOD.....	13
2.3 RESULTS.....	20
2.4 DISCUSSION.....	30
CHAPTER 3: HIGH CIRCULATORY LEPTIN MEDIATED NOX-2 PEROXYNITRITE-MIR21 AXIS ACTIVATE MESANGIAL CELLS AND PROMOTES RENAL INFLAMMATORY PATHOLOGY IN NONALCOHOLIC FATTY LIVER DISEASE.....	44
3.1 INTRODUCTION.....	46
3.2 MATERIALS AND METHODS.....	49
3.3 RESULT.....	56
3.4 DISCUSSION.....	62



CHAPTER 4: MICROCYSTIN EXPOSURE MODULATES NOX-2-MIR21 AXIS IN ECTOPIC GLOMERULAR TOXICITY IN UNDERLYING NONALCOHOLIC FATTY LIVER DISEASE (NAFLD).....	75
4.1 INTRODUCTION.....	77
4.2 MATERIALS AND METHODS.....	80
4.3 RESULT.....	86
4.4 DISCUSSION.....	92
CHAPTER 5: CONCLUSION.....	105
REFERENCES.....	110
APPENDIX A PERMISSION OF AMERICAN JOURNAL OF PHYSIOLOGY FOR REPRINTING MANUSCRIPT USED IN CHAPTER 2.....	124

## LIST OF FIGURES

Figure 2.1 NAFLD potentiates metabolic oxidative stress via CYP2E1 and caused increased lipid peroxidation in proximal tubular cells.....	35
Figure 2.2CYP2E1 metabolism in NAFLD causes increased secretion of proinflammatory cytokines in renal proximal tubules.....	36
Figure 2.3 NAFLD-induced CYP2E1 metabolism leads to increased MC proliferation and TGF- $\beta$ production.....	37
Figure 2.4 NAFLD potentiation of immunotoxicity via CYP2E1-mediated oxidative stress increases T cell presence in the renal microenvironment.....	38
Figure 2.5 Proximal tubule immunotoxicity in NAFLD potentiation of CYP2E1-mediated renal inflammation is exacerbated in mice deficient in NKT cells.....	39
Figure2.6 MC proliferation and TGF- $\beta$ production were increased in mice deficient in NKT cells.....	40
Figure 2.7 NAFLD potentiation of renal inflammation induced by MCs causes increased levels of proximal tubular HMGB1 levels and apoptosis in part via the TLR4 pathway with exacerbation after lack of CD1D-dependent NKT cells .....	41
Figure 2.8 Exacerbation of immunotoxicity in NAFLD kidneys after reductive metabolism of CYP2E1 is mediated by TLR4 activation.....	42
Figure 3.1Increased circulatory leptin in NASH causes mesangial cell activation in Kidney.....	66
Figure 3.2 Leptin causes NOX2 activation and increased peroxynitrite generation in kidney.....	67
Figure 3.3.NOX2 activation leads to mesangial cell priming and increased TLR4 expression in the renal tissue.....	68
Figure 3.4 NOX2 activation leads to a surge of proinflammatory mediators in NAFLD-Kidney .....	69
Figure 3.5 NOX2-derived peroxynitrite causes generation of tyrosyl radicals in mesangial cells.....	70

Figure 3.6 Leptin signaling in mesangial cells induce tyrosyl radicals that is peroxynitrite dependent.....	71
Figure3.7 Leptin-NOX2-Peroxynitrite axis causes mesangial cell activation via miR21.	72
Figure 3.8 MiR21 increase causes kidney inflammation.....	73
Figure 4.1 Microcystin-LR exposure causes glomerular immune cellular infiltrations and glomerular damage in present of NAFLD.....	96
Figure 4.2 Microcystin exposure augment mesangial cell activation in present of NAFLD condition.....	96
Figure 4.3Microcystin exposure heighten glomerular inflammation in NAFLD exist.....	97
Figure 4.4 Microcystin exposure activate mesangial cell NOX2.....	98
Figure 4.5 Microcystin mediates mesangial cell NOX2 generated peroxynitrite.....	99
Figure 4.6 Microcystin administration upregulates Mesangial cell miR21 expression...	100
Figure4.7 miR21 high expression causes mesangial cell activation.....	101
Figure 4.8 Peroxynitrite- miR21 axis drives mesangial cell activation and death.....	102
Figure 4.9 miR21 activates mesangial cell toxicity via increasing TGF- $\beta$ .....	103
Figure 4.10 NOX2- miR21 axis heightens mesangial cells activation via PTEN decreasing.....	104

## LIST OF TABLES

Table 2.1: List of primers used in chapter 2.....	18
Table 3.1: List of primers used in chapter 3.....	54
Table 4.1: List of primers used in chapter 4.....	84

## CHAPTER 1

### INTRODUCTION

Nonalcoholic liver fatty disease (NAFLD) is now becoming the most common chronic liver disease worldwide and it occurs in people who do not consume a high amount of alcohol. NAFLD is prevalent in about 30% of the general western countries population and around 4% of the world population (1). Moreover, the number of NAFLD patients is growing rapidly and the disease is becoming a public health encumbrance (2). NAFLD is a wide spectrum with a progression of stages beginning with the accumulation of excessive fat in hepatic cells, steatohepatitis, and cirrhosis, as well as sometimes including hepatocellular carcinoma (3). Nonalcoholic steatohepatitis (NASH) is a progressive stage of NAFLD. It is prevalent in 5% of the general NAFLD population and is the third most common liver disease in the United States (4). NASH is necroinflammation histological condition in hepatic cells caused by liver injury and inflammation after fat accumulation (5). Cirrhosis is irreversible, and the final phase of NAFLD (6). Instead of alcoholic liver fatty disease, which is caused by alcohol consumption, different risk factors can cause NAFLD. Some primary risk factors for NAFLD are Diabetes Mellitus type two, hypertension, obesity, and metabolic syndrome, while uncommon risk factors for NAFLD include disorders of lipid metabolism, hepatitis infection type C, lipodystrophy, and some medications such as corticosteroids and tamoxifen (3,7). Obesity is prevalent in 32% of adults and there is a correlation between the prevalence of obesity and NAFLD (8,9). Although NAFLD affects

both obese and non-obese individuals, overweight and obese patients with NAFLD are four times more than normal weight patients with NAFLD (10).

Obesity is a condition where the subjects have a body mass index (BMI) more than 30. This excessive amount considers adipose tissue because of triglyceride accumulation (11). In addition to work as a storage to the energy, adipose tissue can release different cytokines, hormones, and other molecules, which together is called Adipokines (12). Accumulation of fat causes adipocytes hypertrophy results in adipocytes damage and the release of pro inflammatory cytokines. Adipocytes damage in visceral adipose tissue lead to fibrosis, which in result leads to deposit fat in other organs, such as the liver and muscles (13,14). The number of NAFLD patients and NAFLD severity correlates with metabolic syndrome severity and progression (15). Thus, many studies considered NAFLD to be a hepatic manifestation of metabolic syndrome with a risk factor that involves insulin resistance development, which itself is considered a core feature of metabolic syndrome (16). Different cohort studies found that patients with type 2 diabetes have an increased a risk of NAFLD, and patients who suffer from NAFLD will have an increased chance of developing type 2 diabetes (17, 18). Regarding which disease is developing first, NAFLD and type 2 diabetes can occur due to exists and progresses of another disease. This correlation may be due to the insulin molecule. In NAFLD condition, fat accumulates in the liver results in high amount of insulin becoming necessary to fuel the body and that causes type 2 diabetes to progress. Meanwhile, in type 2 diabetes, there is not enough insulin to metabolize liver fat, which causes the development of NAFLD from steatosis to NASH (17,19,20,21).

Since both NAFLD and NAFLD progression link to other disorders, such as metabolic syndrome and type 2 diabetes, NAFLD damage is not restricted to the liver, it can be an extrahepatic problem. Cardiovascular disease and ecological diseases are the main reason for death in NAFLD patients (22). Although the mechanical link between NAFLD and cardiovascular disease is unclear, insulin resistance is widely considered the most possible link between NAFLD and cardiovascular disease (23). NAFLD patients, especially patients in the NASH stage, have shown endothelium dysfunction, which is a hallmark of cardiovascular disease (24). In addition, patients proven to NAFLD also likely have hyperlipidemia, increased low-density lipoprotein cholesterol (LDL) level, and decreased high-density lipoprotein cholesterol level (HDL) (24). Type 2 diabetes is associated with NAFLD and increases the risk of NASH. Furthermore, patients with type 2 diabetes and diagnosed with NAFLD are more susceptible to have chronic kidney disease compared to patients without NAFLD (25,26,27). Prevalence of chronic kidney disease is twice likely in patients with NAFLD compared to patients without NAFLD. Although mechanistically, there are different theories of how NAFLD can link with kidney diseases, like chronic kidney disease (CKD), fully understood of the mechanism does not yet exist. One pathophysiological factor is that NAFLD and NASH cause increase releasing biomarkers and proinflammatory cytokines, like  $TNF\alpha$ ,  $TGF\beta$ , IL-6 from hepatocytes and Kupffer cells. In turn, these biomarkers can circulate and promote chronic kidney disease (28). Another pathway which can trigger kidney in the presence of NAFLD that NAFLD leads to insulin resistance in the liver and then in the whole body, which in consequence causes CRD (29). Decreasing adiponectin level via the progression of NAFLD can impact the energy sensor 5'-AMP activated protein kinase (AMPK) pathway, which is important

to Podocytes function, and results in the end stage renal disease ESRD (30). On another hand, Georgescu EF showed that renin angiotensin system involved in insulin resistance, resulting in promoting liver fibrogenesis (31,32).

Since chlorination disinfection method has been added to the drinking water for a long-time word wild, disinfection by products are found in the water source. (33). Although disinfection water by chlorine is an important way to protect humans from microorganisms, there is a link between disinfection by products (DBP) and organic toxicity, which results in carcinogenic effect and disfunction in some organs, such as reproductive system and liver (34, 35). Trihalomethanes (THMs), chloroform, bromoform, bromodichloromethane (BDCM), and dibromochloromethane (DBCM), is a DBP existed when chlorine is used in water to disinfect water from microorganisms. These THMs components are considered the most abundant DBPs studied in epidemiological studies due to its public health problems. BDCM impacts liver functions and develops NAFLD condition to NASH when used as a second hit (35). Different studies found BDCM metabolized inside the liver though xenobiotic metabolism enzyme (cytochrome P450), especially CYP2E1 (36). Admission of BDCM can increase oxidative stress and release free radicals. Experimental studies found that obese mice exposed to BDCM can cause NASH (37). Patients with CYP2E1 polymorphisms are more susceptible to have NASH caused by environmental factors since BDCM metabolize primarily by CYP2E1(38). Although THMs been highlighted in multiple recent studies, different molecules impacted by exposure to THMs are present. Recently, an experimental study from our lab found that Purinergic receptor X7 (P2X7) can modulate NASH progression in obese mice after BDCM exposure (37,39).



Cyanobacteria, is a common bacterium, present in fresh water over the entire globe, and can grow and produce blooms under a specific environment like eutrophic water. Cyanobacteria produce secondary metabolites as toxins which can harm other organs when they grow excessively and cause accumulation of toxins (40). Cyanobacteria can produce several toxins such as a microcystin, a potent toxin able to cause damage in multi organs (41). The molecular weight of microcystin, heptapeptide structure, varies between 900 and 1,100 Daltons and its amino acid positions are different within the X and Y directions. Despite that, many types of microcystin are identified, Microcystin-LR is a potent toxic member of the microcystin family which is a common in nature (42). Diffusion of microcystin across the membrane is not possible due to its high molecular weight. Cells take up microcystin by using transporters which help it cross the cell membrane (40). Inherently, many transporters respond to endogenous and exogenous chemicals up taken by cells including microcystin. These transporters include the organic anion transporting polypeptides (Oatps), Nat-taurocholatecotransporting polypeptide (Ntcp), organic anion transporters (Oats), and organic cation transporters (43-45). OATPs are very important transporters in the liver, kidney, heart, and blood brain barrier (40). Microcystin-LR interacts with serine/threonine protein phosphatases (protein phosphatases) such as PP1 and PP2a after cell exposed to microcystin (46). These enzymes are critical to cell processing like cell apoptosis and proliferation (47). Plenty of molecules are controlled by phosphorylation and dephosphorylation of protein phosphatase, for instance, NEK2, MAPKs, and P53 (48-50). Reactive oxygen species (ROS) is mainly generated in mitochondria to play a role in cellular processes from cell proliferation to apoptosis (51). ROS generation is due to expenditure of glutathione, which is a necessary component to

prevent cellular damage due to ROS (52). Microcystin-LR induces ROS and lipid peroxidation, decreases cell viability, reduces mitochondrial membrane potential, and finally induces cell apoptosis (52,53). Microcystin-LR leads to surge calcium in mitochondria. Calcium surge leads to onset of mitochondrial permeability transition pore (MPT). The consequence of MPT is changes in inner mitochondrial membrane performance and generation of ROS (54-59). Nicotinamide adenine dinucleotide phosphate (NADPH) oxidase is a dominant source of ROS in the biologic system. There are several isoforms of NADPH oxidase such as NOX1-5 and Doux1-2. NOX2 and NOX4 have been implicated in ROS production in the kidney during pathologic conditions (60-61). NOX2 was first NADPH oxidase subunit discovered in Phagocytes, however, recently, several studies found NOX2 expression in different types of cells like smooth muscle cells and kidney mesangial cells (62).

MicroRNAs (miRNA) are small noncoded RNA about 22 nucleotides which can control gene expression. In cytoplasm, miRNAs form mRNA silencing complexes which regulate mRNA expression at transcriptions level (63). Among all miRNAs, miRNA21 is highly expressed in different renal diseases such as Diabetic nephritis (DN) (64). Inhibition of miRNA 21 in experimental models attenuated mesangial extra cellular matrix (65). In this thesis, I inspect the mechanism pathway of different environmental toxins like BDCM and microcystin in augmented NAFLD causing glomerulonephritis and kidney inflammation

CHAPTER 2

**NKT CELL MODULATES NAFLD POTENTIATION OF  
METABOLIC OXIDATIVE STRESS-INDUCED MESANGIAL CELL  
ACTIVATION AND PROXIMAL TUBULAR TOXICITY**

---

Firas Alhasson<sup>1</sup>, Diptadip Dattaroy<sup>1</sup>, Suvarthi Das<sup>1</sup>, Varun Chandrashekar<sup>1</sup>, Ratanesh Kumar Seth<sup>1</sup>, Rick G. Schnellmann<sup>2</sup> and Saurabh Chatterjee<sup>1\*</sup>. Alhasson F, Dattaroy D, Das S, Chandrashekar V, Seth RK, Schnellmann RG, et al. NKT cell modulates NAFLD potentiation of metabolic oxidative stress-induced mesangial cell activation and proximal tubular toxicity. American journal of physiology Renal physiology. 2016;310:F85-F101. Reprinted here with the permission of the publisher.

1Environmental Health and Disease Laboratory, Department of Environmental Health Sciences, Arnold School of Public Health, University of South Carolina, Columbia SC 29208.

Drug Discovery and Biomedical Sciences, Medical University of South Carolina, Charleston, SC, United States.

Running Title: Liver CYP2E1 mediates kidney inflammation

Author for correspondence:

1\*Dr. Saurabh Chatterjee, Ph.D. Environmental Health and Disease Laboratory, Department of Environmental Health Sciences, University of South Carolina, Columbia 29208 USA. Email: schatt@mailbox.sc.edu; Tel: 803-777-8120; Fax: 803-777-3391

Key words: 4HNE,  $\alpha$ 14, CD1d, CXCL16, HMGB1 TLR4.

GRANTS This work has been supported by National Institute of Environmental Health Sciences Pathway to Independence Award 4-R00-ES-019875-02 (to S. Chatterjee)

**Abstract:**

Obesity and nonalcoholic fatty liver disease (NAFLD) are associated with the development and progression of chronic kidney disease. We recently showed that NAFLD induces liver-specific cytochrome P-450 (CYP)2E1-mediated metabolic oxidative stress after administration of the CYP2E1 substrate bromodichloromethane (BDCM) (Seth RK, Das S, Kumar A, Chanda A, Kadiiska MB, Michelotti G, Manautou J, Diehl AM, Chatterjee S. Toxicol Appl Pharmacol 274: 42–54, 2014; Seth RK, Kumar A, Das S, Kadiiska MB,

Michelotti G, Diehl AM, Chatterjee S. *Toxicol Sci* 134:291–303, 2013). The present study examined the effects of CYP2E1-mediated oxidative stress in NAFLD leading to kidney toxicity. Mice were fed a high-fat diet for 12 wk to induce NAFLD. NAFLD mice were exposed to BDCM, a CYP2E1 substrate, for 4 wk. NAFLD + BDCM increased CYP2E1-mediated lipid peroxidation in proximal tubular cells compared with mice with NAFLD alone or BDCM-treated lean mice, thus ruling out the exclusive role of BDCM. Lipid peroxidation increased IL-1 $\beta$ , TNF- $\alpha$ , and interferon- $\gamma$ . In parallel, mesangial cell activation was observed by increased  $\alpha$ -smooth muscle actin and transforming growth factor- $\beta$ , which was blocked by the CYP2E1 inhibitor diallyl sulphide both in vivo and in vitro. Mice lacking natural killer T cells (CD1d knockout mice) showed elevated (>4-fold) proinflammatory mediator release, increased Toll-like receptor (TLR)4 and PDGF2 mRNA, and mesangial cell activation in the kidney. Finally, NAFLD CD1D knockout mice treated with BDCM exhibited increased high mobility group box 1 and Fas ligand levels and TUNEL-positive nuclei, indicating that higher cell death was attenuated in TLR4 knockout mice. Tubular cells showed increased cell death and cytokine release when incubated with activated mesangial cells. In summary, an underlying condition of progressive NAFLD causes renal immunotoxicity and aberrant glomerular function possibly through high mobility group box 1-dependent TLR4 signaling and mesangial cell activation, which, in turn, is modulated by intrinsic CD1D dependent natural killer T cell.

## 2.1 INTRODUCTION

over the last decade, there has been a phenomenal rise in obesity and metabolic syndrome. The obesity phenotype is often associated with fatty liver (steatosis), leading to hepatic inflammation, sinusoidal injury, and fibrosis (109). Fatty liver is also observed with liver-

specific insulin and leptin resistance, leading to metabolic complications referred to as nonalcoholic fatty liver disease (NAFLD) (78, 109). Advanced and progressive NAFLD with inflammation with or without fibrosis and sinusoidal injury is termed “nonalcoholic steatohepatitis” (NASH) (69). NAFLD/NASH is linked to extrahepatic comorbidities like cardiovascular and renal complications (72, 108). For example, the cumulative evidence to date suggests that individuals with NAFLD exhibit an increased risk of developing cardiovascular disease, especially atherosclerosis and portal hypertension, type 2 diabetes, and chronic kidney disease (CKD) (22). Advanced NAFLD/NASH was associated with a higher prevalence (odd ratio: 2.53, 95% confidence interval: 1.58–4.05) and incidence (hazard ratio: 2.12, 95% confidence interval: 1.42–3.17) of CKD than simple steatosis when assessed in cross-sectional and longitudinal studies with the severity of advanced NAFLD/NASH being positively associated with CKD stages (90). The strong association of advanced NAFLD/NASH with kidney disorders may lie in common factors underlying the pathogenesis of NAFLD and CKD, including insulin resistance, oxidative stress, activation of the reninangiotensin system, and secretion of inflammatory cytokines by the steatotic and inflamed liver (70, 94, 103).

We have previously shown that oxidative stress is key for the progression of NAFLD to NASH (110). Oxidative stress pathways like cytochrome P-450 (CYP)mediated lipid peroxidation and NADPH oxidase can trigger the release of multiple proinflammatory mediators that affect distal organs like the kidney (74, 100). It is equally important that the intrinsic properties of proximal tubule cells act as immune responders and producers of a wide range of immunological, ischemic, or toxic injury that may arise from the liver (91). It is therefore not surprising that events in the proximal tubule are closely related to the

pathogenesis of a vast array of kidney diseases (91). In parallel, proinflammatory mediators in the circulation are filtered through the glomerulus, and those that are secreted locally from the kidney epithelia can exert autocrine and paracrine effects on mesangial cells (MCs), fibroblasts, vascular smooth muscle cells, and proximal tubular cells, which are crucially involved in progressive renal diseases (68, 71). The kidney immunotoxicity and inflammatory insult can be magnified by the activation of MCs, which are often found in the vicinity of Bowman's capsule. Hyperplasia of MCs precedes or accompanies progressive glomerular scarring, as seen in chronic glomerulonephritis and diabetic glomerulosclerosis (101). MCs also generate soluble mediators that can, in a paracrine fashion, attract and activate inflammatory cells (platelets, monocytes/macrophages, and granulocytes). For example, IL-6, IL-8, monocyte chemoattractant protein-1, and granulocyte-macrophage colony-stimulating factor exert autocrine effects on MCs, such as by promoting MC proliferation (by PDGF, IL-1, and IL-6) or extracellular matrix production [by transforming growth factor (TGF) $\beta$  and IL-1] and might play a prominent role in the initiation and progression of glomerular inflammation (101). MCs also resort to proliferation upon activation by proinflammatory mediator-induced oxidative stress. This is accompanied by the de novo expression of  $\alpha$ -smooth muscle actin ( $\alpha$ -SMA) and TGF- $\beta$  secretion (76, 87, 95, 97, 110). In parallel to studies regarding the role of MCs in chronic kidney immunotoxicity, there is evidence of immunosuppressive roles of a class of T cells including invariant and CD1D-dependent natural killer (NK)T cells (80). Invariant NKT cells have been shown to inhibit the development of experimental crescentic glomerulonephritis primarily via the involvement of dendritic cells and chemokine (C-X-C motif) receptor (CXCR)6 and CXCR16 (96, 107). However, the cross talk between the

regulatory and immunosuppressive NKT cells that have a prominent role in NAFLD has never been explored for their role in NAFLD-induced kidney immunotoxicity.

Thus, it is justifiable to assume that a preexisting condition of advanced NAFLD/NASH that has higher CYP2E1-mediated oxidative stress, release of damage associated molecular patterns (DAMPs), higher insulin and leptin levels, and higher inflammatory mediators in the circulation can cause oxidative stress distant to the liver, especially in renal tubular cells. The presence of varied cell types within Bowman's capsule and an activated proinflammatory phenotype of MCs raise the possibility of significant cross talk between these cells and other proximal tubular cells via autocrine and paracrine mechanisms, thus exacerbating renal injury in advanced NAFLD/NASH. In the present study, we used a diet-induced NAFLD model where hepatotoxin bromodichloromethane (BDCM) was used to generate CYP2E1-mediated oxidative stress and act as a “second hit” to allow the liver to progress into advanced NAFLD/NASH with steatohepatitis and fibrosis (35). Here, we show, using both in vivo and in vitro models, that advanced NAFLD/NASH affected kidneys with a second hit in the form of increased lipid peroxidation followed by MC activation and immunotoxicity in proximal tubular cells. Interestingly, CD1D-dependent NKT cells were also present in advanced NAFLD/NASH-affected kidneys and played a crucial role in modulating the MC-induced immunotoxicity in the proximal tubule.



## 2.2 MATERIALS AND METHODS:

BDCM and corn oil were purchased from Sigma-Aldrich (St. Louis, MO). Diallylsulfide (DAS) was purchased from Santa Cruz Biotechnology (Santa Cruz, CA). Anti-4-hydroxynonenal (4-HNE), anti-IL1 $\beta$ , anti-TNF- $\alpha$ , anti-interferon (IFN)- $\gamma$ , anti-high mobility group box 1 (HMGB1), anti-chemokine (C-X-C motif) ligand (CXCL)16, anti-TGF- $\beta$ , anti-Toll-like receptor (TLR)4, anti-CD4, anti-CD8, anti-F4/80, and anti- $\alpha$ SMA primary antibodies were purchased from Abcam (Cambridge, MA). Species-specific biotinylated conjugated secondary antibody and streptavidin-horseradish peroxidase were purchased from Vector Laboratories (Vectastain Elite ABC kit, Burlingame, CA). Wild-type and gene-specific knockout (KO) mice were purchased from The Jackson Laboratories (Bar Harbor, ME) and Taconic Farms (Hudson, NY). Animal diets were purchased from Research Diets (New Brunswick, NJ). All other chemicals were of analytic grade and were purchased from Sigma-Aldrich unless otherwise specified. Paraffinized tissue sections on slides were done by the Instrumentation Resource Facility of the University of South Carolina School of Medicine and AML Laboratories (Baltimore, MD).

**Mouse models:** All mice were housed with 1 mouse/cage at 23–24°C on a 12:12-h light/dark cycle with libitum access to food and water. All animals had been treated in strict accordance with the National Institutes of Health guidelines for the humane care and use of laboratory animals and local Institutional Animal Care and Use Committee standards. All experiments were approved by the institutional review board at the National Institute of Environmental Health Sciences, Duke University, and University of South Carolina Columbia, SC). Mice were given either 60% kcal high-fat diet or chow diet. After the

animal experiment was completed, mice of all study groups were euthanized for kidney tissues and serum samples were taken for further experiments.

**Mouse model of NAFLD:** Male pathogen-free C57BL/6J background mice were used as wild-type mice for the NAFLD model. These mice were fed a high-fat diet (60% kcal) from 6 wk until 16 wk. All experiments were conducted in the 16-wk age group. Age matched lean control (LC) mice were fed a diet having 10% kcal fat. Animals were housed at 1 mouse/cage before any experimental use. Mice that contained the disrupted CD1D gene (B6.129S6-Cd1d1/Cd1d2 < tm1Spb >/J), PFP/Rag2 dual gene deletion (B6.129S6-Rag2tm1FwaPrf1tm1Clrk N12, Taconic Farms), and disrupted TLR4 gene (B6.B10ScN-Tlr4lps-del/JthJ) were fed a high-fat diet and treated identically to the NAFLD mouse model.

**Administration of BDCM and induction of kidney injury:** High-fat diet-fed wild-type mice (NAFLD model) and high-fat diet-fed gene KO mice (except for TLR4 gene KO mice) at 16 wk were administered BDCM (1 mmol/kg, diluted in corn oil) intraperitoneally for twice a week for 4 wk to assess the effects of chronic exposure to BDCM. High-fat diet-fed TLR4 gene KO mice at 16 wk were administered with the same dose of BDCM via an intraperitoneal injection for 1 wk. A set of high-fat diet-fed mice (NAFLD model) were not injected with BDCM and served as controls against high-fat diet-fed BDCM-injected wild-type mice (NAFLD + BDCM mice). A group of chow diet fed LC mice was also treated with the same dose of BDCM for 1 mo (LC + BDCM mice). LC mice not injected with BDCM were used as a control against the LC + BDCM model.

**Inhibition of CYP2E1 by DAS (CYP2E1 inhibitor):** A set of high-fat diet-fed BDCM treated mice was administered with 50 mg/kg DAS (diluted in corn oil) via an

intraperitoneal injection at twice a week for 1 mo. This group was termed the NAFLD + BDCM + DAS group.

**Cell culture:** A kidney MC line (CRL-1927) and kidney tubular cell line (CRL-2038) were purchased from the American Type Culture Collection (Manassas, VA) and maintained in DMEM (Corning, Tewksbury, MA) and DMEM-F-12 (1:1, American Type Culture Collection), respectively. Media were supplemented with 10% FBS (Atlanta Biologicals, Norcross, GA), 2 mM glutamine, 100 U/ml penicillin, and 100 µg/ml streptomycin (GIBCO, Grand Island, NY) at 37°C in a humidified atmosphere of 5% CO<sub>2</sub>. MCs were treated with 1 µM 4-HNE (Cayman Chemicals, Ann Arbor, MI) for 48 h, and equal amounts of ethanol were added to control plates. The diluent for 4-HNE and the media were collected for further experiments. Tubular cells were cultured in six well plates. After allowing for the attachment of cells, the media were changed to obtain the following groups: the control group containing fresh DMEM, the control group with DMEM and 1 µM 4-HNE, media collected from MCs treated with alcohol only, and media collected from MCs treated with 1 µM 4-HNE for 48 h. Cells were then lysed in TRIZol (Invitrogen, Grand Island, NY) for mRNA extraction. Cells were plated on coverslips by putting the coverslips on each well of the six-well plates, maintaining the aforementioned conditions, and cells adhered on coverslips were used for immunofluorescence staining after completion of the treatment. To perform the apoptosis assay, tubular cells were seeded in 2-cm<sup>2</sup> dishes with attached coverslips (MatTek, Ashland, MA). After attachment, the media were changed to give the groups described above for 48 h.

**Immunohistochemistry:** Kidneys were collected from each animal and fixed in 10% neutral buffered formalin (Sigma-Aldrich). These formalin-fixed paraffin-embedded

tissues were cut into 5- $\mu$ m-thick sections. These sections were deparaffinized using a standard protocol (35). Epitope retrieval of the deparaffinized sections was performed using epitope retrieval solution and steamer (IHC-World, Woodstock, MD) following the manufacturer's protocol. H<sub>2</sub>O<sub>2</sub> (3%) was used for 5 min to block endogenous peroxidases. Primary antibodies, such as anti-CD4, anti-CD8, anti-4-HNE, anti-IL-1 $\beta$ , anti-TNF- $\alpha$ , anti-IFN- $\gamma$ , anti-HMGB1, anti-CXCL16, anti-TGF- $\beta$ , and anti- $\alpha$ -SMA, were used in the recommended dilutions. Species-specific biotinylated conjugated secondary antibody and streptavidin conjugated with horseradish peroxidase were used to perform antigen-specific immunohistochemistry following the manufacturer's protocols. 3,3'Diaminobenzidine (Sigma-Aldrich) was used as a chromogenic substrate. Tissue sections were counterstained using Mayer's hematoxylin (Sigma-Aldrich). PBS was used as wash three times between the steps. Sections were finally mounted in Simpo mount (GBI Laboratories, Mukilteo, WA) and observed under  $\times 20$  and  $\times 60$  objectives using an Olympus BX51 microscope (Olympus America, Center Valley, PA). Morphometric analysis was done using CellSens Software from Olympus America. For immunohistochemical dual labeling of  $\alpha$ -SMA-IL-1 $\beta$  and  $\alpha$ -SMA-TGF- $\beta$ , the primary antibodies were used as described above. After epitope retrieval, those deparaffinized sections with an Enzo immunohistochemical dual labeling kit (Farmingdale, NY) were used following the manufacturer's protocol.

**Picrosirius red staining:** Picrosirius red staining of kidney slices was done using a Nova ultra-sirius red stain kit following manufacturer's instructions (IHC-World). Sections were observed using a  $\times 20$  objective under a light microscope.

**Immunofluorescence:** Formalin-fixed paraffin-embedded tissues sections were subjected to deparaffinization using a standard protocol. Epitope retrieval of the deparaffinized

sections was done using epitope retrieval solution and steamer (IHC World) following the manufacturer's instructions. The primary antibody F4/80 (Abcam) as used at the recommended dilution. Species-specific anti-IgG secondary antibodies conjugated with Alexa fluor 633 (Invitrogen) were used. Sections were mounted in a ProLong gold antifade reagent with 4',6-diamidino-2-phenylindole (Life Technologies, Eugene, OR). Images were taken under a  $\times 10$  objective using the Olympus BX51 microscope. After cells were plated and treatments were completed as described above, cells attached on coverslips were fixed using 10% neutral buffered saline. Cells were washed with PBS containing 0.1% Triton X-100 (Sigma) and then blocked using 3% BSA, 0.2% Tween 20 (Fisher), and 10% FBS in PBS. Cells were incubated with  $\alpha$ -SMA primary antibody (Abcam) followed by species-specific Alexa fluor 488 (Invitrogen) for immunofluorescence dual labeling staining. Stained cells attached on coverslips were mounted on slides using ProLong gold antifade reagent with 4',6-diamidino-2 phenylindole (Life Technologies) and viewed under a  $\times 10$  objective using the Olympus BX51 microscope.

**Quantitative real-time PCR:** Gene expression (mRNA) levels in kidney tissue samples were measured by quantitative real-time RT-PCR. Total RNA was isolated from mouse kidney tissues, and cells were treated using TRIzol reagent (Life Technologies) following the manufacturer's protocol. RNA was purified using RNeasy mini kit columns (Qiagen, Valencia, CA). An iScript cDNA synthesis kit (Bio-Rad) was used to convert 1  $\mu$ g of purified RNA to cDNA. Quantitative real-time RT-PCR was performed with gene specific primers using SsoAdvanced Universal SYBR Green supermix (Bio-Rad) and a CFX96 thermal cycler (Bio-Rad). Threshold cycle (Ct) values for genes of interest were normalized against 18S (internal control) values in the same sample. Reactions were

carried out in triplicate for each gene and each tissue sample. The relative fold change was calculated by the  $2^{-\Delta\Delta C_t}$  method. The sequences for the mouse-specific primers.

**Table 2.1:** Table showing the primer sequences for the different targets genes.

Gene	Sense	Antisense
IL-1 $\beta$	CCTCGGCCAAGACAGGTC GC	TGCCCATCAGAGGCAAGGAGGA
TNF $\alpha$	CAACGCCCTCCTGGCCAAC G	TCGGGGCAGCCTTGTCCCTT
IFN $\gamma$	TGCGGGGTTGTATCTGGGG GT	GCGCTGGCCCGGAGTGTAG
$\alpha$ -SMA	GGAGAAGCCCAGCCAGTC GC	ACCATTGTCGCACACCAGGGC
CD4	CACACACCTGTGCAAGAA GC	GCGTCTTCCCTTGAGTGACA
CD8	GCCCTTCTGCTGTCCTTGA T	TAGTTGTAGCTTCCTGGCGG
FasL	GCAGCAGCCCATGAATTA CC	AGATGAAGTGGCACTGCTGTCT AC

**TUNEL assay:** Paraffin-embedded mouse kidney tissue sections (5  $\mu$ m thick) were used for a TUNEL assay using an Apoptag Fluorescein In-Situ Apoptosis Detection Kit (Millipore, Temecula, CA) following the manufacturer's protocol. Tissue sections were

counterstained with propidium iodide in antifade reagent (Millipore). Stained sections were imaged at magnification of  $\times 20$  using the Olympus BX51 microscope. Tubular cells were grown in 2-cm<sup>2</sup> dishes in the conditions described above. Attached cells were used for the TUNEL assay using the Apoptag Fluorescein In Situ Apoptosis Detection Kit (Millipore) following the manufacturer's protocol. Propidium iodide in antifade reagent (Millipore) was used as a counterstain. Stained cells were imaged using a  $\times 20$  objective.

**BUN assay:** Blood urea nitrogen (BUN) was measured (in mg/dl) in mouse serum samples using a BUN colorimetric detection kit (Arbor Assays) following the manufacturer's instructions.

**Renal inflammation and fibrosis scores:** A blind folded analysis of renal pathology was carried out to assess renal inflammation and fibrosis using a standard grading system. To analyze tubulointerstitial fibrosis in the renal compartments, lesions were scored using a semiquantitative scoring system (105). For inflammation, grade 0 = no foci of inflammation, grade 1 = less than one foci per two  $\times 20$  fields, grade 2 = 1 foci per two  $\times 20$  fields to one foci per one  $\times 20$  fields, grade 3 = one to two foci per one  $\times 20$  fields, and grade 4 = more than two foci per one  $\times 20$  fields. Interstitial fibrosis was graded according to the following scale: 0 = no evidence of interstitial fibrosis, 1 = less than 25% involvement, 2 = 25–50% involvement, and 3 = less than 50% involvement.

**Statistical analyses:** Statistical analysis was done by ANOVA followed by Bonferroni post hoc correction for intergroup comparisons. P values of  $<0.05$  were considered statistically significant.

## 2.3 RESULTS

NAFLD potentiates metabolic oxidative stress via CYP2E1 and caused increased lipid peroxidation in proximal tubular cells. NAFLD shows increased CYP2E1 induction (66). We have previously shown that metabolic oxidative stress in NAFLD/NASH causes lipid peroxidation primarily dependent on CYP2E1 in the liver (35). BDCM is a substrate of CYP2E1 and is known to cause lipid peroxidation through reductive metabolism (35). The results showed that lipid peroxidation marker 4-HNE was significantly higher in the NAFLD + BDCM kidney group compared with the LC, LC + BDCM, or NAFLD alone groups ( $P < 0.05$ ; Fig. 1, A and B). Mice treated with the CYP2E1 inhibitor DAS, a relatively specific inhibitor of CYP2E1, showed a significant decrease in lipid peroxidation, as assessed by decreased staining of 4-HNE. Peroxidation was primarily localized in proximal tubular cells and podocytes (Fig. 1A). The results suggested that a condition of NAFLD characterized by increased steatosis and metabolic oxidative stress via CYP2E1 exacerbated the lipid peroxidation in the NAFLD + BDCM kidney group and was not a result of the metabolism of the toxin alone since kidneys from the LC + BDCM group had significantly decreased 4-HNE staining compared with the NAFLD + BDCM group (Fig. 1A).

### **CYP2E1 metabolism in NAFLD causes increased secretion of proinflammatory cytokines in renal proximal tubules.**

Oxidative stress due to reductive metabolism of CYP2E1 has been shown to increase proinflammatory cytokine release (35). We studied the role of CYP2E1 reductive metabolism and its corresponding lipid peroxidation in the release of proinflammatory cytokines in NAFLD kidneys after BDCM administration. The results showed that there



was a significant increase in the levels of IL-1 $\beta$  in the LC+BDCM group compared with the LC group ( $P < 0.05$ ; Fig. 2B). Levels of the cytokine also increased in the NAFLD + BDCM group compared with the NAFLD alone group (Fig. 2, A and B), as shown by immunohistochemistry, compared with the NAFLD alone group, whereas the administration of DAS significantly decreased levels of IL-1 $\beta$  primarily in proximal tubular cells (Fig. 1, A and B). mRNA expression of IL1 $\beta$  also showed a significant increase in the NAFLD + BDCM group compared with NAFLD alone group, whereas the NAFLD + BDCM + DAS group showed a significant decrease in mRNA levels, as assessed by quantitative RT-PCR (Fig. 2C). Oxidative stress and other inflammatory stimuli of a primarily systemic nature have been shown to increase TNF- $\alpha$  levels and TNF- $\alpha$  release from proximal tubular cells, podocytes, and MCs (76, 87, 91, 97). The results showed that levels of TNF- $\alpha$  were significantly increased primarily in tubular cells, podocytes, and MCs in the NAFLD + BDCM group compared with the NAFLD alone group ( $P < 0.05$ ; Fig. 2, D and E). No significant change was observed between the LC and LC + BDCM groups. The administration of DAS significantly decreased TNF- $\alpha$  levels compared with the NAFLD + BDCM group ( $P < 0.05$ ; Fig. 2, D and E). The increased protein levels were due to increased protein synthesis, as explained by the increased mRNA expression of the cytokine in the NAFLD + BDCM group compared with the NAFLD alone group or DAS-administered group ( $P < 0.05$ ; Fig. 2F). Although the proinflammatory cytokines IL-1 $\beta$  and TNF- $\alpha$  were found to be increased in proximal tubular cells in the NAFLD + BDCM group, we investigated the role of IFN- $\gamma$ , a regulatory cytokine, in the kidney. IFN- $\gamma$  has been found to often be associated with a regulatory role in the kidney, especially by suppressing angiotensinogen levels via suppressor of cytokine signaling 1 (99). To study the role of

CYP2E1-mediated oxidative stress in regulating the role of IFN- $\gamma$ , immunohistochemistry was performed. The results showed that IFN- $\gamma$  protein was primarily localized in proximal tubular cells and other cell types (Fig. 2G). Levels of IFN- $\gamma$  were significantly increased in the NAFLD + BDCM group compared with the NAFLD alone group, whereas only a slight but significant change was observed between LC and LC + BDCM groups ( $P < 0.05$ ; Fig. 2, G and H). The administration of DAS significantly decreased IFN- $\gamma$  levels in these cells compared with the NAFLD + BDCM group ( $P < 0.05$ ; Fig. 2H). mRNA expression of IFN- $\gamma$  also showed a significant increase in the NAFLD + BDCM group compared with both the NAFLD alone group and DAS-administered group ( $P < 0.05$ ; Fig. 2I), confirming that the increase in the levels of IFN- $\gamma$  was because of increased mRNA expression and most likely by increased protein synthesis. The results assumed significance since IFN- $\gamma$  can be secreted from infiltrating or resident T cells, including NKT cells, which have been shown to be protective in various forms of glomerulonephritis (107).

### **NAFLD-induced CYP2E1 metabolism leads to increased MC proliferation and TGF- $\beta$ production.**

MCs have long been regarded as mediators of CKD (81). Hypertrophy of MCs and tubular cells is common in the progression of CKD (81). To study the involvement of MC activation, proliferation and hypertrophy in the NAFLD potentiation of CYP2E1-induced oxidative stress, and the subsequent immunotoxicity in the kidney, protein levels and localization of  $\alpha$ -SMA were analyzed by immunohistochemistry (79). The results showed that there was a significant increase in the immunoreactivity of  $\alpha$ -SMA in the glomerulus and proximal tubular cells in the NAFLD + BDCM group compared with the NAFLD alone group, whereas no significant change was observed between LC and LC + BDCM groups

( $P < 0.05$ ; Fig. 3, A and B). DAS-administered mice had a significant decrease in immunoreactivity to  $\alpha$ -SMA compared with the NAFLD + BDCM group ( $P < 0.05$ , Fig. 3, A and B). mRNA expression of  $\alpha$ -SMA was significantly higher in the NAFLD + BDCM group compared with both the NAFLD alone group or DAS-administered group, suggesting that the protein synthesis of  $\alpha$ -SMA was intrinsic to the kidney ( $P < 0.05$ ; Fig. 3C). Since MC-mediated fibroproliferative effects, especially mesangial matrix formation, are via TGF- $\beta$  production, we studied the immunoreactivity of TGF- $\beta$  in the glomerulus and proximal tubular cells (83, 86). The results showed that the NAFLD + BDCM group showed significantly higher protein levels of TGF- $\beta$  compared with the NAFLD alone group, whereas DAS administration significantly decreased TGF- $\beta$  immunoreactivity compared with the NAFLD + BDCM group ( $P < 0.05$ ; Fig. 3, D and E). Interestingly, the LC + BDCM group showed a significant increase in the level of the cytokine compared with the LC group (Fig. 3E). There was increased mRNA expression of TGF- $\beta$  in the NAFLD + BDCM group compared with the NAFLD alone group or NAFLD + DAS group ( $P < 0.05$ ; Fig. 3F). The results suggest that MC proliferation, in part, is a significant event in NAFLD potentiation of immunotoxicity, although other cell types cannot be ruled out at this stage. MCs incubated with 4-HNE showed increased expression of IL-1 $\beta$ , TNF- $\alpha$ , PDGF2, TLR4, and  $\alpha$ -SMA (Fig. 3, G–K).  $\alpha$ -SMA protein expression and its myofibroblastic phenotype were also evident by immunofluorescent microscopy in the 4-HNE-treated group compared with the cells + vehicle-treated group (Fig. 3L).

## **NAFLD potentiation of immunotoxicity via CYP2E1-mediated oxidative stress increases T cell presence in the renal microenvironment.**

Differential roles of various T cell subsets have been reported in CKD (89). Our previous data in this study showed an increased IFN- $\gamma$  immunoreactivity in the NAFLD + BDCM group, whereas administration of DAS had decreased protein levels of this T cell cytokine (Fig. 2, G–I). To study the presence of T cells in the NAFLD kidney after increased CYP2E1-mediated oxidative stress, quantitative real-time PCR was used to analyze the fold expression of CD4, CD8, Va14, and NK1.1 genes. The results showed that mRNA expression of CD4, CD8, Va14, and NK1.1 was significantly higher in the NAFLD + BDCM group compared with the NAFLD alone group ( $P < 0.05$ ; Fig. 4, A–D), whereas the administration of DAS significantly decreased mRNA expression of T cell subset markers in the kidney. Interestingly, use of CD1D KO mice, which were deficient in CD1d-dependent NKT cells, had significantly decreased mRNA expression of Va14, CD4, and CD8, whereas the expression of NK1.1 was unchanged ( $P < 0.05$ ; Fig. 4). Expression of Va14 was significantly higher in the NAFLD + DAS group, suggesting that CYP2E1 reductive metabolism might have a role in the repression of invariant NKT cells and that the administration of DAS significantly upregulated NKT cell expression of Va14 (Fig. 4C). However, protein expression of CD4 and CD8 was significantly higher in CD1d KO mice, despite the low mRNA expression of these T cell markers (Fig. 4, E and F). The observed data of higher CD4 and CD8 protein in CD1d KO mice might be due to other T cell subsets in CD1d KO mice. To show the presence of infiltrating macrophages, F4/80 immunofluorescence staining was performed. The results showed that there was no marked difference between groups. The reactivity was also diffused due to the presence of red

blood cells in the kidney (Fig. 4G). These data thus suggested that CD1d-dependent NKT cells with CD4 and/or CD8 expression might be involved, although in part, in the modulation of immunotoxicity in the NAFLD kidney.

**Proximal tubule immunotoxicity in NAFLD potentiation of CYP2E1-mediated renal inflammation is exacerbated in mice deficient in NKT cells.**

Based on the data of increased T cell presence in the NAFLD kidney and the increased expression of CD4, CD8, and Va14, we used mice deficient in CD1D-specific NKT cells to study the role of these T cell subsets in the NAFLD kidney. The results showed that the proinflammatory cytokines IL1- $\beta$  and TNF- $\alpha$  were localized in proximal tubular cells and were significantly higher in CD1D KO mouse kidneys compared with the NAFLD + BDCM group ( $P < 0.05$ ; Fig. 5, A, B, D, and E). The increase was three- to fourfold higher in CD1D-deficient mice. mRNA expression of the cytokines IL-1 $\beta$  and TNF- $\alpha$  was also significantly higher in CD1D KO mice (3.5-fold), suggesting an intrinsic response from the cells, most likely NKT cells dependent on CD1D ( $P < 0.05$ ; Fig. 5, C and F). The results strongly suggested that the absence of CD1D significantly exacerbated the NAFLD kidney immunotoxicity. However, the increased CD4 and CD8 protein in CD1D KO mice and their strong correlation with tubular immunotoxicity in the absence of CD1D-dependent NKT cells might possibly be due to infiltrating and/or resident T cells, which are capable of increasing cytotoxicity. The study also analyzed the expression of NAFLD kidney secretion of PDGF2 and TLR4. Since there was a strong indication of the activation of MCs and the proinflammatory pathway that is downstream of TLR4 signaling, such as IL-1 $\beta$  and TNF- $\alpha$ , expression of both PDGF2 and TLR4 was performed. The results showed that mRNA expression of TLR4 was significantly higher in the NAFLD + BDCM group

but was lower in the NAFLD + BDCM + DAS group (Fig. 5G). CD1D-deficient mice had a significant increase in the expression of TLR4 compared with the NAFLD + BDCM group ( $P < 0.05$ ; Fig. 5G). Interestingly, BDCM administration to LC mice did not significantly increase the expression of TLR4 or PDGF2 compared with the LC alone group (Fig. 5, G and H). The results suggested that the expression of TLR4 correlated well with CD1D deficiency and tubular immunotoxicity. MC activation is often associated with an increase in PDGF2 (79, 97). The results showed that PDGF2 expression was significantly higher in the NAFLD + BDCM group compared with the NAFLD alone group ( $P < 0.05$ ; Fig. 5H). The administration of DAS significantly decreased its expression, whereas lack of CD1D had a significant increase in its expression compared with the NAFLD + BDCM group ( $P < 0.05$ ; Fig. 5H). The results suggested that MC activation and the release of proinflammatory mediators were strong possibilities due to a reductive metabolism of CYP2E1 and NKT cell deficiency intrinsic to the kidney in addition to infiltrating T cell subsets (CD4+ and CD8+) might be regulating its activation and immunotoxicity.

**MC proliferation and TGF- $\beta$  production were increased in mice deficient in NKT cells.**

To show that CD1D-dependent NKT cells regulated the MC proliferation, we studied the protein levels of  $\alpha$ -SMA and TGF- $\beta$  in the NAFLD kidney. The results showed that immunoreactivity of  $\alpha$ -SMA and TGF- $\beta$  were significantly increased in the NAFLD + BDCM group compared with the NAFLD alone group ( $P < 0.05$ ;  $\alpha$ -SMA: Fig. 6, A and C, and TGF- $\beta$ : Fig. 6, B and D), whereas mice deficient in CD1D-dependent NKT cells showed a significant increase in both  $\alpha$ -SMA and TGF- $\beta$  immunoreactivity compared with

the NAFLD + BDCM group. Dual labeling of IL1 $\beta$ / $\alpha$ -SMA and TGF- $\beta$ / $\alpha$ -SMA showed a significant increase in immunoreactivity in CD1D KO mice. Interestingly, mice lacking T, B, and NK cells showed a significant decrease in  $\alpha$ -SMA levels. The results suggested that MC activation ( $\alpha$ -SMA + ve cells), at least in part, is dependent on the presence of NKT cells and that lack of NKT cells significantly enhanced immunotoxicity. In the absence of T, B, or NK cells, there was no significant increase in MC activation (Fig. 6, E,v and F,v).

**NAFLD potentiation of renal inflammation induced by MCs causes increased levels of proximal tubular HMGB1 levels and apoptosis in part via the TLR4 pathway with exacerbation after lack of CD1D-dependent NKT cells.**

Our results showed that MCs were activated after CYP2E1-induced oxidative stress. Reductive metabolism of CYP2E1 has been shown to cause cell death and the release of DAMPs in the circulation (39). HMGB1 is known to be an established DAMP and a ligand for TLR4 activation (73, 82). Our previously described results in this study have shown TLR4 activation in the NAFLD kidney that was dependent on CYP2E1 reductive metabolism and the presence of CD1D. To show the presence of HMGB1 in the NAFLD kidney, we studied the immunoreactivity of HMGB1 in kidney tissues. The results showed that HMGB1 immunoreactivity was significantly higher in the NAFLD + BDCM group compared with the NAFLD alone group ( $P < 0.05$ ; Fig. 7, A and B), whereas deficiency of CD1D significantly increased HMGB1 protein in this group compared with the NAFLD + BDCM group ( $P < 0.05$ ; Fig. 7, A and B). Further apoptotic cell death, as indicated by TUNEL-positive nuclei, was significantly increased in the NAFLD + BDCM group compared with the NAFLD alone group ( $P < 0.05$ ; Fig. 7, C and D). Deficiency of CD1D further increased apoptosis compared with the NAFLD + BDCM group (Fig. 7, C and D).

These results suggested that increased HMGB1 was partly due to the repression of NKT cell function in NAFLD and may be responsible for the proinflammatory surge in the kidneys. Interestingly, apoptosis indicated by TUNEL assay also followed a similar pattern, being controlled in part by NKT cells intrinsic to the kidneys. The apoptosis might be mediated by CD95L (Fas ligand) since mRNA expression was significantly higher in the NAFLD + BDCM group compared with the NAFLD alone group, whereas CD1D-deficient mice had a further increase in the expression of Fas ligand ( $P < 0.05$ ; Fig. 7E). To show the role of MCs in proximal tubular immunotoxicity, conditioned medium from MCs was used to incubate proximal tubular cells. The results showed that proximal tubular cells had a significant increase in chemokine (C-C motif) ligand 5 (regulated on activation, normal T cell expressed and secreted) and endothelin-1 expression ( $P < 0.05$ ; Fig. 7, F and G). Tubular cells also had a significant increase in the expression of IL-1 $\beta$  and monocyte chemoattractant protein-1 (Fig. 7, H and I). These cells also exhibited more apoptotic cell death, as indicated by increased TUNEL-positive nuclei (shown by yellow; Fig. 7J). The data showed that activated MCs caused tubular cell toxicity.

**Exacerbation of immunotoxicity in NAFLD kidneys after reductive metabolism of CYP2E1 is mediated by TLR4 activation.**

A significant role of CYP2E1 in inflammation has been documented (67). The mechanisms, although unclear, might proceed through an oxidative stress-DAMP-TLR4 signaling pathway. To study whether the strong correlation of the events that we observed in the NAFLD kidney might be via TLR4 signaling, we used TLR4 KO mice kidneys treated identically. The results showed that the immunotoxicity was significantly decreased in TLR4 KO mouse kidneys compared with the NAFLD + BDCM group for IL-1 $\beta$ , TNF-



$\alpha$ , and Fas ligand, whereas the expression of IL-6 was unchanged ( $P < 0.05$ ; data not shown and Fig. 8A). LC mice treated with BDCM had a marked increase in the expression of Fas ligand compared with the LC group and NAFLD + BDCM group (Fig.8A). HMGB1 immunoreactivity was unchanged in TLR4 KO mice, indicating that HMGB1 was upstream of TLR4 signaling, as may be perceived since HMGB1 is a known inducer of TLR4 signaling (Fig. 8, B and C). The results suggested a strong involvement of TLR4 signaling in the immunotoxicity of the kidney of mice that had NAFLD and CYP2E1 activation.

**Exacerbation of immunotoxicity in NAFLD kidneys by reductive metabolism of CYP2E1 increases the levels of CXCL16.**

CXCL16 has been shown to be a proinflammatory mediator mostly released by dendritic cells and is bound by NKT cells through their surface moiety CXCR6 (96). To show whether CYP2E1 reductive metabolism in NAFLD causes an increase in levels of CXCL16 in the kidneys, we performed immunohistochemistry and mRNA expression profiles of this important cytokine. The results showed that there was a significant increase in the immunoreactivity of CXCL16 in the NAFLD + BDCM group compared with the NAFLD alone group ( $P < 0.05$ ; Fig. 9, A and B). The administration of DAS significantly decreased the immunoreactivity of CXCL6, whereas CD1D-deficient mouse kidneys did not show any significant difference ( $P < 0.05$ ). mRNA expression of CXCL16 also showed a similar trend while indicating that the expression was intrinsic to the kidneys ( $P < 0.05$ ; Fig. 9C). These results suggested that there might be a strong correlation with increased CXCL16 in the kidneys and increased NKT cell activation, as shown in this study, because NKT cells

are attracted due to the higher presence of cognate ligand and chemokine (CXCL16) in the renal microenvironment (96).

### **NAFLD-induced CYP2E1 activity and metabolic oxidative stress cause kidney injury and affect glomerular function.**

To show whether CYP2E1-mediated oxidative stress affected glomerular function, mouse blood was analyzed for BUN concentrations as an indicator of glomerular function. The results showed that BUN increased significantly in the LC + BDCM group compared with the LC alone group ( $P < 0.05$ ; Fig. 10A). The administration of the CYP2E1 inhibitor showed a significant decrease in BUN values. However, an underlying condition of NAFLD and metabolic oxidative stress significantly increased the concentration of BUN (>3-fold) compared with the NAFLD alone or LC groups (Fig. 10A). Picrosirius red staining, an indicator of collagen deposition, showed a marked increase in the NAFLD + BDCM group compared with the NAFLD alone group, whereas administration of the CYP2E1 inhibitor attenuated the collagen deposition (Fig. 10B). Histological scores showed that the NAFLD + BDCM group had higher inflammation fibrosis than the NAFLD alone group, whereas the CD1D KO group showed higher scores for these two indexes compared with the NAFLD + BDCM group. TLR4 KO mice had lower inflammation and fibrosis.

## **2.4 DISCUSSION**

In the present study, we show that an underlying condition of progressive NAFLD in mice exacerbated proximal tubular immunotoxicity and affected glomerular function after a second hit from metabolic oxidative stress via CYP2E1. The heightened inflammation in

proximal tubular cells might have resulted from MC proliferation, as indicated by increased  $\alpha$ -SMA protein and increased TGF- $\beta$  production (76, 92). Furthermore, the heightened inflammation was mediated in part by a TLR4-dependent mechanism, as shown by the abrogation of the inflammatory phenotype in TLR4 KO mouse kidneys. Finally, the study showed that the proinflammatory nature of the immunotoxicity in NAFLD kidneys that had metabolic oxidative stress via CYP2E1 metabolism was modulated by NKT cells, as evidenced by 1) increased immunotoxicity in NKT cell-deficient mice and 2) higher localization of CXCL16 protein, a ligand that binds to CXCR6 on NKT cells to promote its activation in the kidneys (96).

There is increasing evidence that a condition of NAFLD, which has high risks of progressing to NASH, cirrhosis, and hepatocellular carcinoma, can have comorbidities that may include renal and cardiovascular complications (72). The more progressive form of NAFLD is termed NASH and is likely caused by a second or multiple hits from oxidative stress, inflammatory adipokines, activation of pattern recognition receptors, glucose intolerance, and insulin resistance (69). More recently, there have been significant studies that have shown the role of CYP2E1 in modulating the progression of NAFLD to NASH via metabolic oxidative stress (66, 84, 85, 93). In the present study, we used BDCM as a substrate for the generation of metabolic oxidative stress that aids in the progression of NASH (88). Interestingly, CYP2E1 reductive metabolism of BDCM caused lipid peroxidation in proximal tubular cells of the kidney, as shown by 4-HNE staining, whereas the administration of DAS, a specific inhibitor of CYP2E1, attenuated the peroxidation. The increased oxidative stress was not due to the toxin administration alone since LC mice, which did not have symptoms of NAFLD and did not have steatosis or insulin resistance,

did not show the exacerbation in oxidative stress. The results strongly suggested that CYP2E1-mediated oxidative stress in the liver might be a strong mediator of ectopic manifestations in distant organs, such as the kidney, via soluble mediators of inflammation or DAMPs that can be released in the circulation and further cause lipid peroxidation in the kidneys (73, 106). It is highly unlikely that the toxin alone could cause a parallel oxidative stress damage in the kidneys via CYP2E1 metabolism since it is known that the kidneys possess only 5% of CYP2E1 protein compared with the liver (98). However, the mechanisms were elusive at this juncture.

Metabolic syndrome and diabetes have been found to be among the many reasons responsible for CKD (77). CKD is often associated with proximal tubular inflammation, glomerulonephritis, and glomerulosclerosis. Our study investigated the proinflammatory events in the glomerulus and proximal tubules after progressive NAFLD (NAFLD with inflammation and fibrosis in the liver) in mice. Furthermore, we aimed at identifying the cell types that might be primarily responsible for the heightened proinflammatory phenotype by targeting MCs, since it has been shown that MCs have a strong role to play in the development of CKD (83). The results showed that there was a significant increase in the levels of lipid peroxidation, IL-1 $\beta$ , and TNF- $\alpha$  in proximal tubular cells and podocytes. There was a significant increase in the levels of  $\alpha$ -SMA, a proliferative marker of MCs, along with levels of TGF- $\beta$ . Interestingly, levels of IFN- $\gamma$  and the T cell markers CD4, CD8, and Va14 (an invariant NKT cell marker) were also increased in proximal tubules. The strong inflammatory phenotype and increased levels of  $\alpha$ -SMA and TGF- $\beta$  levels showed a strong bias toward the role of MCs in proinflammatory processes in the tubule, but a role of endothelial cells also could not be ruled out (101). The rationale that

MC activation caused proximal tubular immunotoxicity was further strengthened by results where conditioned medium from MCs enhanced tubular cell expression of proinflammatory cytokines and cell death (Fig. 7, F–J). It was highly unlikely that the infiltrating macrophages were responsible since there was equal F4/80 staining in kidney sections, including the CD1D KO group (Fig. 4G).

The data showed a prominent inflammatory pattern in tubules, but the presence of T cells also increased the possibility of a regulatory role of these cells in the kidney after NAFLD progression. The argument in favor of the regulatory role of T cells could not be ignored since glomerulonephritis has been shown to be attenuated by the presence of NKT cells primarily in the kidney (107). Moreover, the significant increase in the mRNA expression of Va14, a marker of invariant CD1D-dependent NKT cells, also indicated the involvement of these cell types (107). We used CD1D KO mice to probe the involvement of NKT cells since use of mice that were deficient for T, B, and NK cells did not alter the immunotoxic phenotype in the kidneys, especially regarding the activation of MCs (Fig. 6, E and F). The use of CD1D KO mice significantly exacerbated the proinflammatory phenotype in the kidneys by three- to fourfold compared with the NAFLD + BDCM group (which harbors the kidney disease phenotype).

Ectopic manifestation of the effects of progressive NAFLD, especially in conditions of NASH, has been shown (72). DAMPS can be released in the circulation after liver injury (39). HMGB protein, adipokine leptin, or TNF- $\alpha$  in the circulation has been shown to cause lipid peroxidation in distant organs (102). Furthermore, HMGB1 can act as an endogenous ligand for TLR4 receptors and increase immunotoxicity (75). Our data showed increased levels of HMGB1 protein in proximal tubular cells, whereas lack of NKT

cells showed a further increase in the levels of HMGB1, suggesting a modulatory role of NKT cells in preventing DAMP-induced kidney injury. However, the exact mechanism by which NKT cells can modulate the release of DAMPs is not understood in this study. To show whether HMGB1 mediated the proximal tubular inflammation through the TLR pathway, we used TLR4 KO mice. The results indicated that the mRNA expression of IL-1 $\beta$  and TNF- $\alpha$  was significantly decreased in TLR4 KO mouse kidneys, suggesting a strong involvement of TLR4 pathway activation, probably through endogenous ligands. However, the data are clearly of an indicative nature since endotoxin leaching via the gut could not be ruled out, as has been predicted in alcoholic liver disease (104).

Taken together, we report a possible mechanistic investigation of ectopic immunotoxicity in kidney proximal tubular cells after heightened CYP2E1 metabolism in progressive NAFLD. The increased oxidative stress caused MC activation and proinflammatory cytokine release, thus accentuating extracellular matrix formation via TGF- $\beta$  production. The resultant immunotoxicity possibly mediated the altered glomerular function, as indicated by increased BUN values. The proinflammatory events were likely mediated by the TLR4 pathway, and the presence of NKT cells was found to be protective in the NAFLD potentiation of proximal tubular immunotoxicity. On the other hand, NKT cells, which might be activated in parallel by oxidative stress, played a major protective role via binding to CXCL16, which also has been shown in this study to be increased in the kidneys after reductive metabolism of CYP2E1. Future studies will need to focus on both DAMP-induced TLR4 pathway activation and a concomitant regulatory mechanism by CD1D-dependent NKT cells or other regulatory T cells.

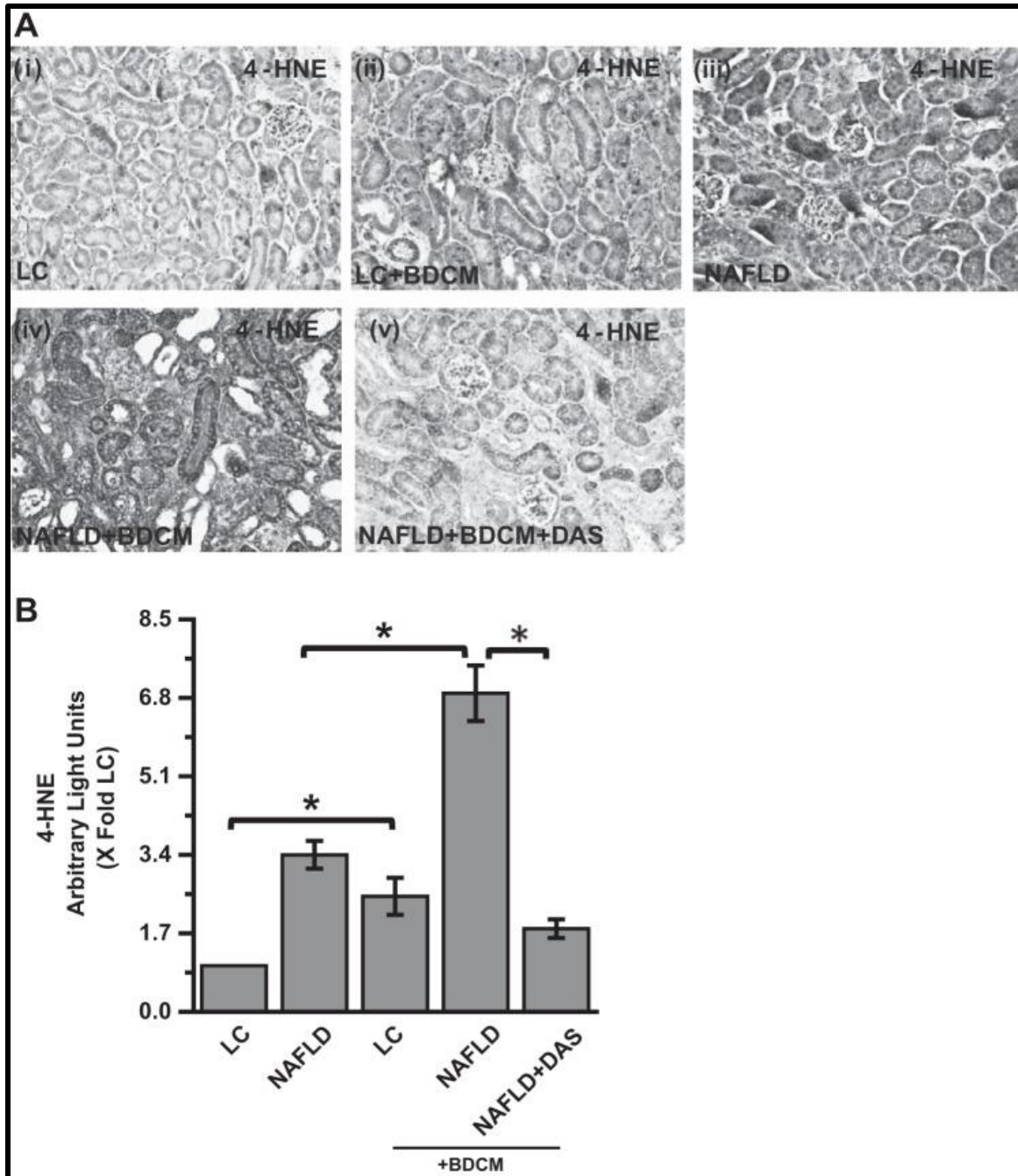


Figure 2.1A: 4-hydroxynonenal (4-HNE; a marker for lipid peroxidation) immunoreactivity, as shown by immunohistochemistry in kidney slices from mice fed a chow diet [lean control (LC); i], LC mice exposed to bromodichloromethane (BDCM; ii), mice fed a high-fat diet (60% kcal fat) and used as a model of nonalcoholic fatty liver disease (NAFLD; iii), NAFLD mice exposed to BDCM (iv), and NAFLD mice coexposed to BDCM and diallylsulfide (DAS; v), a known cytochrome P-450 (CYP)2E1 inhibitor. Images were taken at  $\times 20$  magnification. B: morphometric analysis of 4-HNE

immunoreactivity (mean data from 3 separate microscopic fields were plotted on the yaxis) in the LC, LC + BDCM, NAFLD, NAFLD + BDCM, and NAFLD + BDCM + DAS groups. \*P < 0.05.

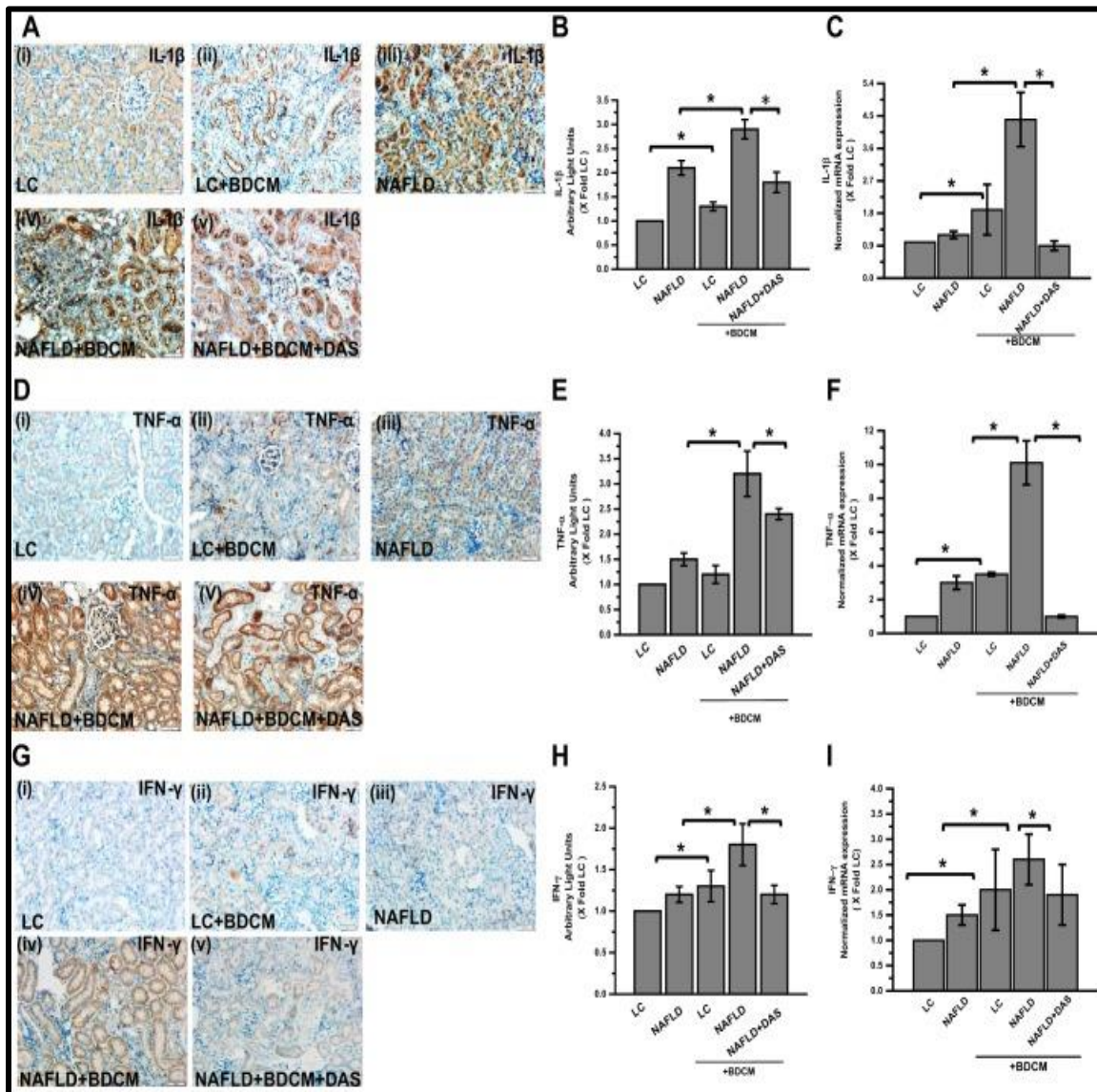


Figure 2.2A: immunoreactivity of IL-1β, as shown by immunohistochemistry in kidney slices from LC(i), LC + BDCM (ii), NAFLD (iii), NAFLD + BDCM (iv), and NAFLD + BDCM + DAS (v) groups of mice. B: morphometric analysis of IL-1β immunoreactivity in the LC, LC + BDCM, NAFLD, NAFLD + BDCM, and NAFLD + BDCM + DAS groups. \*P < 0.05. C: mRNA expression of IL-1β in kidney tissue of LC, LC + BDCM, NAFLD, NAFLD + BDCM, and NAFLD + BDCM + DAS groups of mice. D: immunoreactivity of TNF-α, as shown by immunohistochemistry in kidney slices from LC (i), LC + BDCM (ii), NAFLD (iii), NAFLD + BDCM (iv), and NAFLD + BDCM + DAS



(v) groups of mice. E: morphometric analysis of TNF- $\alpha$  immunoreactivity in the LC, LC + BDCM, NAFLD, NAFLD + BDCM, and NAFLD + BDCM + DAS groups. \*P < 0.05. F: mRNA expression of TNF- $\alpha$  in kidney tissue of LC, LC + BDCM, NAFLD, NAFLD + BDCM, and NAFLD + BDCM + DAS groups of mice. G: immunoreactivity of interferon (IFN)- $\gamma$ , as shown by immunohistochemistry in kidney slices from LC (i), LC + BDCM (ii), NAFLD (iii), NAFLD + BDCM (iv), and NAFLD + BDCM + DAS (v) groups of mice. H: morphometric analysis of IFN- $\gamma$  immunoreactivity in the LC, LC + BDCM, NAFLD, NAFLD + BDCM, and NAFLD + BDCM + DAS groups. \*P < 0.05. F: mRNA expression of IFN- $\gamma$  in kidney tissue of LC, LC + BDCM, NAFLD, NAFLD + BDCM, and NAFLD + BDCM + DAS groups of mice. All immunohistochemistry images were taken at  $\times 20$  magnification, and morphometric analysis results were plotted as mean data (immunoreactivity measured in arbitrary light units) from three separate microscopic fields plotted on the y-axis. All mRNA expression was assessed by quantitative real-time PCR, and expression was normalized against the LC group. \*P < 0.05.

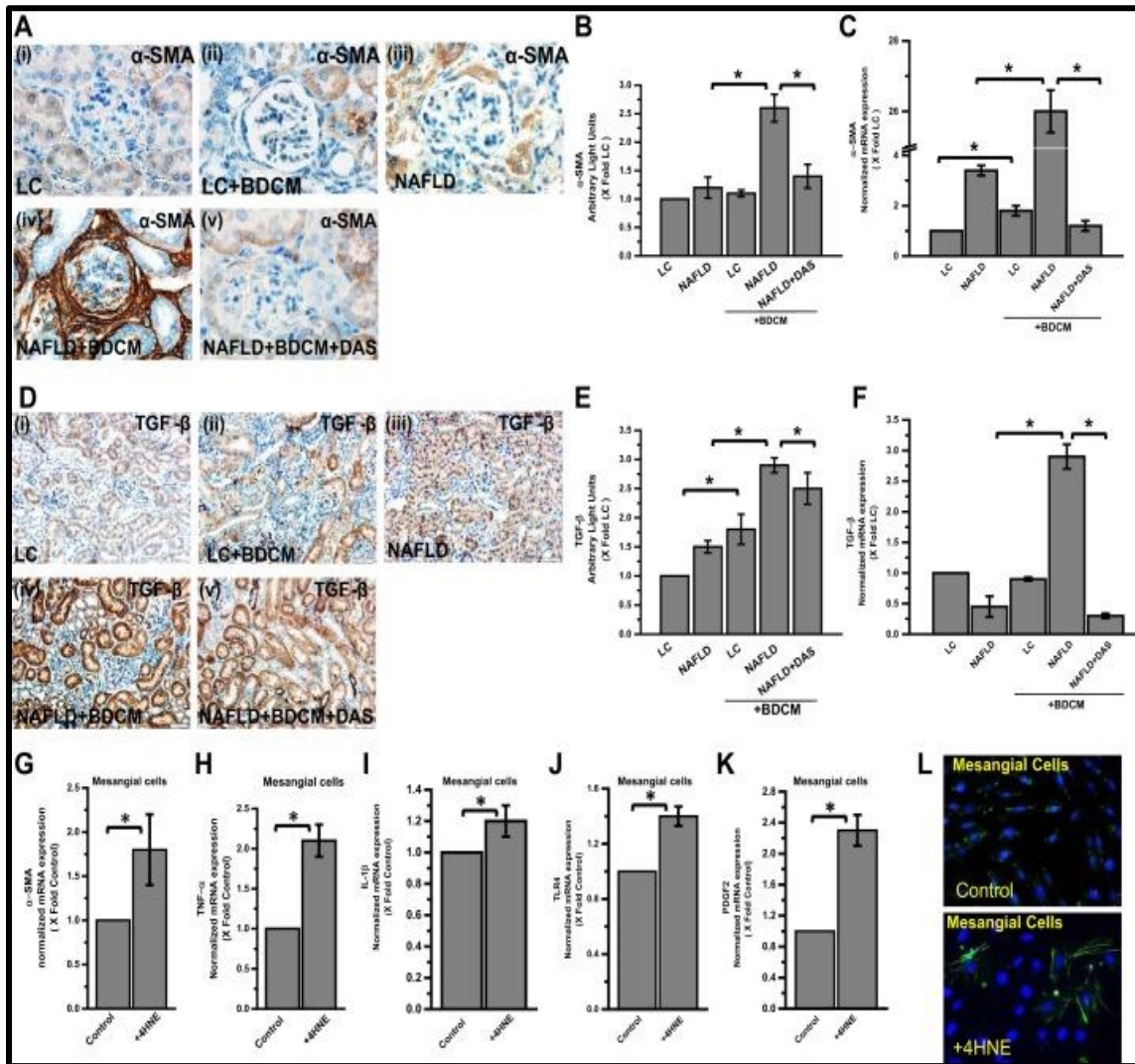


Figure 2.3 A: immunoreactivity of  $\alpha$ -smooth muscle actin ( $\alpha$ -SMA), as shown by immunohistochemistry in kidney slices from LC(i), LC + BDCM (ii), NAFLD (iii), NAFLD + BDCM (iv), and NAFLD + BDCM + DAS (v) groups of mice. All images were taken at  $\times 60$  oil magnification. B: morphometric analysis of  $\alpha$ -SMA immunoreactivity in the LC, LC + BDCM, NAFLD, NAFLD + BDCM, and NAFLD + BDCM + DAS groups. \*P < 0.05. C: mRNA expression of  $\alpha$ -SMA gene in kidney tissue of LC, LC + BDCM, NAFLD, NAFLD + BDCM, and NAFLD + BDCM + DAS groups of mice. D: immunoreactivity of transforming growth factor (TGF)- $\beta$ , as shown by immunohistochemistry in kidney slices from LC(i), LC + BDCM (ii), NAFLD (iii), NAFLD + BDCM (iv), and NAFLD + BDCM + DAS (v) groups of mice. All images were taken at  $\times 20$  magnification. E: morphometric analysis of TGF- $\beta$  immunoreactivity in the LC, LC + BDCM, NAFLD, NAFLD + BDCM, and NAFLD + BDCM + DAS groups. \*P < 0.05. F: mRNA expression of TGF- $\beta$  in kidney tissue of LC, LC + BDCM, NAFLD, NAFLD + BDCM, and NAFLD + BDCM + DAS groups of mice. Morphometric analysis was plotted as mean data (immunoreactivity measured in arbitrary light units) from three separate microscopic fields plotted on the y-axis. All mRNA expression was assessed by quantitative real-time PCR, and expression was normalized against the LC group. \*P < 0.05. G-K: mRNA expression of  $\alpha$ -SMA, TNF- $\alpha$ , IL-1 $\beta$ , Toll-like receptor (TLR)4, and PDGF2 in cell lysates of a kidney mesangial cell (MC) line (CRL-1927) treated with 4-HNE, a lipid peroxidation product. MCs treated with ethanol were used as a control (CTL). L: immunofluorescence images of CRL-1927 cells treated with either alcohol or 4-HNE for assessment of myofibroblastic phenotype ( $\alpha$ SMA immunoreactivity).

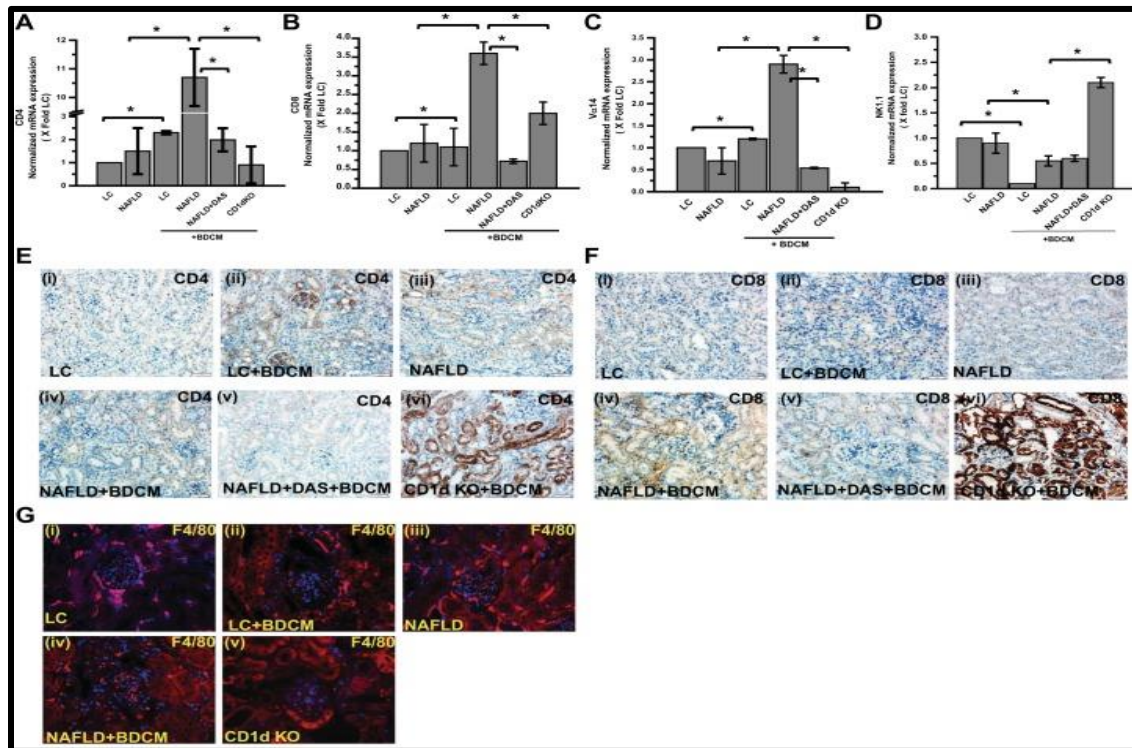


Figure 2.4 A–D: mRNA expression of CD4, CD8, Va14, and NK1.1 genes in kidney tissue from LC, LC + BDCM, NAFLD, NAFLD + BDCM, NAFLD + BDCM + DAS groups of mice as well as CD1d-deficient [CD1d knockout (KO)] mice fed a high-fat diet and exposed to BDCM. mRNA expression was assessed by quantitative real-time PCR, and expression was normalized against the LC group. \*P < 0.05. E and F: immunoreactivity of tissue sections against CD4 (E) and CD8 (F), as assessed by immunohistochemistry from LC(i), LC + BDCM (ii), NAFLD (iii), NAFLD + BDCM (iv), NAFLD + BDCM + DAS (v), and CD1d KO + BDCM (vi) groups of mice. G: immunofluorescence microscopy for F4/80 immunoreactivity in kidney slices from LC (i), LC + BDCM (ii), NAFLD (iii), NAFLD + BDCM (iv), and CD1d KO (v) groups, as shown by red fluorescence.

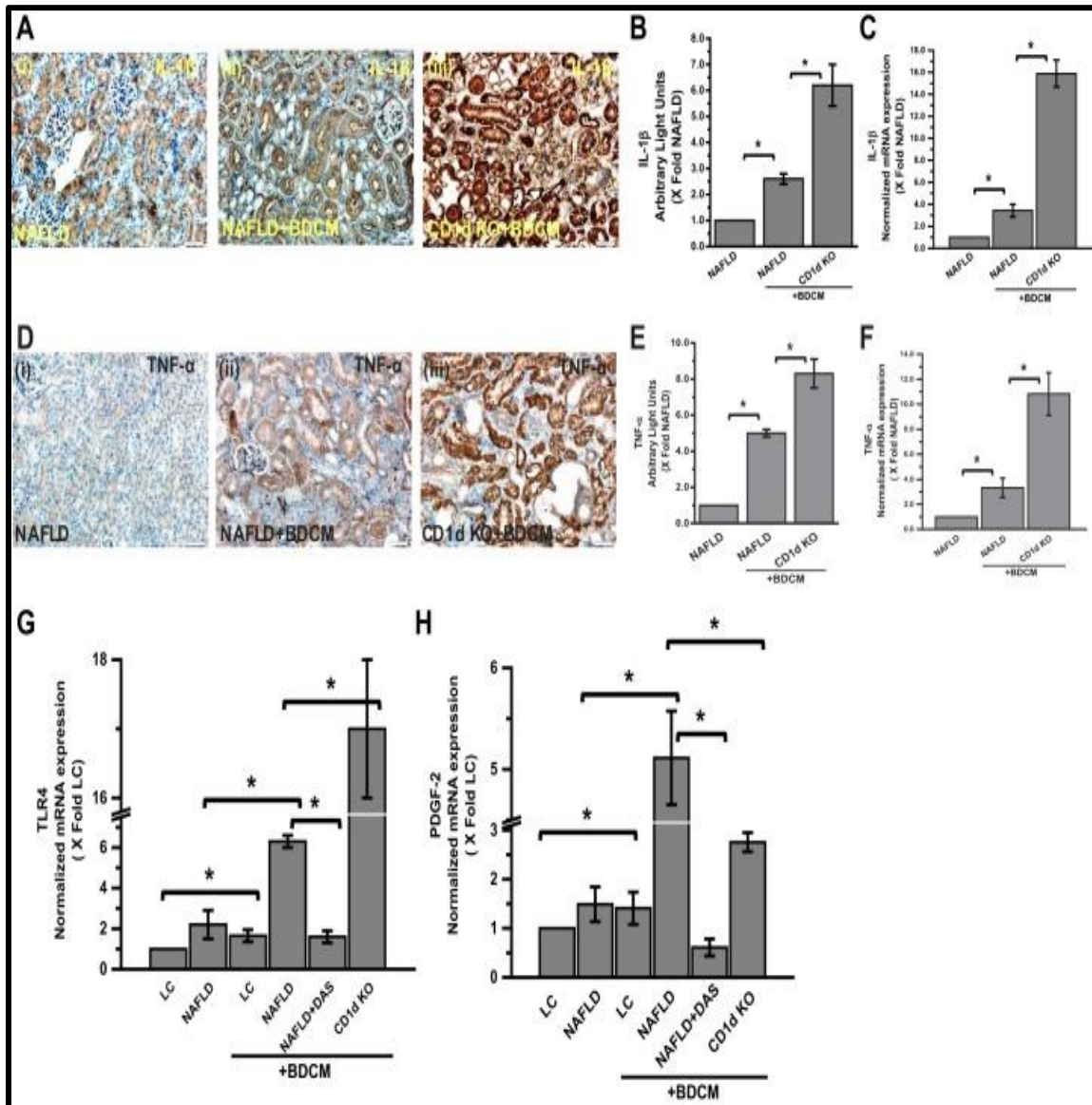


Figure 2.5 A: immunoreactivity of IL-1 $\beta$ , as shown by immunohistochemistry in kidney slices from NAFLD (i), NAFLD + BDCM (ii), and CD1d KO + BDCM (iii) groups. B: morphometric analysis of IL-1 $\beta$  immunoreactivity in NAFLD, NAFLD + BDCM, and CD1d KO + BDCM groups of mice. Data were normalized against the NAFLD group. \*P < 0.05. C: mRNA expression of IL-1 $\beta$  in kidney tissue of NAFLD, NAFLD + BDCM, and CD1d KO + BDCM groups of mice. D: immunoreactivity of TNF- $\alpha$ , as shown by immunohistochemistry in kidney slices from NAFLD (i), NAFLD + BDCM (ii), and CD1d KO + BDCM (iii) groups. E: morphometric analysis of TNF- $\alpha$  immunoreactivity in NAFLD, NAFLD + BDCM, and CD1d KO + BDCM groups of mice. Data were normalized against the NAFLD group. \*P < 0.05. F: mRNA expression of TNF- $\alpha$  in kidney tissue of NAFLD, NAFLD + BDCM, and CD1d KO + BDCM groups of mice. G and H: mRNA expression of TLR4 and PDGF2 in kidney tissue of LC, LC + BDCM, NAFLD, NAFLD + BDCM, NAFLD + BDCM + DAS, and CD1d KO + BDCM groups of mice. All immunohistochemistry images were taken at  $\times 20$  magnification, and morphometric analysis was plotted as mean data (immunoreactivity measured in arbitrary light units) from three separate microscopic fields plotted on the y-axis. All mRNA expression was assessed by quantitative real-time PCR, and expression was normalized against the LC group. \*P < 0.05.

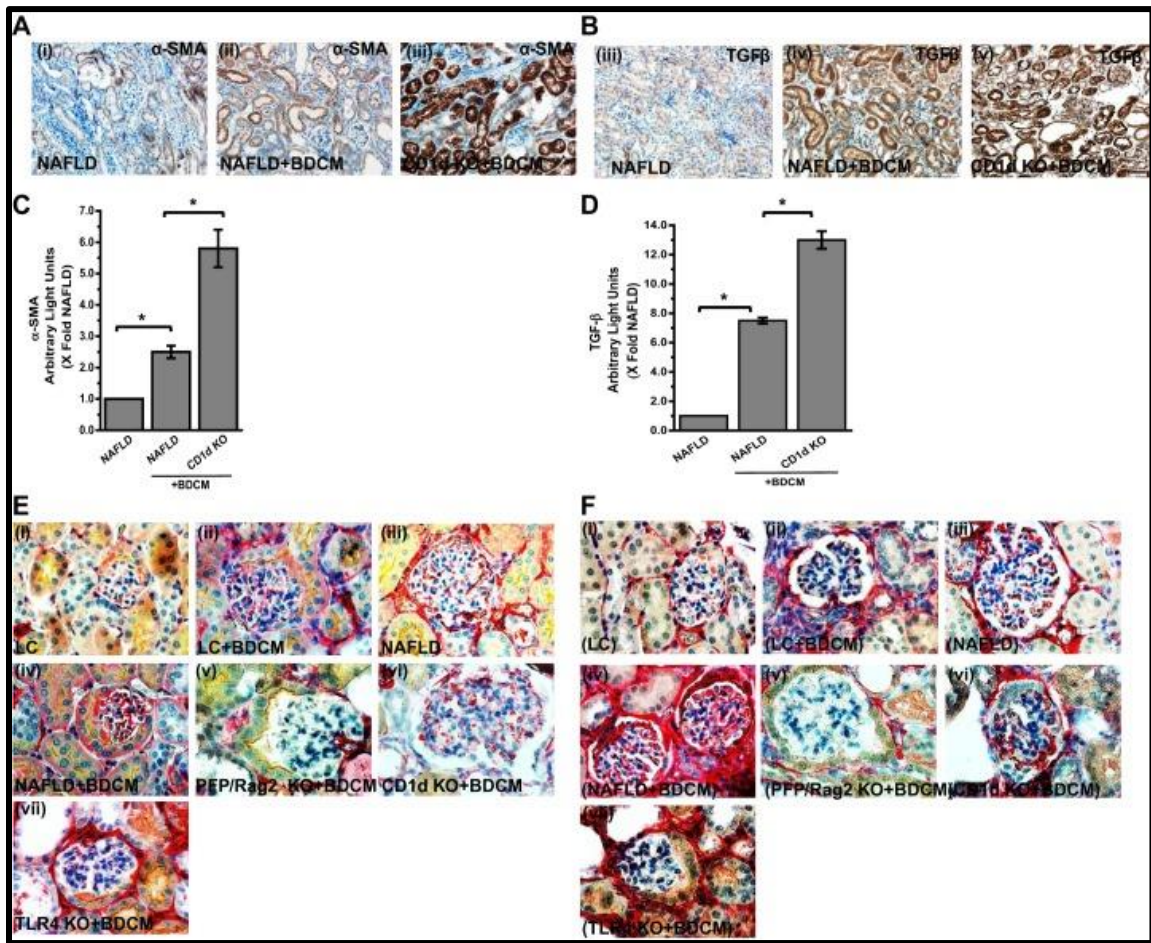


Figure 2.6A: immunoreactivity of  $\alpha$ -SMA, as shown by immunohistochemistry in kidney slices from the NAFLD (i), NAFLD + BDCM (ii), and CD1d KO + BDCM (iii) groups. B: immunoreactivity of TGF- $\beta$ , as shown by immunohistochemistry in kidney slices from the NAFLD (i), NAFLD + BDCM (ii), and CD1d KO + BDCM (iii) groups. C and D: morphometric analysis of  $\alpha$ -SMA (C) and TGF- $\beta$  (D) immunoreactivity in NAFLD, NAFLD + BDCM, and CD1d KO + BDCM groups of mice. All immunohistochemistry images were taken at  $\times 20$  magnification, and morphometric analysis was carried out as mean data (immunoreactivity measured in arbitrary light units) from three separate microscopic fields plotted on the y-axis. \* $P < 0.05$ . E: immunohistochemistry images of kidney tissue slices showing immunoreactivity against both  $\alpha$ -SMA (red) and IL-1 $\beta$  (yellow). F: immunohistochemistry images of kidney tissue slices showing immunoreactivity against both  $\alpha$ -SMA (red) and TGF- $\beta$  (yellow).

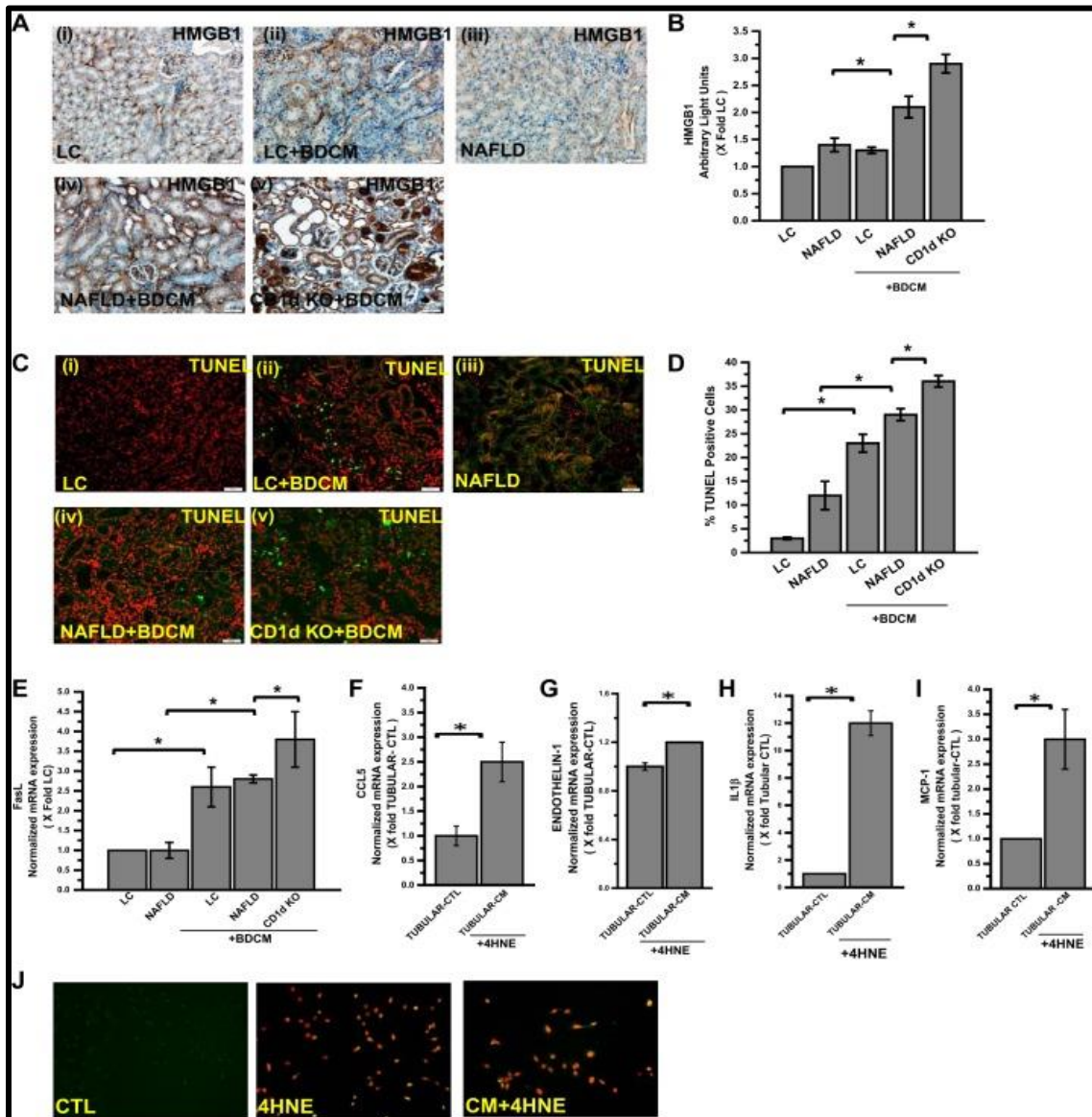


Figure 2.7A: immunoreactivity of high mobility group box (HMGB)1, as shown by immunohistochemistry in kidney slices from LC (i), LC + BDCM (ii), NAFLD (iii), NAFLD + BDCM (iv), and CD1d KO + BDCM (v) groups of mice. B: morphometric analysis of HMGB1 immunoreactivity in LC, LC + BDCM, NAFLD, NAFLD + BDCM, and CD1d KO + BDCM groups of mice. Mean data (immunoreactivity measured in arbitrary light units) from three separate microscopic fields were plotted on the y-axis. \*P < 0.05. C: number of apoptotic nuclei as shown by TUNEL immunofluorescence staining in kidney slices from LC (i), LC + BDCM (ii), NAFLD (iii), NAFLD + BDCM (iv), and CD1d KO + BDCM groups of mice. The number of TUNEL-positive cells identified by their green-stained nuclei against the nuclear fast red-stained nuclei corresponds to the number of apoptotic events. Images were taken at  $\times 20$  magnification. D: percentage of TUNEL-positive cells (obtained by morphometric analysis done on images from three separate microscopic fields) in LC, LC + BDCM, NAFLD, NAFLD + BDCM, and CD1d KO + BDCM groups. \*P < 0.05. E: mRNA expression of Fas ligand (FasL) in kidney tissue of LC, LC + BDCM, NAFLD, NAFLD + BDCM, and CD1d KO + BDCM groups of mice. F–I: a kidney MC line (CRL-1927) and kidney tubular cell line (CRL-2038) were used for these experiments. CRL-2038 cells were incubated with conditioned medium (CM) from MC + 4-HNE. mRNA expression was then assessed by quantitative real-time PCR using primers for chemokine (C-C motif) ligand 5, endothelin-1, IL-1 $\beta$ , and monocyte chemoattractant protein (MCP)-1 (P < 0.05). J: cell death (apoptotic) as shown by TUNEL (green)-stained nuclei (red). Nuclei positive for TUNEL show a yellow appearance and were markedly higher in cells + CM + 4-HNE compared with the other groups.

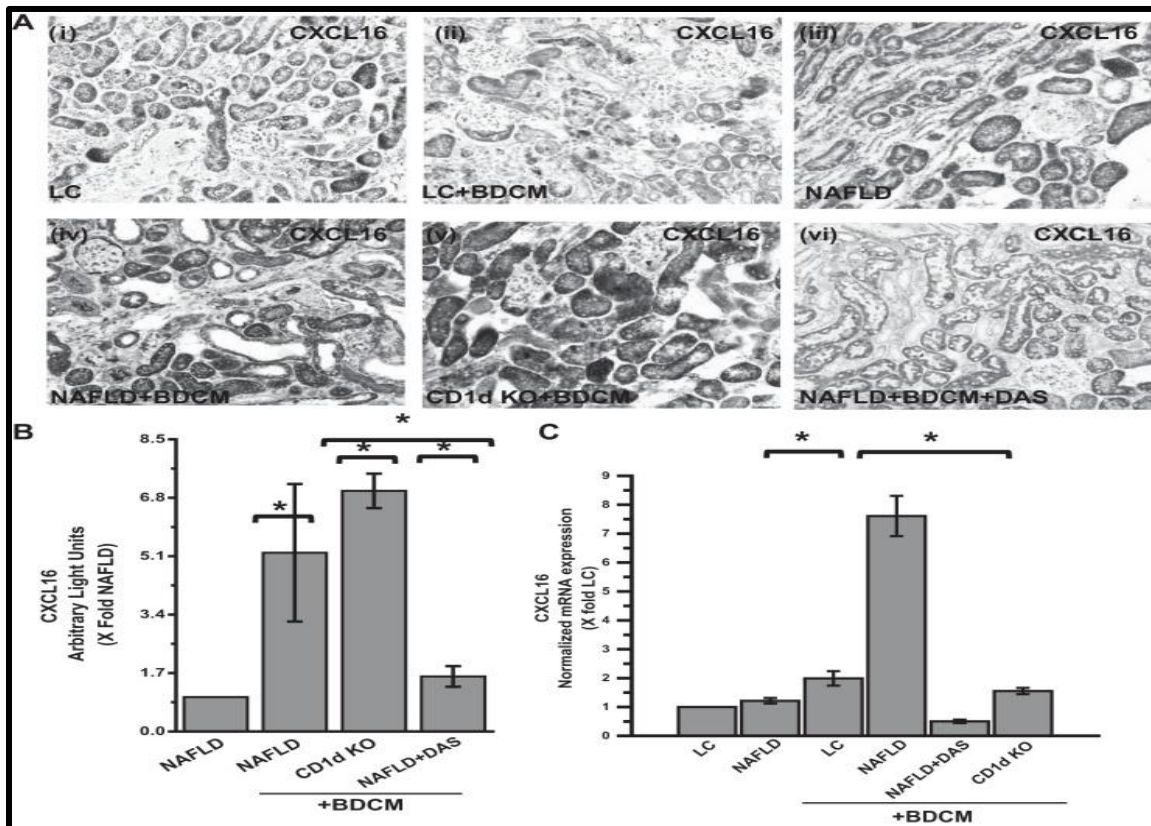


Figure 2.8 A: mRNA expression of IL-1 $\beta$ , IL-6, TNF- $\alpha$ , and FasL in kidney tissue of LC, LC + BDCM, NAFLD, NAFLD + BDCM groups as well as TLR4 gene-deficient (TLR4 KO) mice fed a high-fat diet and exposed to BDCM. All mRNA expression was assessed by quantitative real-time PCR, and expression was normalized against the NAFLD group. \*P < 0.05. B: immunoreactivity of HMGB1, as shown by immunohistochemistry in kidney slices from LC (i), LC + BDCM (ii), NAFLD (iii), NAFLD + BDCM (iv), and TLR4 KO + BDCM (v) groups. All images were taken at  $\times 20$  magnification. All mRNA expression was assessed by quantitative real-time PCR, and expression was normalized against the LC group. \*P < 0.05. C: immunoreactivity of HMGB1. \*P < 0.0

## CHAPTER 3

# **HIGH CIRCULATORY LEPTIN MEDIATED NOX-2 PEROXYNITRITE-MIR21 AXIS ACTIVATE MESANGIAL CELLS AND PROMOTES RENAL INFLAMMATORY PATHOLOGY IN NONALCOHOLIC FATTY LIVER DISEASE**

---

Firas Alhasson<sup>1</sup>, Ratanesh Kumar Seth<sup>1</sup>, Diptadip Dattaroy<sup>1</sup>, Varun Chandrashekar<sup>1</sup>,  
Geoffrey I Scott<sup>1</sup>, Mitzi Nagarkatti<sup>2</sup> Prakash Nagarkatti<sup>2</sup>, Anna Mae Diehl<sup>3</sup> and Saurabh  
Chatterjee<sup>1\*</sup> To be submit to Journal of Redox Biology.



To whom correspondence should be addressed:

\*Dr. Saurabh Chatterjee, Ph.D. Environmental Health and Disease Laboratory,

Department of Environmental Health Sciences, University of South Carolina, Columbia

29208 USA. Email: schatt@mailbox.sc.edu; Tel: 803-777-8120; Fax: 803-777-3391

Key Words: Leptin, NOX-2, NADPH, Mesangial Cells, miR21, Oxidative stress,

NAFLD, JAK/STAT

Conflict of Interest: The authors declare that there is no conflict of interest.

Running Title: High circulatory leptin causes renal inflammation in NAFLD.

Grant Support: This work has been supported by NIH Pathway to Independence Award,

R00ES019875 and P01AT003961 to Saurabh Chatterjee, R01DK053792 to Anna Mae

Diehl, P01AT003961, P20GM103641, R01AT006888, R01ES019313, R01MH094755

and VA Merit Award BX001357 to Mitzi Nagarkatti and Prakash S. Nagarkatti.

**Abstract:**

High circulatory insulin and leptin followed by underlying inflammation is often ascribed to the ectopic manifestations in non-alcoholic fatty liver disease (NAFLD) but the exact molecular pathways remain unclear. We have shown previously that CYP2E1-mediated oxidative stress and circulating leptin in NAFLD is associated with renal disease severity. Extending the studies, we hypothesized that high circulatory leptin in NAFLD causes renal mesangial cell activation and tubular inflammation via a NOX2 dependent pathway that upregulates proinflammatory miR21. High fat diet (60%kcal) was used to induce fatty liver

phenotype with parallel insulin and leptin resistance. The kidneys were probed for mesangial cell activation and tubular inflammation that showed accelerated NASH phenotype and oxidative stress in the liver. Results showed that NAFLD kidneys had significant increases in  $\alpha$ -SMA, a marker of mesangial cell activation, miR21 levels, tyrosine nitration and renal inflammation while they were significantly decreased in leptin and p47 phox knockout mice. Micro RNA21 knockout mice showed decreased tubular immunotoxicity and proinflammatory mediator release. Mechanistically, use of apocynin or phenyl boronic acid (FBA) or DMPO or miR21 antagomir inhibited leptin primed-miR21-mediated mesangial cell activation in vitro suggesting a direct role of leptin-mediated NOX-2 in miR21-mediated mesangial cell activation. Finally, JAKSTAT inhibitor completely abrogated the mesangial cell activation in leptin-primed cells suggesting that leptin signaling in the mesangial cells depended on the JAK-STAT pathway. Taken together the study reports a novel mechanistic pathway of leptin mediated renal inflammation that is dependent on NOX-2-miR21 axis in ectopic manifestations underlying NAFLD-induced co-morbidities.

### **3.1 INTRODUCTION:**

Fatty liver is the most common cause of chronic liver injury (111). Non-alcoholic fatty liver disease (NAFLD) is well-defined as the excessive accumulation of fat (>5%) in the liver without excessive consumption of alcohol and often considered as a benign disease in the background of altered mediators of metabolic syndrome and pro-inflammatory immune response (111,112). If untreated, NAFLD can progress from simple steatosis to complex stage of nonalcoholic steatohepatitis (NASH), hepatic fibrosis and hepatocellular carcinoma (113) following a second or multiple hits from oxidative stress, underlying low

grade sterile inflammation or environmental factors (5). The contribution of NAFLD/NASH in several ectopic diseases and pathological conditions such as type 2 diabetes (T2DM), cardiovascular disease (CVD), Chronic Kidney Disease (CKD) has been discussed in previous studies (114,115). Recently, enormous interest has been generated following multiple studies dealing with NAFLD/NASH-associated CKD. (116). We have shown previously that accelerated glomerular pathology follows a NASH phenotype (117). Additionally, CKD represents a major health concern in adults over age 65 years and it covers 25% of the western populations (118). Commonly, CKD is described as decreased estimated glomerular filtration (eGFR) and/or increased proteinuria. At the advanced stage, CKD patients develop the end-stage renal disease because of the high risk of cardiovascular disease. Further, NAFLD is characterized by metabolic disturbances including insulin resistance and leptin resistance and inflammatory response in the liver. Leptin is a cytokine mainly produced by adipocytes and plays a proinflammatory role in the liver (119,120). The primary function of leptin is to regulate satiety and control fat metabolism (121). The increased levels of circulatory leptin (hyperleptinemia) found in NAFLD can influence inflammatory response in an ectopic organ such as the kidney in addition to other comorbidities already reported in the clinics (116, 122, 123]. In the advanced stage of NAFLD/NASH, the common factor associated with NAFLD/NASH progression such as oxidative stress, activations of JAK/STAT, TGF- $\beta$  signaling, renin-angiotensin system, TLR4 pathways and release of inflammatory cytokine may strongly associate with kidney disease (117, 74-103). We and others have previously shown that oxidative stress is the key regulator in NASH via second hit/multiple hit theory (119, 125-127]. The redox stress generated by xenobiotic enzyme Cytochrome p450 2E1 (CYP2E1)

via a free-radical mechanism generates reactive oxygen species (ROS) and reactive nitrative species (RNS) in the liver (128). The oxidative stress resulted from reductive metabolism of CYP2E1, can accelerate metabolic disturbances, leptin release and trigger host innate immune response (ref). The cascade of redox signaling, presence of damage associated molecular patterns (DAMPS) and presence of high circulatory leptin can stimulate NADPH oxidase system in distal organs such as the kidney (119, 39, 129). The NADPH oxidase (NOX) is commonly expressed in both phagocytic and non-phagocytic cells (130). In Kidney, NADPH oxidases have divergent localization in the renal cells which include mesangial cells, tubular cells endothelial cells and podocytes (131). Though NOX4 is predominant in the kidney, NOX-2 is primarily expressed on mesangial cells and podocytes, but their functional significance remains unclear (132). The NOX2 is primarily composed of several subunits mainly GP91 phox (membrane subunits) and P47 phox (cytosolic subunit) (130). When the proper signal stimulates NOX2 activation it leads to the alignment of the cytosolic subunit (p47phox) to the membrane subunit (gp91phox). Localized NOX2 is involved in superoxide generation and can lead to the increased burden of oxidative stress and kidney inflammation (133). NOX2 has also been shown to activate the TLR4 system which includes recruitment of TLR4 into lipid rafts and further receptor dimerization and activation in several inflammatory responses (126, 134). Previously, we and others have shown that NOX2, when stimulated by leptin, can generate peroxynitrite in different disease model such as intestinal inflammation or inflammatory bowel disease (IBD), liver inflammation in NASH, (124, 129, 135). Since evidence is scarce to explain the specific NOX2 mediator involved in TLR4 activation in the mesangial cell, we chose to investigate the role of peroxynitrite in NOX2 mediated TLR4 activation in kidney

inflammation. Recently, it has been shown that the highly reactive oxidant, peroxynitrite mediates glomerular lesion by JAK/STAT signaling pathway (136). In our previous studies, Leptin has been shown to stimulate epigenetic regulation and microRNA induction in experimental NASH (137). The Non-coding microRNA (miR) negatively regulates target protein by degrading mRNA (transcript degradation) and/or interfering in the process of protein translation. miR21 has been significantly upregulated in several inflammatory responses such as experimental NASH, hematopoietic cells, and allergic response (137-139). In both liver and kidney injury, miR21 plays a key role in fibroblast activation and is a prominent regulatory factor in Smad7/TGF-beta signaling (74, 140, 141). Considering these facts, in the present study, we hypothesize that increased circulatory leptin due to CYP2E1-induced oxidative stress in NAFLD activates mesangial cells and renal inflammatory response. Further leptin, acting via JAK/STAT-mediated NOX2 activation in the glomerulus induces miR21-mediated proinflammatory pathway that affects progression of kidney disease. This present study uses an established *in vivo* mouse model of CYP2E1-primed NASH, leptin knockout (KO) mice, p47 phox KO mice and miR21 KO mice along with kidney mesangial cells to show the mechanism of NOX2-initiated renal inflammation.

### **3.2 MATERIALS AND METHODS**

Bromodichloromethane (BDCM), a known substrate for CYP2E1-mediated oxidative stress in the liver and corn oil were purchased from Sigma-Aldrich (St. Louis, MO). Anti- $\alpha$ SMA, anti-IL1 $\beta$ , anti-TNF $\alpha$ , anti-TLR4, Anti-3-Nitrotyrosine (3NT), anti P47phox and anti GP91phox primary antibodies were purchased from Abcam (Cambridge, MA). Species-specific biotinylated conjugated secondary antibody and streptavidin -HRP were

purchased from Vectastain Elite ABC kit (Vector Laboratories, Burlingame, CA). Wild-type and gene-specific KO mice were purchased from The Jackson Laboratories (Bar Harbor, ME) and Taconic Farms Inc. (Hudson, New York). Fluorescence-conjugated (Alexa fluor) secondary antibodies and ProLong Gold antifade mounting media with DAPI were bought from Thermo Fisher Scientific (Waltham, MA) Animal diets were purchased from Research Diets (New Brunswick, NJ). All other chemicals were purchased from Sigma Aldrich unless otherwise specified. Paraffinized tissue sections on slides were done by IRF, University of South Carolina School of Medicine and AML laboratories (Baltimore, MD).

Cell culture: Kidney Mesangial cell line (CRL-1927) was purchased from ATCC (Manassas, VA) and maintained in Dulbecco's modified eagles medium, Corning (Tewksbury, MA). The media was supplemented with 10% fetal bovine serum, Atlanta Biologicals (Norcross, GA), 2mM glutamine, 100U/ml Penicillin, and 100ug/ml streptomycin; Gibco (Grand Island, NY) at 37°C in a humidified atmosphere of 5% CO<sub>2</sub>. Cells had been serum-starved (DMEM with 0.25% FBS) overnight before cell were given any treatment. The cells were then treated with Leptin 100ng/ml, Biovision (Milpitas, CA), mir21 inhibitor 20 µM (Qiagen, Valencia, CA), JAK-STAT inhibitor (Ruxolitinib) 10 µM (Invivogen, San Diego, CA), separately or in combination with Leptin and Apocynin 100 µM an inhibitor of NADPH oxidase activity. Phenyl Boronic Acid (FBA) 100 µM was used as a scavenger for Peroxynitrite. Spin trap DMPO 100 µM (5,5 dimethyl-1- Pyrroline N- oxide) (Alexis biochemical San Diego, CA) was used to scavenge free radicals via spin trapping. Cells were lysed in Trizol, Invitrogen (Grand Island, NY) for mRNA extraction or plated on coverslips MatTek Corp, (Ashland, MA) on each well of 6 well plates

maintaining the aforementioned conditions and the adhered cells on coverslips were used for immune-luorescence staining after completion of the treatment.

**Mouse Models:** All mice were housed one per cage at 23-24°C with a 12-h/12-h light/dark cycle with ab-libitum access to food and water. The mice had been treated in strict accordance with the NIH guideline for Humane Care and Use of Laboratory Animals and local IACUC standards. All experiments have been approved by the University of South Carolina at Columbia. Pathogen-free, adult male, C57BL/6J background mice were used as wild-type mice for nonalcoholic fatty liver disease (NAFLD) model. These mice and mice that contained the disrupted *ob/ob* gene (B6.V Lepob/J) (Jackson Laboratories) (Leptin KO), *miRNA21* gene (B6;129S6-Mir21atm1Yoli/J) and *P47phox* gene (alias *Ncf1*) (KO; B6.129S2-Ncf1tm1shl N14; Taconic, Cranbury, NJ) were fed a high fat diet (60% kcal) from 6 weeks until 16 weeks. After the completion of animal xperiments, mice of all study groups were sacrificed. Immediately after anesthesia, blood from the mice was drawn using cardiac puncture to collect serum for the experiments. The mice kidneys were removed right after terminal surgery and dissected out and were fixed by using 10% formalin.

**Induction of CYP2E1-mediated redox stress in underlying NAFLD:** We and others have shown previously that CYP2E1-mediated redox stress is a determining factor for progressive disease development in NAFLD. The high-fat diet fed wild-type mice (NAFLD model) and high-fat diet fed gene knockout mice at 16 weeks were administered BDCM (1mmol/kg, diluted in corn oil) via intraperitoneal route, twice a week for 4 weeks to estimate the effects of chronic CYP2E1-mediated redox stress. A group of high-fat diet fed mice (NAFLD) that had simple steatosis and were not injected with BDCM and served

as a non-redox primed control against high-fat diet fed wild-type mice injected with BDCM (NAFLD+BDCM).

**Immunohistochemistry:** The kidneys were collected from each mouse and fixed in 10% neutral buffered formalin (Sigma Aldrich, Missouri, USA) and paraffin embedded. These formalin-fixed, paraffin embedded tissues were cut in 5 $\mu$ m thick sections. These sections were deparaffinized using a standard protocol. Briefly, sections were put in xylene twice for 3 min, then with xylene:ethanol (1:1) for 3 minutes, and rehydrated via a series of ethanol (twice with 100%, 95%, 70%, 50%) 3 minutes each, twice with distilled water, and finally rinsed twice with PBS (Sigma-Aldrich). Epitope retrieval of the sections was completed using epitope retrieval solution and steamer (IHC-World, Woodstock, MD) for 45 minutes. 3% H<sub>2</sub>O<sub>2</sub> was used for 10 minutes to block the endogenous peroxidases. The primary antibodies like anti- $\alpha$ SMA, anti-IL1 $\beta$ , anti-TNF $\alpha$ , anti-TLR4 (Abcam, Cambridge, MA) were used overnight in recommended dilutions. Species-specific biotinylated conjugated secondary antibody and streptavidin conjugated with HRP were used to perform antigen-specific immunohistochemistry following manufacturer's protocols. 3,3' Diaminobenzidine (Sigma-Aldrich, St.Louis, MO) was used as a chromogenic substrate. Kidney sections were counter-stained with Mayer's hematoxylin (Sigma-Aldrich). Phosphate buffer saline was used for washing three times between the steps. Sections were finally mounted in Simpo mount (GBI Laboratories, Mukilteo, WA) and observed under a 20x and 60x objectives using an Olympus BX51 microscope (Olympus, America). Morphometric analysis was done using CellSens Software from Olympus America (Center Valley, PA).



**Immunofluorescence: For tissue:** Formalin-fixed, paraffin-embedded tissues sections were deparaffinized using a standard protocol. Epitope retrieval of the deparaffinized sections was completed using epitope retrieval solution and steamer (IHC-World, Woodstock, MD) following the manufacturer's instructions. The primary antibody 3NT (Abcam, Cambridge, MA) and anti-gp-91phox, anti-p47phox (purchased from Santa Cruz Biotechnology, Santa Cruz, CA) dual labeling were used at the recommended dilution. Species-specific anti-IgG secondary antibodies conjugated with Alexa Fluor 633 (Invitrogen, California, USA) was used against anti-3NT and anti-gp-91phox, and Alexa Fluor 488 (Invitrogen) was used against anti-P-47phox. The sections were mounted in a ProLong gold antifade reagent with DAPI (Life technologies, EU, OR). Lastly, images were taken under 40X objectives using Olympus BX51 microscope.

**Cultured cells:** After completion of the treatments of the aforementioned cell culture section, cells attached on coverslips were fixed with 10% neutral buffered saline. After the cells were washed with PBS containing 0.1% Triton X (Sigma), they were blocked with 3% BSA, 0.2% Tween (Fisher), 10% FBS in PBS. Cells were incubated with primary antibodies anti- $\beta$  Actin (Abcam) and anti-3NT (Abcam), for immunofluorescence dual-labeling staining, followed by species-specific Alexa Fluor 488 was used against anti-  $\beta$ -Actin and Alexa Fluor 633(described above) was used against anti- 3NT. The stained cells attached on the coverslips were mounted on slides with ProLong Gold antifade reagent with DAPI (Life Technologies) and viewed under 40X objectives with an Olympus BX51 microscope.

**Quantitative Real-Time Polymerase Chain Reaction:** Gene expression levels in kidney tissue samples and Mesangial cells were measured by two-step qRT-PCR. Total RNA was

isolated from kidney tissue and cells using TRIzol reagent (Invitrogen) according to the manufacturer's instructions and purified with the use of RNeasy mini columns (Qiagen, Valencia, CA). Purified RNA was converted to cDNA using iScript cDNA synthesis kit (Bio-Rad) following the manufacturer's standard protocol. qRT-PCR was performed with the gene-specific primers using SsoAdvanced SYBR Green Supermix (Bio-Rad) and CFX96 thermal cycler (Bio-Rad). Threshold Cycle (Ct) values for the selected genes were normalized against 18S (internal control) in the same sample. The relative fold change was calculated by the  $2^{-\Delta\Delta Ct}$  method. The sequences for the mouse-specific primers used for real-time PCR are provided in table-2.

Table 3.1: Table showing the primer sequences for the different targets used in this study.

Gene	Sense	Antisense
IL-1 $\beta$	CCTCGGCCAAGACAGGTC GC	TGCCCATCAGAGGCAAGGAGGA
TNF $\alpha$	CAACGCCCTCCTGGCCAAC G	TCGGGGCAGCCTTGTCCCTT
IFN $\gamma$	TGCGGGGTTGTATCTGGGG GT	GCGCTGGCCCGGAGTG TAG
$\alpha$ -SMA	GGAGAAGCCCAGCCAGTC GC	ACCATTGTCGCACACCAGGGC
CD4	CACACACCTGTGCAAGAA GC	GCGTCTTCCCTTGAGTGACA

CD8	GCCCTTCTGCTGTCCTTGA T	TAGTTGTAGCTTCCTGGCGG
FasL	GCAGCAGCCCATGAATTA CC	AGATGAAGTGGCACTGCTGTCT AC

miR21 expression levels in kidney tissues: Total miRNA was isolated from cells grown in a monolayer by homogenization in Qiazol reagent (Qiagen) following the manufacturer's instructions. The purification was done by using miRNeasy mini kit (Qiagen). Purified miRNA (1,000 ng) was converted to cDNA using miScript cDNA synthesis kit (Qiagen) following the manufacturer's protocol. qRT-PCR was performed with miRNA-21 specific primers (Qiagen) using miScript SYBR Green PCR master mix (Qiagen) and CFX96 thermal cycler (Bio-Rad). Ct values for the selected gene were normalized against RNU6-2 (internal miR expression control) values in the same sample.

**Western blot:** Western blot for serum leptin was performed by using the standard protocol as described by Seth et.al. 2017 (27913210). Briefly, 20 µg of denatured serum protein resolved on novex 4–12% bis-tris gradient gel. Resolved protein bands were transferred to nitrocellulose membrane using Trans-Blot Turbo transfer system. Further, blots were blocked with 5% non-fat milk solution for 1 h and then incubated with antileptin antibody for overnight at 4 °C. Species-specific anti-IgG secondary antibody conjugated with HRP was used to tag primary antibody. ECL western blotting substrate was used to develop the blot. Finally, the blot was imaged using G:Box Chemi XX6 and subjected to densitometry analysis using Image J software.

**Statistical Analyses:** The statistical analysis was completed by analysis of variance (ANOVA) followed by Bonferroni post-hoc correction for intergroup comparisons \*p<0.05 is considered statistically significant.

### 3.3 RESULTS:

#### **Increased circulatory leptin in NASH causes mesangial cell activation in Kidney.**

We have shown previously that NASH in an underlying condition of obesity causes an increase in hepatic CYP2E1 activity with concomitant free radical damage to lipids and proteins (128). The adipokine, leptin is mainly produced by adipocytes in obesity and poses inflammatory response in the liver. In CYP2E1 priming progressive NASH, BDCM (Bromodichloromethane, or xenobiotics) act as a second hit and causes liver injury and activation of Hepatic stellate cells (120, 35). Hepatocytes and Hepatic stellate cells produce endogenous leptin and further causes increase in circulatory leptin and leptin resistance (120, 39). Our results in this study also showed that serum leptin was significantly increased in BDCM exposed group (NAFLD+BDCM) as compared to NAFLD alone group (control) (Fig. 1A, B) (p<0.05). In a previously published study, it has been shown that circulatory leptin plays a significant role in CKD. To study the involvement of increased circulatory leptin in CYP2E1-primed NAFLD in progression of ectopic kidney disease; we tested the immunoreactivity and localization of  $\alpha$ -SMA, a mesangial cell activation marker. The results showed that there was a significant increase in  $\alpha$ -SMA immunoreactivity in glomerular lesions of the NAFLD+BDCM group as compared to NAFLD alone (Fig. 1C, D; P <0.05). Xenobiotic metabolism mediated Mesangial cell activation was completely diminished in Leptin KO groups (Fig. 1C, D; P <0.05). The results suggest that the increased circulatory leptin play a crucial role in mesangial cell activation and

inflammatory response in the kidney. Although we cannot rule out the involvement of another kidney cell types at this stage, it appeared that mesangial cell activation and proliferation is an extensive event in NAFLD associated renal disease.

### **Leptin causes NOX2 activation and increased peroxynitrite generation in kidney**

Though leptin involves in the regulation of food intake and energy metabolism hyperleptinemia found in obesity and NAFLD generates oxidative stress mediated by NADPH oxidase activation (142). The NADPH oxidase isoform 2 (NOX2) is one of the several isoforms of the gp91 phox catalytic subunit of NADPH oxidase (143). To see the activation of NADPH oxidase system dual-labeled (gp91 phox-Red and p47phox-green) immunofluorescence microscopy was carried out. The result showed that there was a significant increase in gp91 phox-p47phox co-localization (yellow) events in the glomerulus of BDCM exposed group as compared to NAFLD group alone (Fig.2A, B) ( $p < 0.05$ ). The leptin KO mice exposed to BDCM showed decreased co-localization of both subunits and suggested decreased NADPH oxidase activation in glomerulus in the absence of leptin. The activation of NADPH oxidase system is further associated with higher oxidative stress, as evident from the increased tyrosyl radical formation (3-nitrotyrosine immunoreactivity) in the glomerulus and other tubular structures (133, 119). Further, the results showed that the mice exposed with BDCM had significantly increased 3-nitrotyrosine immunoreactivity as compared to NAFLD group alone that was significantly decreased in p47phox KO mice fed with a high fat diet exposed to BDCM (Fig 2C, D) ( $p < 0.05$ ). The data suggest that higher leptin induced NOX2 assembly that was essential for activation of NADPH oxidase system and perpetuated nitrative stress generation in the kidney.

### **Leptin-NOX2 axis causes mesangial cell activation and renal inflammation.**

The role of NADPH oxidase has been demonstrated in several experimental models of renal injury such as Diabetic nephritis (144) a hHcys model of glomerulosclerosis (145). To study the role of leptin-induced activation of NADPH system complex and peroxynitrite generation in mesangial cell injury, mouse kidney tissue was evaluated for  $\alpha$ -Smooth Muscle Actin ( $\alpha$ -SMA) immunoreactivity by immunohistochemistry. The result showed that mesangial cell activation marker,  $\alpha$ -SMA was significantly increased in BDCM exposed N AFLD group as compared with NAFLD alone group (Fig. 3A, C)( $p < 0.05$ ). P47phox KO mice group exposed with BDCM showed significantly decreased immunoreactivity for  $\alpha$ -SMA (Fig. 3A, C)( $p < 0.05$ ). The data strongly suggested that mesangial cell activation was dependent on oxidative stress mediated by active NADPH oxidase assembly. The glomerular mesangial when activated imposes not only the thickening glomerular lining but also plays a crucial role in chronic renal inflammation (146). NADPH oxidase-mediated 3-nitrotyrosine has also been studied in several inflammatory diseases (124, 191, 147, 148). To study the role of NOX2 mediated renal inflammation in this study, qRTPCR, and immunoreactivity of TLR4 and inflammatory cytokines were carried out. Results showed that TLR4 expression was significantly increased in BDCM exposed NAFLD group (NAFLD+BDCM) as compared to NAFLD alone group, while the P47phox KO+BDCM group showed a significantly decreased TLR4 expression (Fig 3B,D,E) ( $p < 0.05$ ). The qRTPCR analysis of inflammatory cytokines and markers of proinflammatory T cell subtypes showed significantly increased expression of IL1 $\beta$ , IFN $\gamma$ , CD4, CD8 and TNF- $\alpha$  in BDCM exposed NAFLD kidney when compared with NAFLD alone while they were significantly decreased in P47phox KO mice group

exposed with BDCM (Fig 4A) ( $p < 0.05$ ). A similar data was also obtained in the glomerular regions where immunoreactivity of IL1 $\beta$  and TNF- $\alpha$  showed a significant increase in NAFLD mice exposed with BDCM (NAFLD+BDCM) and a parallel significant decrease in the P47phox+BDCM group (Fig 4B-D) ( $p < 0.05$ ). Results also showed a significantly increased migration of CD4+ T-cells (12 folds) in comparison to CD8+ T-Cells (2.5 folds) in a NAFLD+BDCM group of mice as compared to NAFLD alone and significantly decreased in P47phox KO+BDCM group suggesting a strong T cell inflammatory phenotype (Fig 4A) ( $p < 0.05$ ). The above data suggest that mesangial cell activation and inflammation in the kidney is dependent on activation of NADPH oxidase system.

### **Leptin-mediated increased peroxynitrite generation in mesangial cell is NOX2**

**dependent** To study the mechanism of Leptin-induced NOX2 activation and subsequent peroxynitrite generation in mesangial cells of the kidney, experiments were performed with mesangial cell culture primed with adipocytokine leptin. The immunofluorescence images (Red: 3-nitrotyrosine) of cultured mesangial cells showed that cells primed with leptin caused a significant increase in 3-nitrotyrosine immunoreactivity when compared with corresponding vehicle control (Fig 5A-B) ( $p < 0.05$ ). However, leptin primed mesangial cells co-treated with Apocynin (NADPH oxidase nonspecific inhibitor), or DMPO (free radical spin trap) or FBA (peroxynitrite scavenger) showed a significant decrease in 3-nitrotyrosine immunoreactivity as compared to leptin-treated cells alone (Fig 5A-B) ( $p < 0.05$ ). The results suggest that the leptin-mediated generation of 3 Nitrotyrosine in the mesangial cell was NOX2 and peroxynitrite dependent. Further to explore how leptin activates NOX2-induced peroxynitrite generation and tyrosyl radical formation, we used a JAK- STAT inhibitor to block leptin signaling. Results showed a significant decrease in 3-

nitrotyrosine immunoreactivity in JAK-STAT treated cells primed with leptin when compared to cells primed with leptin alone (Fig. 6A-B) ( $p < 0.05$ ). The data suggested that leptin activated NOX2 via a JAK-STAT pathway and ruled out an endogenous mesangial specific in situ activation independent of leptin.

### **Leptin-NOX2-peroxynitrite-axis causes miR21 upregulation and mesangial cell activation.**

We and others have shown that miR21 plays a crucial role in modulating inflammation in liver disease (137, 149). It has been demonstrated that the expression and function of miR21 is regulated by NADPH oxidase-dependent reactive oxygen species in prostate cancer (150). In Kidney, the miR21 expression is associated with renal fibrosis and inflammation (151). To study how leptin-mediated NOX2 induction and its downstream peroxynitrite caused miR21 upregulation, we used mesangial cell culture primed with leptin and co-treated with Apocynin or FBA or DMPO or a widely used JAK/STAT inhibitor. Results showed that miR21 expression in mesangial cells were significantly increased in leptin primed cells as compared to vehicle control group alone (Fig 7A) ( $p < 0.05$ ). Interestingly, miR21 expression was significantly decreased in leptin primed mesangial cells co-treated with NADPH oxidase inhibitor (Apocynin) or free radical scavenger (DMPO) or peroxynitrite scavenger (FBA) as compared to leptin primed mesangial cell alone (Fig 7A) ( $p < 0.05$ ). To confirm the role of leptin signaling in the increase of miR21 expression, we co-treated the leptin primed mesangial cells with JAK/STAT inhibitor. The results showed a significant decrease in miR21 expression as compared to leptin alone group (Fig 7A). The data suggested that upregulation of miR21 in the mesangial cell is dependent on the leptin-mediated NOX2 pathway and its



downstream signaling mediators. Further, to explore Leptin-NOX2-peroxynitrite axis induced miR21 as a key event in mesangial cell activation, we co-treated leptin primed mesangial cells with miR21 inhibitor or JAK/STAT inhibitor and tested for mesangial cell activation by qRT-PCR for  $\alpha$ -SMA, an activation marker. Results showed a significant decrease in  $\alpha$ -SMA mRNA expression in miR21 inhibitor or JAK/STAT inhibitor cotreated group as compared to Leptin primed mesangial cells (Fig. 7B, C)( $p < 0.05$ ). In parallel, to prove the results obtained from in vitro mesangial cell culture, BDCM was given intraperitoneally to miR21 KO – NAFLD mice. The in vivo results showed that miR21 KO mice have significantly decreased  $\alpha$ -SMA immunoreactivity as compared to a NAFLD+BDCM group of mice (Fig 7D, E) ( $p < 0.05$ ). Similarly, mRNA expression of  $\alpha$ SMA in miR21 KO treated with BDCM was significantly decreased as compared to NAFLD+BDCM mice or NAFLD mice alone (Fig. 7F) ( $p < 0.05$ ). Taken together, In vitro and in vivo results suggested that leptin-induced NOX2-peroxynitrite signaling causes mesangial cell activation via an increased expression of miR21.

**Leptin-NOX2-peroxynitrite-axis induced miR21 upregulation causes an inflammatory response in the kidney.**

MiR21 induction has been reported in several inflammatory diseases (137, 149). To study the role of elevated miR21 in the kidney due to NOX2 induced by leptin, we treated miR21 KO mice with BDCM and observed the inflammatory markers typical to glomerulonephritis and tubular disease. Results showed that the mRNA expression of pro-inflammatory cytokines IL-1 $\beta$ , TNF- $\alpha$  and IFN- $\gamma$  were significantly elevated in BDCM treated NAFLD mice (NAFLD+BDCM) as compared with NAFLD group alone (Fig. 8A) ( $p < 0.05$ ). However, miR21 gene deleted mice treated with BDCM (miR21 KO+BDCM)

showed a significant decrease in mRNA expression of these proinflammatory markers when compared with a NAFLD+BDCM group of mice (Fig. 8A) ( $p<0.05$ ). Also, the protein levels of IL-1 $\beta$  showed significantly increased IL-1 $\beta$  immunoreactivity in BDCM treated NAFLD mice (NAFLD+BDCM) as compared with NAFLD mice alone (Fig.8B, C) ( $p<0.05$ ). However, miR21 KO treated with BDCM showed significantly decreased IL-1 $\beta$  immunoreactivity as compared with a NAFLD+BDCM group of mice (Fig.8B, C) ( $p<0.05$ ). The results suggested that miR21 plays a crucial role in kidney inflammation especially related to glomerulonephritis.

### 3.4 DISCUSSION

There is mounting evidence in the clinics of a higher prevalence of chronic kidney diseases in patients with advance stages of NASH (152, 90). With NAFLD/NASH being considered a global pandemic, it is important that increased research emphasis be provided for understanding of the pathology and ectopic mediators of NAFLD/NASH. Our present report builds logically from our previous findings that showed a strong link to glomerular inflammation in murine models of NAFLD (117). We and others have shown that high circulatory leptin in NASH is proinflammatory and generates a high flux of reactive oxygen species generation primarily through the activation of NOX2 in the liver (119). In the present study we argued that high circulatory leptin that is a result of either leptin resistance or increased hepatic production of the protein might be a causal link to the inflammation observed in distal organ systems including the cardiac and renal organs. We found that NAFLD-induced high leptin was responsible for increased mesangial cell immunoreactivity for  $\alpha$ -SMA, a marker for its activation. Interestingly both acute and chronic kidney disease show increased activation of the mesangial cells that lead to

increased inflammation by release of proinflammatory cytokines and concomitant increase in TGF-beta signaling (117, 153). Results in the present study also showed that absence of leptin abrogated the mesangial cell activation while deletion of p47phox in mice produced the same result. The activation of NOX2 in mesangial cells responsible for oxidative stress was significantly high in mice that had advance form of NAFLD when primed with a CYP2E1 ligand, while the response was blunted in the absence of leptin. It appears from the data that higher circulatory leptin induced an ectopic NADPH oxidase activation in the distal mesangial cells. The NOX2 activation caused a significant increase in proinflammatory mediators like IL1 $\beta$ , TNF  $\alpha$  and IFN- $\gamma$  in addition to higher CD4 and CD8 expression suggesting an elicitation of a strong innate and adaptive immune response in the kidney. However, the use of whole body systemic knockouts for leptin and p47 phox, do not clearly support the cause that underlines the role of leptin and NOX2 in the kidney alone. Underlying adiposity that is a hallmark of the present model can also produce low lying systemic inflammation that can augment mesangial cell NOX2 activation. The use of kidney specific deletion of NOX2 might have answered the above limitation of the study. Interestingly our results using a mesangial cell line that is primed with identical concentrations of leptin that was found in the systemic circulation caused a similar NOX2 activation and tyrosine nitration suggesting that the lack of kidney specific knockout did not alter our interpretations of an endocrine role of leptin in NAFLD/NASH. Our in vitro results further showed that a higher NOX2 activation led to an increased peroxynitrite generation that was abrogated by the use of both DMPO, a spin trap and FBA, a specific peroxynitrite scavenger. The results suggested that higher NOX2 activation was able to produce sufficient localized peroxynitrite generation that has been found to initiate redox

signaling primarily through activation of the AKT pathway or rapidly nitrating enzymes like CPB1 thus rendering them inactive and allowing uninterrupted inflammation, though such an interpretation is speculative at this time (133). Since glomerular inflammation has been shown to be associated with a higher miR21 levels, a mediator of inflammation, we sought to study the role of NOX2-derived peroxynitrite in modulating the levels of miR21 (154). Results showed that peroxynitrite was instrumental in increasing miR21 levels in the mesangial cells since use of FBA decreased its levels. However, it remains to be seen whether peroxynitrite might have directly induced miR21 levels or it has done so by increasing TLR4 activation. The chances of the latter in the present model is more likely since use of p47phox KO mice decreased kidney TLR4 expression and use of FBA decreased TLR4 expression (data not shown) with a parallel decrease in miR21. We have shown previously that NOX2-derived peroxynitrite was instrumental in trafficking TLR4 to lipid rafts, an essential mechanistic event in TLR4 activation (124). Thus, increased TLR4 expression coupled with its activation might be a likely cause of increased miR21 levels in the mesangial cells. This result is supported by the fact that miR21 coupled with other miRs are induced by TLR4 dependent mechanisms (138).

Having observed an increase in miR21 levels in the mesangial cells primarily driven by leptin induced NOX2, we chose to study the effect of the inducible miR21 on the mesangial cell activation, release of proinflammatory mediators and glomerular inflammation. Results showed a significant increase in mesangial cell mediated expression of  $\alpha$ -SMA, that was inhibitable following the use of miR21 specific antagomir. Further, the data was supported by the corresponding use of miR21 KO mice that showed decreased mesangial cell activation and expression of proinflammatory mediators in the NAFLD-

Kidney tissue suggesting that the above cited miR was downstream of a NOX2-mediated peroxynitrite surge essentially caused by higher circulating leptin.

Thus, in summary the present study addresses a novel and timely issue of NAFLD-induced ectopic manifestation of kidney disease and underlines a mechanistic role of NOX2 induced redox signaling that can be a future basis for therapeutic intervention in such pathology. The above mechanism can also be used to understand the pathways that exist in other comorbidities of NAFLD such as cardiovascular and neuronal complications. Further, use of miR21 as a clinical biomarker for kidney complications in NAFLD can be strengthened by the observations of this study and use of miR21 antagomirs can be used as future therapeutic tools.

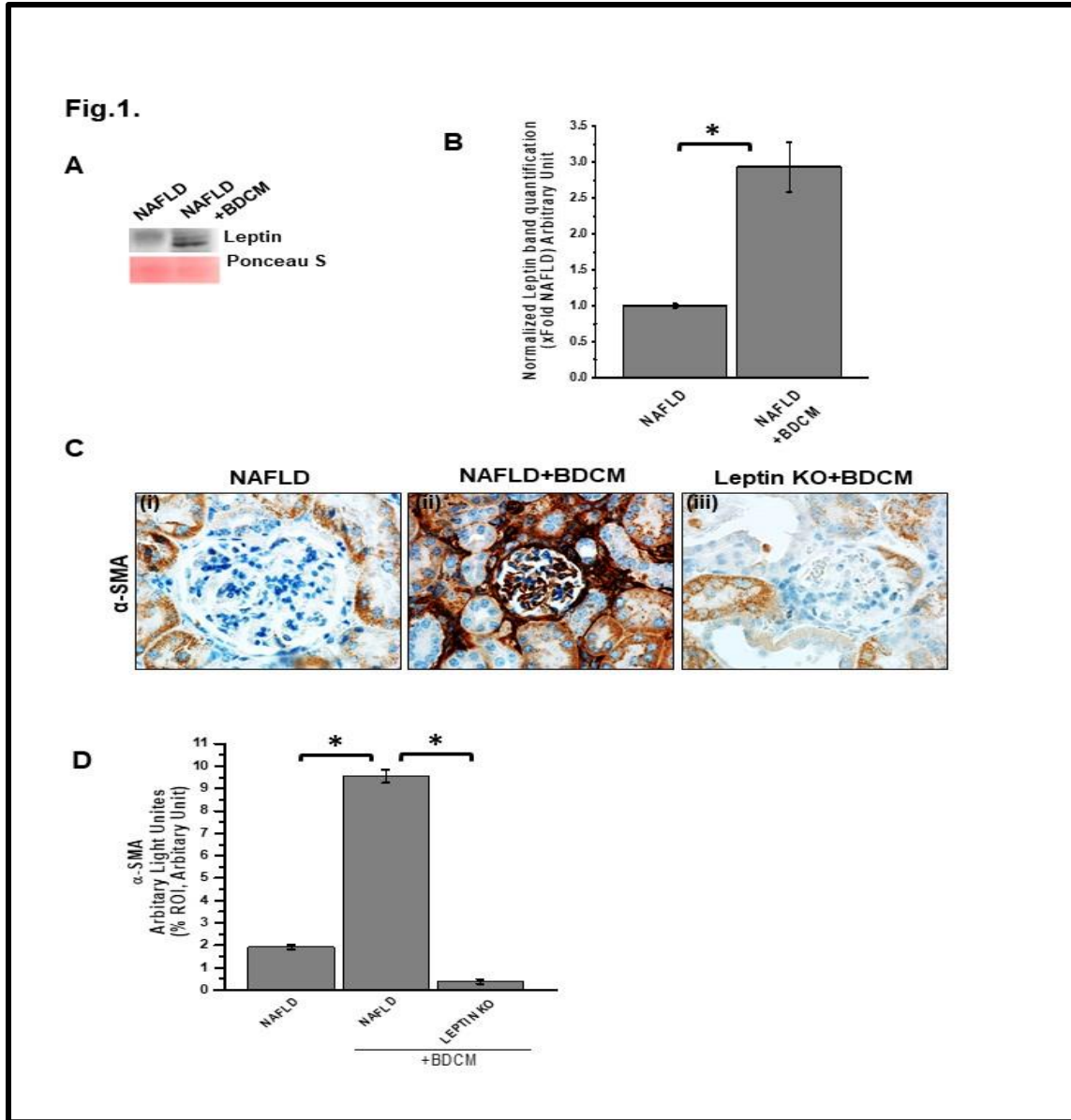


Figure 3.1 Increased circulatory leptin causes mesangial cell activation in the NAFLD-Kidney. **A.** Western blot analysis for serum leptin in NAFLD group and NAFLD group treated with BDCM. **B.** The morphometric analysis of the western blot normalized with ponceau S band. **C.** Immunoreactivity of alpha-smooth muscle actin ( $\alpha$ -SMA, a marker for mesangial cell activation) as shown by immunohistochemistry in kidney slices from mice fed with high fat diet (60% kcal fat) NAFLD serve as a control, NAFLD mice exposed to BDCM (NAFLD+BDCM), Leptin gene-deficient (Leptin KO) mice fed with high fat diet and exposed to BDCM. Images were taken at 60X. **D.** Morphometric analysis of  $\alpha$ -SMA immunoreactivity (mean data measured as arbitrary light units from three separate microscopic fields were plotted on y-axis) in NAFLD, NAFLD+BDCM, and Leptin KO+BDCM groups (\* $P < 0.05$ ).

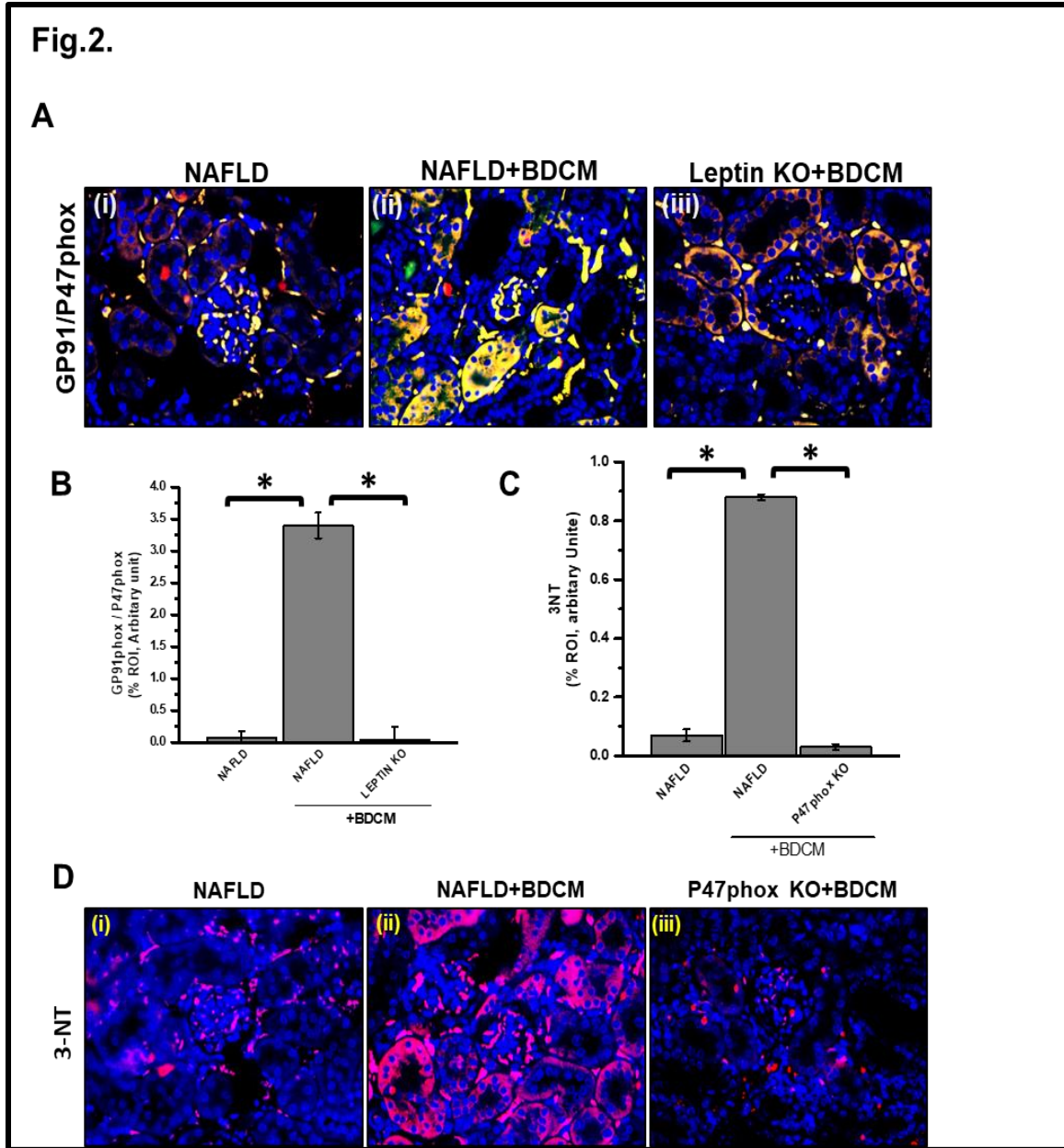


Figure 3.2 Leptin induces renal NOX2 activation and subsequent tyrosyl radical formation. A. Colocalization of GP91/ P47phox as shown by immunofluorescence imaging in kidney slices from mice fed with high- fat diet (NAFLD), NAFLD mice exposed to BDCM, and Leptin gene-deficient mice fed with high-fat diet and exposed to BDCM (Leptin KO + BDCM). B Immunoreactivity of 3-nitrotyrosine (3NT) as shown by immunofluorescence imaging in kidney slices from mice fed with high- fat diet (NAFLD), NAFLD mice exposed to BDCM, and P47phox gene-deficient mice fed with high-fat diet and exposed to BDCM (P47phox KO + BDCM). C Morphometric analysis of GP91/P47phox colocalized in NAFLD, NAFLD+BDCM, Leptin KO+BDCM group of mice. All immunofluorescent Images were taken at 40X and mean colocalization events were measured as arbitrary light units from three separate microscopic fields (plotted on y-axis)

(\*P<0.05). D Morphometric analysis of 3NT immunoreactivity in NAFLD, NAFLD+BDCM, P47phox KO+BDCM group of mice. Morphometric analysis was performed as mean data (immunoreactivity measured as arbitrary light units) from three separate microscopic fields (plotted on y-axis) (\*P<0.05).

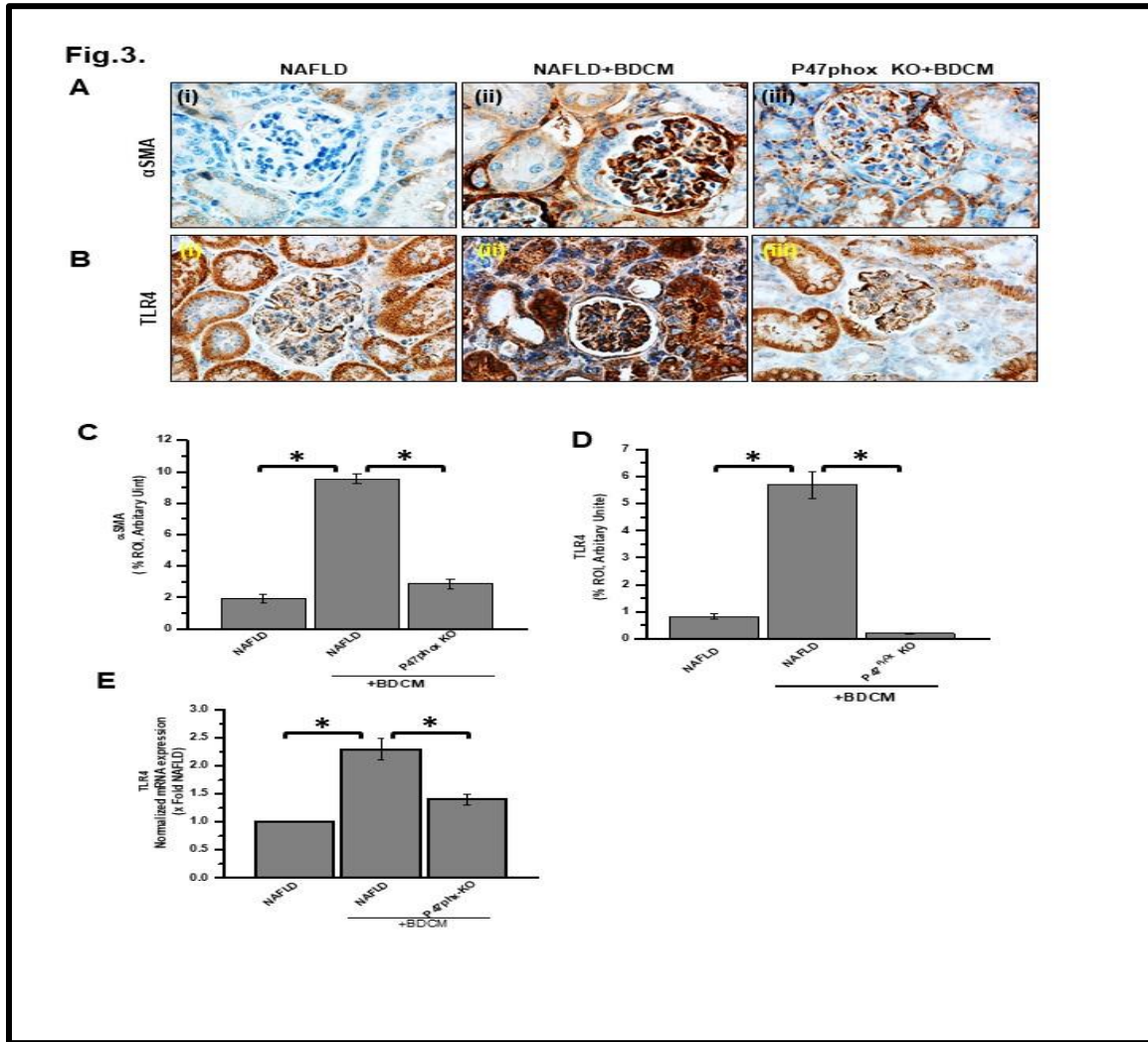


Figure 3.3 NOX2 activation leads to mesangial cell priming and increased TLR4 expression in the renal tissue. A and B Immunoreactivity of  $\alpha$ -SMA and TLR4 respectively as shown by immunohistochemistry in kidney slices from mice fed with high- fat diet (NAFLD), NAFLD mice exposed to BDCM, and P47phox gene-deficient mice fed with high-fat diet and exposed to BDCM (P47phox KO + BDCM). All immunohistochemistry Images were taken at 60X. C Morphometric analysis of  $\alpha$ -SMA immunoreactivity in NAFLD, NAFLD+BDCM, P47phox KO+BDCM group of mice. D Morphometric analysis of TLR4 immunoreactivity in NAFLD, NAFLD+BDCM, P47phox KO+BDCM group of mice. All morphometric analysis was carried out as mean data from three separate microscopic fields. (plotted on y-axis) in NAFLD, NAFLD+BDCM, P47phox KO+BDCM group of mice. E. mRNA expression of TLR4 gene in kidney tissue of NAFLD,



NAFLD+BDCM, P47phox KO+BDCM group of mice fed with high-fat diet. mRNA expression had been appraised by quantitative real-time PCR (qRT-PCR) and expressions were normalized against NAFLD group (\*P<0.05).

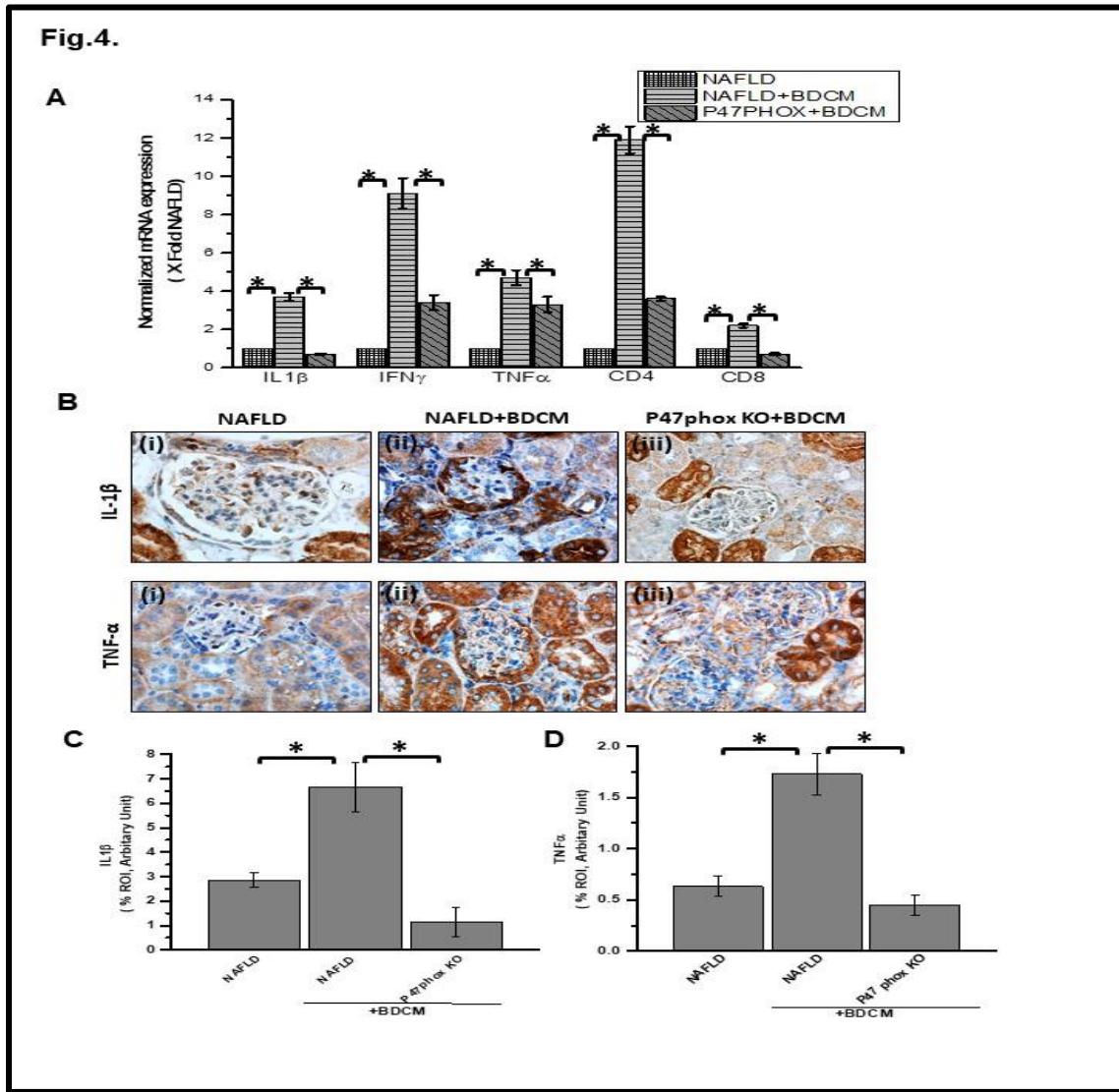


Figure 3.4 NOX2 activation leads to a surge of proinflammatory mediators in NAFLD-Kidney A. mRNA expression analysis of IL-1 $\beta$ , IFN- $\gamma$ , TNF- $\alpha$ , CD4, and CD8 genes in kidney tissue of NAFLD, NAFLD+BDCM, and P47phox KO mice fed with high-fat diet. All mRNA expression had been assessed by quantitative real-time PCR (qRT-PCR) and expressions were normalized against NAFLD group (\*P<0.05). B Kidney tissue slices were probed for IL-1 $\beta$  and TNF- $\alpha$  immunoreactivity in NAFLD group (serve as a control), NAFLD+BDCM, and P47phox mice group. C, D Morphometric analysis of IL-1 $\beta$  and TNF- $\alpha$  immunoreactivity as observed in the region of interest (ROI) (\*P<0.05).

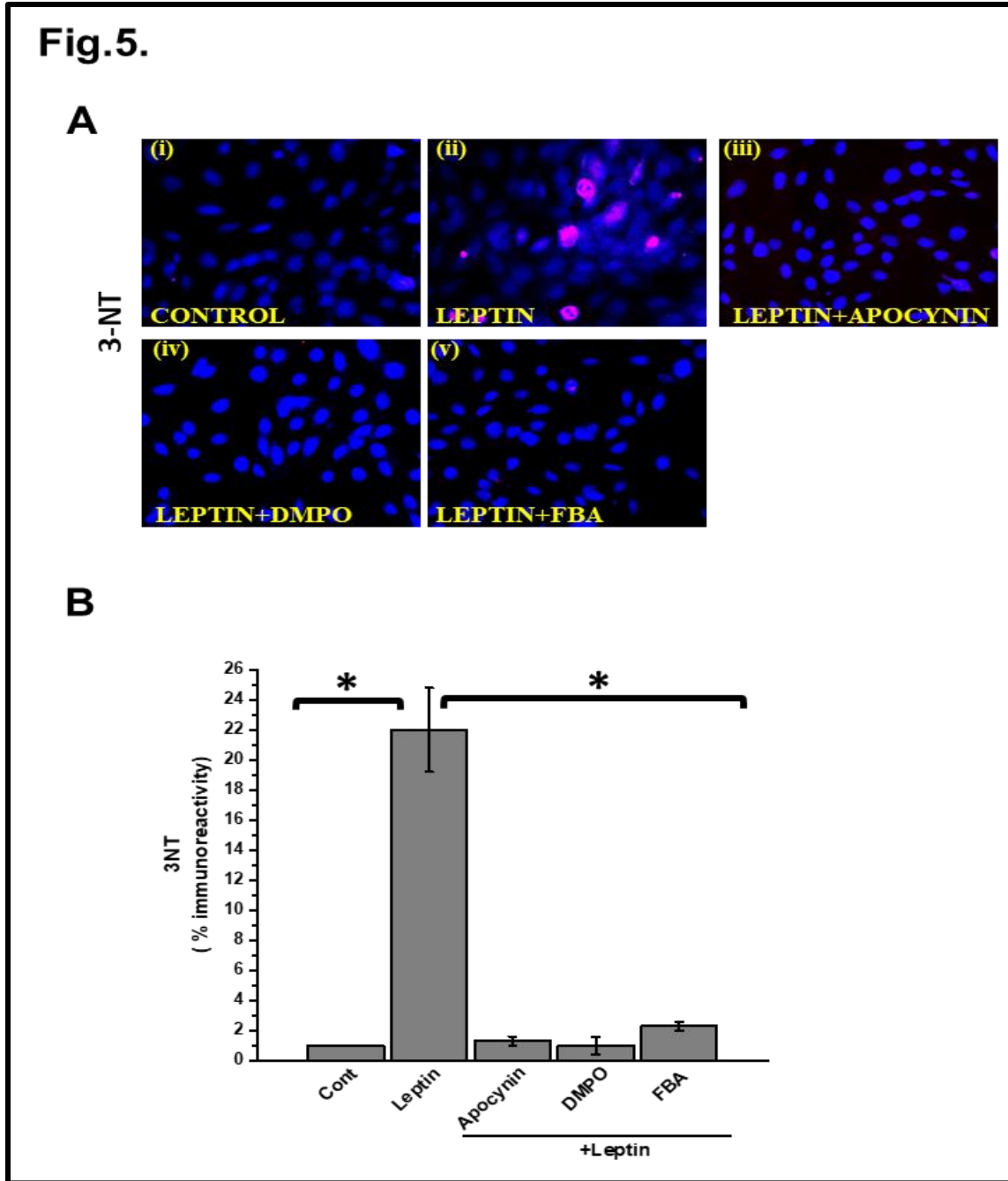


Figure 3.5 NOX2-derived peroxynitrite causes generation of tyrosyl radicals in mesangial cells. **A.** Immunoreactivity of 3NT as shown by Immunofluorescence microscopy in kidney mesangial cell line(CRL-1927). Mesangial cells were treated with media only served as control and other sets of Mesangial cells were treated with leptin, leptin+ Apocynin, leptin+ DMPO, leptin+ FBA. **B** Morphometric analysis of 3NT immunoreactivity in control, leptin, leptin+ Apocynin, leptin+ DMPO, leptin+ FBA groups of mesangial cells (\*P<0.05).

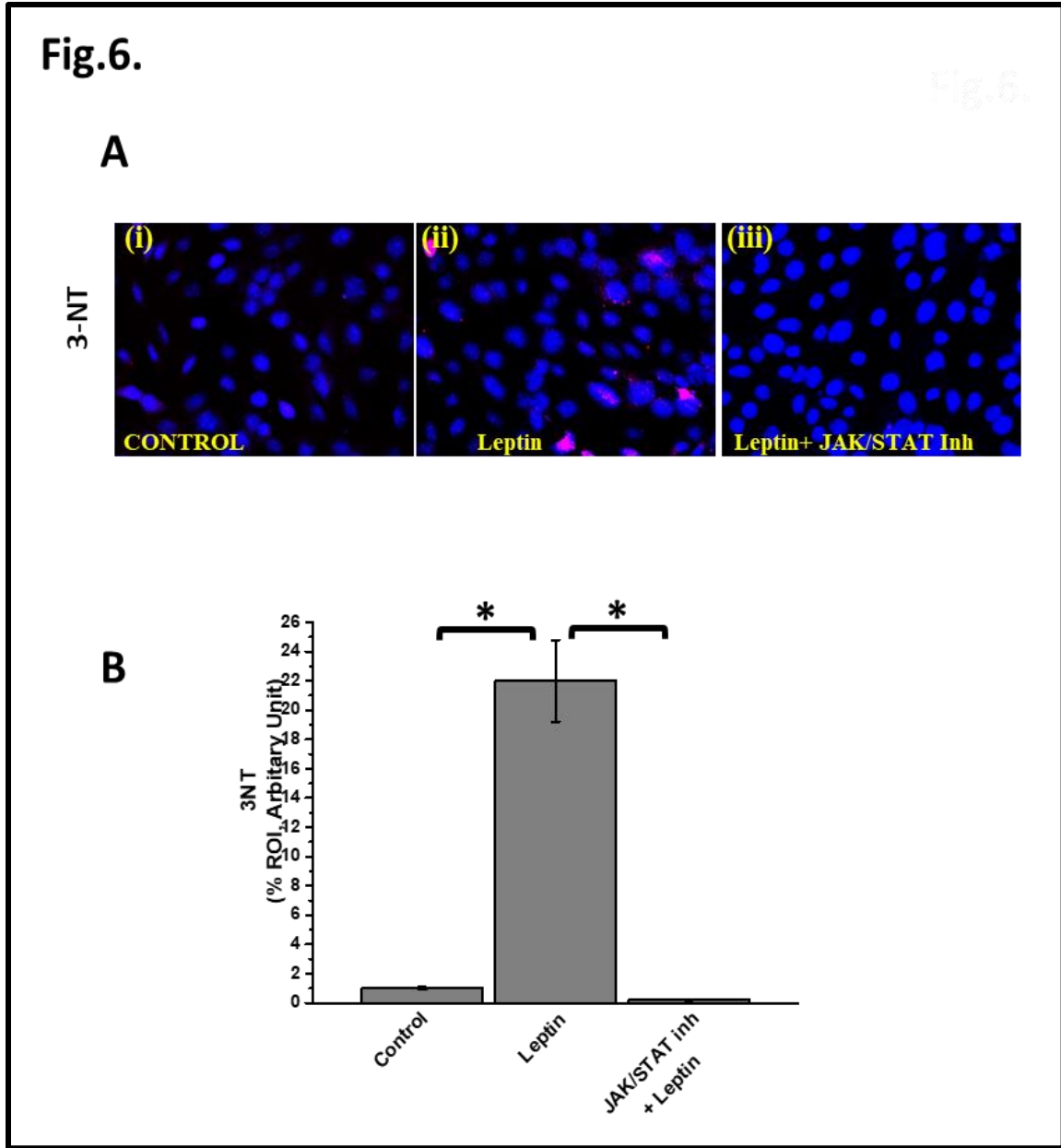


Figure 3.6 Leptin signaling in mesangial cells induce tyrosyl radicals that is peroxynitrite dependent **A**. Immunoreactivity of 3NT as shown by Immunofluorescence microscopy in control, leptin, leptin+ JAK/STAT inhibitor kidney mesangial cell line(CRL-1927) group. Nuclear staining was appeared by DAPI (blue) stain. 3NT immunoreactivity was functioned by Immunofluorescence microscopy after the protein had been labeled with the red fluorescent secondary antibody. Images were taken at 40X. **B** Morphologic analysis of 3NT immunoreactivity in control, leptin, leptin

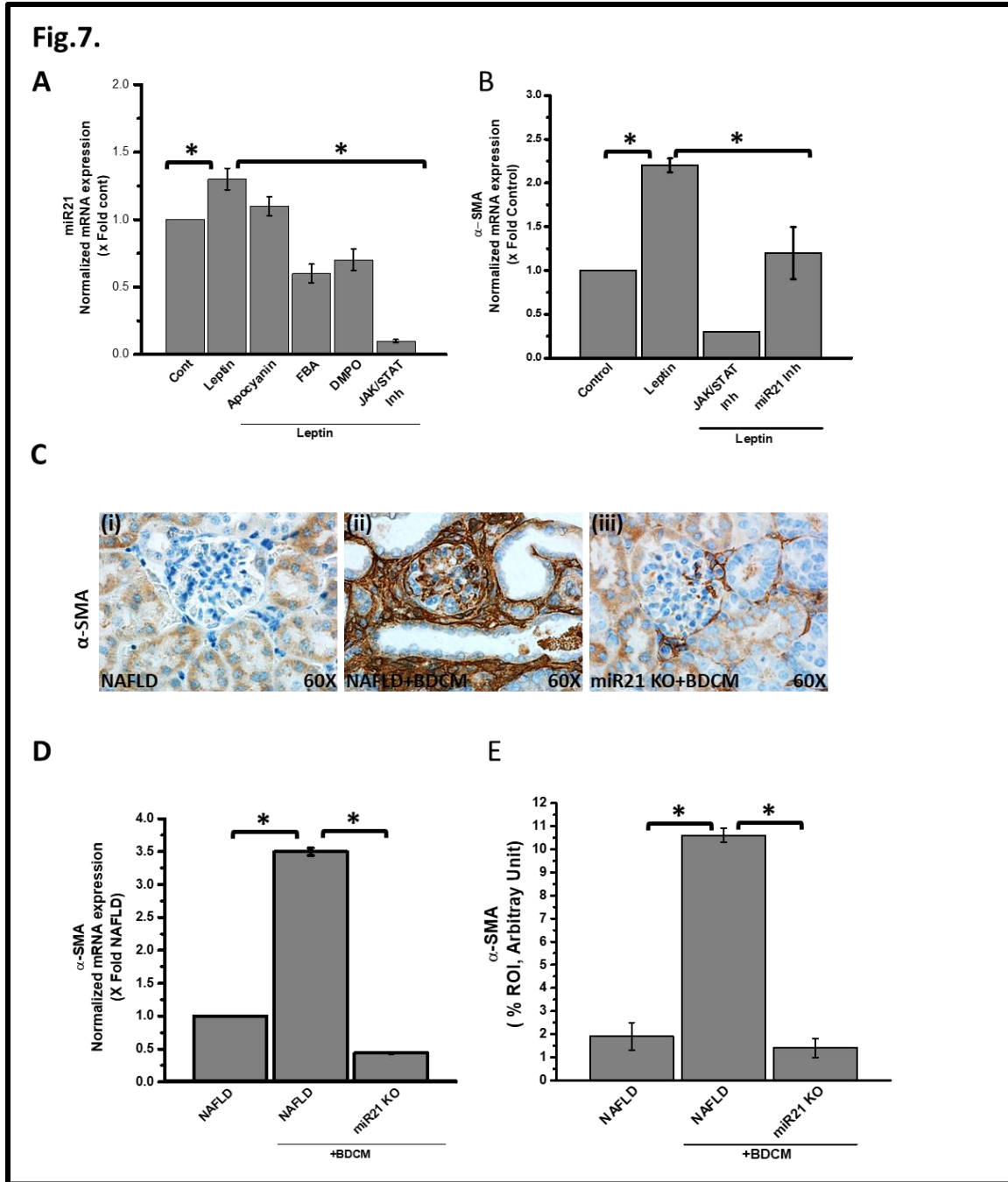


Figure 3.7 Leptin-NOX2-Peroxyntirite axis causes mesangial cell activation via miR21. A. mRNA expression analysis of miRNA 21 (miR21) gene expression in control (mesangial cells line (CRL-1927) treated with media only served as control), mesangial cells treated with leptin (leptin), mesangial cells groups were coexposed with leptin and Apocynin (leptin+ Apocynin), leptin and FBA (leptin+ FBA), leptin and DMPO (leptin+ DMPO), and leptin and JAK/ STAT inhibitor (Leptin+ JAK/STAT inh). miRNA expression had been assessed by quantitative real-time PCR (qRTPCR) and expressions were normalized against control (\*P<0.05). B. mRNA expression analysis of alphaSMA genes in kidney

mesangial cells of control, Leptin, Leptin+ miRNA 21 inhibitor (miR21 inhibitor). mRNA expression has been assessed by quantitative real-time PCR (qRT-PCR) and expressions were normalized against mesangial cell control (\*P<0.05). C Immunoreactivity of  $\alpha$ -SMA as observed by immunohistochemistry in kidney slices from (NAFLD), NAFLD mice exposed to BDCM, and miRNA21 gene-deficient mice fed with high-fat diet and exposed to BDCM (miR21 KO + BDCM). All immunohistochemistry Images were taken at 60X. D Morphometric analysis of  $\alpha$ -SMA immunoreactivity in NAFLD, NAFLD+BDCM, miR21 KO+BDCM group of mice. All morphometric analysis was performed as mean data from three separate microscopic fields (designed on y-axis) in NAFLD, NAFLD+BDCM, miR21 KO+BDCM group of mice(\*P<0.05). E. mRNA expression analysis of  $\alpha$ -SMA gene in kidney tissue of NAFLD, NAFLD+BDCM, and miR21 KO+BDCM mice. mRNA expression has been assessed by qRT-PCR and was normalized against NAFLD group (\*P<0.05).

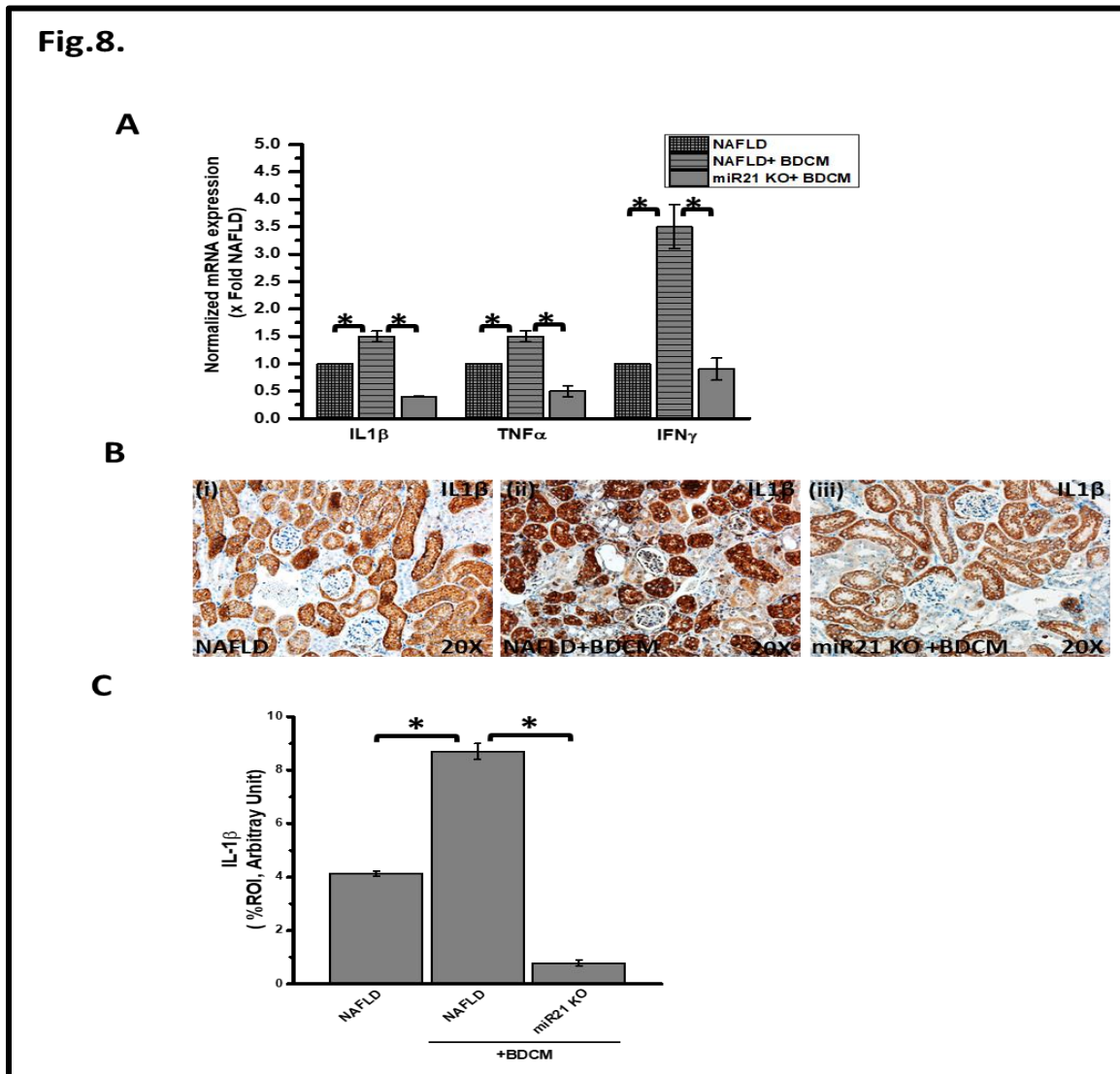


Figure 3.8 miR21 increase causes kidney inflammation. A mRNA expression of IL-1 $\beta$ , TNF $\alpha$ , and IFN $\gamma$  in kidney tissue from mice fed with high-fat diet NAFLD serve as a control, NAFLD mice exposed to BDCM (NAFLD+BDCM), miRNA 21 gene-deficient mice exposed to BDCM (miR21 KO+BDCM) as assessed by quantitative real-time PCR, the expressions were normalized with 18S and compared to the NAFLD group(\*P<0.05). B Immunoreactivity of IL-1 $\beta$  as shown by immunohistochemistry in kidney slices from. of NAFLD, NAFLD+BDCM, and miR21 KO+BDCM group of mice Images were taken at 20X. C Morphometric analysis of IL-1 $\beta$  immunoreactivity in NAFLD, NAFLD+BDCM, and miR21 KO+BDCM group of mice(\*P<0.05).

## CHAPTER 4

# **MICROCYSTIN EXPOSURE MODULATES NOX-2-MIR21 AXIS IN ECTOPIC GLOMERULAR TOXICITY IN UNDERLYING NONALCOHOLIC FATTY LIVER DISEASE (NAFLD)**

---

Alhasson F, Chandrashekar V, Dattaroy D, Seth R, Albadrani M, Scott GI,  
Raychowdhury S, Nagarkatti M, Nagarkatti P, and Chatterjee S. To be submit to Journal  
of Redox Biology.

To whom correspondence should be addressed:

\*Dr. Saurabh Chatterjee, Ph.D. Environmental Health and Disease Laboratory,  
Department of Environmental Health Sciences, University of South Carolina, Columbia  
29208 USA. Email: [schatt@mailbox.sc.edu](mailto:schatt@mailbox.sc.edu); Tel: 803-777-8120; Fax: 803-777-3391

**Key Words:** Leptin, NOX-2, NADPH, Mesangial Cells, miR21, Oxidative stress,  
NAFLD, JAK/STAT

**ACKNOWLEDGMENTS:** The authors gratefully acknowledge the technical services of Benny Davidson at the IRF, University of South Carolina School of Medicine and AML Labs (Baltimore MD). We also thank the Instrumentation resource facility (IRF) at the University of South Carolina for equipment usage and consulting services.

### **Abstract**

NAFLD often results in cardiovascular, intestinal and renal complications. Previous reports from our laboratory exhibited NAFLD induced ectopic inflammatory manifestations in the kidney that gave rise to glomerular inflammation. Extending our studies, we hypothesized that existing inflammatory conditions in NAFLD could make the kidneys more susceptible to environmental toxins. Our results showed that exposure of Microcystin-LR (MC) in NAFLD mice caused a significant increase in mesangial cell activation as evidenced by increased  $\alpha$ -SMA in the extracellular matrix surrounding the glomeruli. Renal tissue surrounding the glomeruli also had increased NOX2 activation as shown by increased co-localization of p47 Phox and its membrane component gp91 that. To show whether NOX2 activation and subsequent NOX2-miR21 axis were key to microcystin exposure and exacerbation of renal toxicity, experiments were designed in vitro with immortalized



mesangial cells of mouse origin. The cells incubated with (a) apocynin and (b) nitron spin trap DMPO and (c) miR21 inhibitor showed significantly decreased  $\alpha$ -SMA, miR21 levels and proinflammatory cytokine release in the supernatant. In parallel, mice lacking miR21, a proinflammatory miR, known to be activated by NOX2, when exposed to MC in NAFLD showed decreased mesangial cell activation. Mechanistically, phenyl boronic acid incubated cells that are exposed to MC showed significantly decreased mesangial cell activation showing that peroxynitrite might be the major reactive species involved in mediation the activation process, release of proinflammatory micro RNAs and cytokines that are crucial for renal toxicity. Thus, in conclusion, MC exposure causes NOX2 activation that leads to mesangial cell activation and toxicity via release of peroxynitrite and miR21.

#### **4.1 INTRODUCTION:**

Cyanobacteria are prokaryotic organisms found in fresh and brackish water throughout the world. It is growing fast under special water climates with certain water nutrients like nitrogen and phosphorus to govern phytoplankton which results in cyanobacteria blooms (155). Each type of cyanobacteria produces a specific toxin which releases after cyanobacteria death (156). Among all cyanotoxins, the microcystin is a very common cyanotoxin, which is widely dispersed throughout aquatic world. The microcystin family, has almost 90 isoforms, consists of heptapeptide ( $\beta$ -amino acid(ADDA), alanine (D-ala), D- $\beta$ -methyl-isoaspartate(D- $\beta$ -Me-isoAsp), and glutamic acid (D-glu)) (157). Microcystin-LR is one of most potent toxins which releases from cyanobacteria and causes different pathological conditions (158). Chronic low dosage of microcystin-LR exposure through different routes, like drinking contaminated water, direct skin contact, or by

inhalation can cause human health problems (159). Although the liver is a primary target for microcystin, different organs can be impacted such as the kidneys and the gut (159,160). Therefore, microcystin exposure links with various diseases like hepatic inflammation, gastroenteritis, and liver and colon cancers (160,161,162). Inhibition of serine/threonine protein phosphatases, especially protein phosphatase 1 (PP1) and protein phosphatase 2- A (PP2A), is the most common pathway of microcystin activity inside cells (163,164,165). Nong *et al* found that microcystin-LR exposure caused reactive oxygen series (ROS) generation through cytochrome P 450 enzyme especially CyP2E1 subunit. Thereby, lipid peroxidation, oxidative stress, and mitochondrial dysfunction can be mediated by microcystin-LR exposure (166).

Obesity is one of the most public health problems in the world, particularly in developed countries because of its prevalence. The consequences of obesity include premature death, disabilities, and a high cost of health care (167). Obesity has several medical complications, which include cardiac diseases, hypertension, and liver abnormalities such as Nonalcoholic fatty liver disease (NAFLD) (168). NAFLD is a wide spectrum phenomenon including a simple form called nonalcoholic fatty liver which characterized by extra fat accumulation without cell damage, and a second form is more progress one called Nonalcoholic steatohepatitis which is characterized by high level of inflammation and cell abnormalities (8,169). Oxidative stress-cytochrome P 450 pathway plays a critical role in augmented NAFL to NASH through mediation of lipid peroxidation and NADPH oxidase activation, which lead in turn to the release of proinflammation cytokines which cause hepatic and extrahepatic cell damage (170). We have previously demonstrated that progressing NASH can cause ectopic glomerulonephritis via mesangial

cells activation (171). In-Vitro mesangial cell activation has been shown high expression of alpha smooth muscle actin ( $\alpha$ SMA) and transforming growth factor- $\beta$  (TGF- $\beta$ ) after treated with 4HNE a marker of lipid peroxidation while mesangial cell proliferation can be attenuated via cytochrome P 450 inhibition by using diallyl sulphide (DAS) (171).

NADPH oxidase is a primary source of reactive oxygen series (ROS) generation. NOX2 has been shown highly expressed in different types of cells including mesangial cells, smooth muscle cells, in addition to macrophages (62). NOX2 expression causes several renal diseases and disfunctions, like ischemia-reperfusion injury (IRI) and diabetic nephropathy (62,172). NOX2 knock out mice showed less reactivity of  $\alpha$ SMA, HNE, picrosirius, and  $\alpha$ SMA – SMAD2 pathway comparing with wildtype mice suffered from IRI in different time points. which suggested that NOX2 associated with oxidative stress released and fibrogenesis activity (173, 174).

MicroRNAs (miRNAs) are small noncoded mRNAs that play a significant role in regulating gene expression during post-transcription. Among all miRNAs, mir21 shows partakes in nephritis and renal fibrosis (155). In the kidney, TGFb – SMAD2/3 signaling pathway upregulates miR21, whilst miR21 can inhibit SMAD7 and P10 causing high expression of TGF-b signaling. Therefore, miR21 and TGF-b are a key for renal fibrosis. (156) The present study examined the hypothesis that microcystin exposure increases NAFLD severity causing renal damage and glomerulonephritis through mesangial cell activation. Mechanistically, our result from in vivo and invitro showed microcystin toxin activated mesangial cell NOX2 mediated miR21 upregulation, resulting in fibrogenesis markers releasing and proinflammatory cytokines releasing induce renal nephrotoxicity.

## 4.2 MATERIAL AND METHODS:

Microcystin-LR was purchased from Cayman (Ann Arbor, MI). Leptin was purchased from BioVision (Milpitas, CA). Anti-3 nitrotyrosine (3NT), anti-TGF- $\beta$ , anti- GP91 phox, anti-P47phox, and anti- $\alpha$ SMA primary antibodies were purchased from Abcam (Cambridge, MA). Species-specific biotinylated conjugated secondary antibody and streptavidin-horseradish peroxidase were purchased from Vector Laboratories (Vectastain Elite ABC kit, Burlingame, CA). Fluorescence conjugated (Alexa fluor) secondary antibodies and ProLong Gold antifade mounting media with DAPI were bought from Thermo Fisher Scientific (Waltham, MA). Wild-type and gene-specific knockout (KO) mice were purchased from The Jackson Laboratories (Bar Harbor, ME). Animal diets were purchased from Research Diets (New Brunswick, NJ). All other chemicals were of analytic grade and were purchased from Sigma-Aldrich unless otherwise specified. Paraffinized tissue sections on slides were done by the Instrumentation Resource Facility of the University of South Carolina School of Medicine and AML Laboratories (Baltimore, MD).

**Animal Model:** Pathogen-free, adult, male mice with C57BL/6J background (Jackson Laboratories, Bar Harbor, ME) were used in the study. They were fed with a methionine and choline deficient (MCD) diet, (Research diets, New Brunswick, NJ) for 8 weeks and used as a model of nonalcoholic fatty liver disease (NAFLD). Mice kept on normal chow diet was used as a lean model. Mice that contained the disrupted P47phox gene (B6(cg)-Ncf1M1J/J(JAC004742) and disrupted miR21 gene (B6.129S6-Mir21tm1 Yoli/J) (Jackson Laboratories, Bar Harbor, ME) were fed a methionine and choline deficient (MCD) and treated identically to the NAFLD mouse model. All mice were housed with 1 mouse/cage

at 23–24°C on a 12:12-h light-dark cycle with libitum access to food and water. All animals were treated in strict accordance with the NIH Guide for the Humane Care and Use of Laboratory Animals, and the experiments were approved by the institutional review board at the University of South Carolina at Columbia.

**Toxin model:** Normal chow diet wild-type mice, methionine and choline deficient (MCD) wild-type mice, and MCD fed gene KO mice (P47phox, miR21) were administered microcystin-LR (10 µg/kg/day) intraperitoneally for five times a week for two weeks to assess the effects of chronic exposure to MC-LR. A set of MCD-fed mice (NAFLD model) were not injected with MC-LR and served as controls in this study.

**Cell culture:** Kidney Mesangial cell line (CRL-1927) was purchased from ATCC (Manassas, VA) and maintained in Dulbeccos modified eagles medium, Corning (Tewksbury, MA). The media was supplemented with 10% fetal bovine serum, Atlanta biologicals (Norcross, GA), 2mM glutamine, 100U/ml Penicillin, and 100ug/ml streptomycin; Gibco (Grand Island, NY) at 37°C in a humidified atmosphere of 5% CO<sub>2</sub>. Cells were serum starved (DMEM with 0.25% FBS) overnight before cell were given any treatment. A set of cells were treated with leptin 100ng/ml, Biovision (Milpitas, CA), another group were treated with MC-LR (20µM) separately or combination with leptin. Other groups of cells were then treated with leptin and MC-LR and were incubated with Apocynin (Sigma-Aldrich) 100 µM an inhibitor of NADPH oxidase activity and thus preventing production of superoxide, Phenyl Boronic Acid (FBA) 100 µM was used as a scavenger for Peroxynitrite, 100 mM the spin trap 3-[[2-(Biotinamido)ethyl] dithio] propionic Acid 4'-(Hydroxymethyl)DMPO ( Alexis biochemical, San Diego, CA), miR21 inhibitor Qiagen ( Valencia, CA). The cells were then lysed in Trizol, Invitrogen (Grand

Island, NY) for mRNA extraction or plated on coverslips MatTek Corp, (Ashland, MA) were used for immune-fluorescence staining after completion of the treatment.

**Hematoxylin and eosin staining (H&E)** Formalin-fixed tissues were paraffin embedded. Liver tissue sections were stained with hematoxylin and eosin by the Instrumentation Resource Facility, University of South Carolina School of Medicine.

**Immunohistochemistry** The kidneys were collected from each animal and fixed in 10% neutral buffered formalin (Sigma Aldrich, Missouri, USA). These formalin-fixed, paraffin embedded tissues were cut in 5 $\mu$ m thick sections. These sections were deparaffinized using a standard protocol. Briefly, sections were incubated with xylene twice for 3 min, washed with xylene: ethanol (1:1) for 3 min, and rehydrated through a series of ethanol (twice with 100%, 95%, 70%, 50%), twice with distilled water, and finally rinsed twice with PBS (Sigma-Aldrich). Epitope retrieval of the deparaffinized sections was performed using epitope retrieval solution and steamer (IHC-World, Woodstock, MD) for 45 minutes. 3% H<sub>2</sub>O<sub>2</sub> was used for 5 minutes to block the endogenous peroxidases. The primary antibody for TGF- $\beta$  (Abcam, Cambridge, MA) were used overnight in recommended dilutions. Species specific biotinylated conjugated secondary antibody and streptavidin conjugated with HRP were used to perform antigen-specific immunohistochemistry following manufacturer's protocols. 3, 3' Diaminobenzidine (Sigma-Aldrich, St.Louis, MO) was used as a chromogenic substrate. Tissue sections were counter-stained with Mayer's hematoxylin (Sigma-Aldrich). Phosphate buffer saline was used for washing three times between the steps. Sections were finally mounted in Simpo mount (GBI Laboratories, Mukilteo, WA) and observed under a 20x and 60x objectives using an Olympus BX51

microscope (Olympus, America). Morphometric analysis was done using CellSens Software from Olympus America (Center Valley, PA).

**Immunofluorescent:** *IN VIVO*, formalin-fixed, paraffin-embedded tissue sections were subjected to deparaffinization according to standard instructions. Epitope retrieval of the deparaffinized sections was done with an epitope retrieval solution and steamer (IHC World) according to the manufacturer's protocol. The primary antibodies anti- $\alpha$ -SMA, anti-gp-91phox, anti-p47phox, and anti-3NT (purchased from Santa Cruz Biotechnology, Santa Cruz, CA, and Abcam) and used at recommended dilutions. Species-specific anti-IgG secondary antibodies conjugated with Alexa Fluor 488 (Invitrogen) were used. The sections were mounted in a ProLong Gold antifade reagent with DAPI (Life Technologies, Carlsbad, CA). Images were taken under  $\times 20$  and  $\times 60$  oil objectives with an Olympus BX51 microscope.

*IN VITRO*, after completion of the treatments under serum-starved conditions as in Cell Culture, cells attached on coverslips were fixed with 10% neutral buffered saline. After the cells were washed with PBS containing 0.1% Triton X (Sigma), they were blocked with 3% BSA, 0.2% Tween (Fisher), 10% FBS in PBS. Cells were incubated with primary antibodies anti- $\alpha$ -SMA, anti-3NT Abcam), followed by species-specific Alexa Fluor 633 and 488. The stained cells attached on the coverslips were mounted on slides with ProLong Gold antifade reagent with DAPI (Life Technologies) and viewed under  $\times 40$  objectives with an Olympus BX51 microscope.

**Quantitative Real-Time Polymerase Chain Reaction** Gene expression levels in kidney tissue samples were grown in a monolayer by homogenization were measured by two-step qRT-PCR. Total RNA was isolated from kidney tissue in TRIzol reagent (Invitrogen)

according to the manufacturer's instructions and purified with the use of RNeasy mini kit columns (Qiagen, Valencia, CA). Purified RNA was converted to cDNA using iScript cDNA synthesis kit (Bio-Rad) following the manufacturer's standard protocol. qRT-PCR was performed with the gene-specific primers using SsoAdvanced SYBR Green supermix (Bio-Rad) and CFX96 thermal cycler (Bio-Rad). Threshold Cycle (Ct) values for the selected genes were normalized against 18S (internal control) values in the same sample. The relative fold change was calculated by the  $2^{-\Delta\Delta Ct}$  method. The sequences for the mouse specific primers used for real time PCR are provided in (table 1). Total miRNA was isolated from cells grown in a monolayer by homogenization in Qiazol reagent (Qiagen) following the manufacturer's instructions. The purification was done by using miRNeasy mini kit columns (Qiagen). Purified miRNA (1,000 ng) was converted to cDNA using miScript cDNA synthesis kit (Qiagen) following the manufacturer's protocol. qRT-PCR was performed with miRNA-specific primers (Qiagen) using miScript SYBR Green PCR master mix (Qiagen) and CFX96 thermal cycler (Bio-Rad). Ct values for the selected gene were normalized against RNU6-2 (internal miR expression control) values in the same sample.

**Table 4.1** Table showing the primer sequences for the different targets genes.

Target	Species	Sequence 5'-3'
MCP-1 F	<i>Mus musculus</i>	GTAGCAGCAGGTGAGTGGGGC
MCP-1 R	<i>Mus musculus</i>	CACAGTTGCCGGCTGGAGCAT
IL-1 $\beta$ F	<i>Mus musculus</i>	CCTCGGCCAAGACAGGTCGC
IL-1 $\beta$ R	<i>Mus musculus</i>	TGCCCATCAGAGGCAAGGAGGA
18SF	<i>Mus musculus</i>	TTCGAACGTCTGCCCTATCAA
18SR	<i>Mus musculus</i>	ATGGTAGGCACGGCGATA
CD68F	<i>Mus musculus</i>	GCTACATGGCGGTGGAGTACAA



CD68R	<i>Mus musculus</i>	ATGATGAGAGGCAGCAAGATGG
-------	---------------------	------------------------

**Western blot** SDS PAGE-Resolved protein bands were transferred to nitrocellulose membrane using precut nitrocellulose/filter paper sandwiches (Bio-Rad Laboratories, Hercules, CA) and Trans-Blot Turbo transfer system (Bio-Rad) in case of low molecular weight proteins and using wet transfer module from Invitrogen for high molecular weight proteins. Primary antibodies (Abcam) were used at recommended dilutions, and compatible horseradish peroxidase-conjugated secondary antibodies were used. Pierce ECL Western Blotting substrate (Thermo Fisher Scientific, Rockford, IL) was used for detection. The blot was imaged using G:Box Chemi XX6 (Syngene imaging systems) and subjected to densitometry analysis using Image J.

**TUNEL assay** Mesangial cells adhered on coverslips were used for a TUNEL assay using an Apoptag Fluorescein in Situ Apoptosis Detection Kit (Millipore, Temecula, CA) following the manufacturer's protocol. The cells were counterstained with propidium iodide in antifade reagent (Millipore). Stained sections were imaged at magnification of  $\times 40$  using the Olympus BX51 microscope.

**Statistical analysis** All in-vivo experiments were repeated three times with 5 mice per group (N=5; data from each group of mice was pooled). The statistical analysis was implemented by analysis of variance (ANOVA) followed by the Bonferroni post hoc correction for intergroup comparisons. Quantitative data from western blots as portrayed by the relative intensity of the bands were analyzed by performing a student's *t*-test.

### **4.3 RESULT:**

#### **Microcystin-LR exposure causes glomerular immune cellular infiltrations and glomerular damage in present of NAFLD.**

Sub-chronic dose of microcystin-LR can cause glomerular damages and infiltration of immune cells especially eosinophils (175). To study whether NAFLD condition causes kidney more vulnerable to microcystin exposure, renal tissue sections were imaged after stained by Hematoxylin and Eosin (H&E). Our result showed thickness in the glomerular wall in mice group fed with methionine and choline deficient (MCD) diet and were exposed to microcystin-LR compared to mice fed with MCD diet without microcystin treatment and normal chow diet mice exposing to microcystin-LR (Fig1). In addition, filtration of immune cells and proliferation of mesangial cell is high in NAFLD group exposed to microcystin. Microcystin-LR exposure showed significant increase of mesangial cell proliferations in mice NAFLD, as assess in high expression of alpha smooth muscle actin ( $\alpha$ -SMA). The reactivity of  $\alpha$ -SMA, which is a specific mesangial cell activation marker, was showed high in NAFLD mice treated with microcystin compared to NAFLD mice and lean mice exposed to microcystin ( $P < 0.05$ ; Fig2, A and B). This result suggested that a condition of NAFLD make glomeruli more susceptible to microcystin intoxication.

#### **Microcystin potentiates NAFLD induced renal inflammation pro inflammatory cytokines secretion in renal tissue.**

We have shown previously that environmental toxin like bromodichloromethane(BDCM), which is metabolized by cytochrome P 450 (Cyp2E1), augmented NAFLD mice model to release significant high level of cytokines in renal tissue (171). To study the effect of microcystin-LR administration to mice models, kidney proinflammatory cytokine gene

levels were analyzed by qRT-PCR. Results showed that mRNA expression of proinflammatory IL-1 $\beta$  was significantly higher in NAFLD mice treated with microcystin-LR compared to NAFLD mice alone and mice were fed with normal chow diet and exposed to microcystin (Fig3, A). Similar results were obtained for mRNA expression of MCP-1, CD68, F4/80 were NAFLD mice treated with microcystin have significant increase of expression compared to NAFLD mice and lean mice exposed to microcystin (Fig3; B, C, and D). This result assumed that microcystin led to potentiate NAFLD releasing proinflammatory cytokines in kidney, which in turn caused renal inflammation and renal tissue damage.

**Microcystin exposure activates mesangial cell NOX2 and mediates mesangial cell NOX2 generated peroxynitrite.**

NOX2 upregulation causes oxidative stress resulting in renal hypertrophy, dysregulate in renal function, inflammation, and fibrosis (176). To prove the role of microcystin in induction of NADPH 2 oxidase (NOX2) in progressive NAFLD, we studied the membrane association of NOX2 two subunits (P47phox and GP91phox) by using immunofluorescence microscopy in mice tissue samples. Results were analyzed regarding to the number of colocalization/overlay events (shown by yellow). Results showed that the NAFLD + microcystin-LR group had a significant increase in the colocalization events compared with the NAFLD only group ( $P < 0.01$ ) (fig.4 A and B). Lean mice group treated was treated with microcystin-LR showed less colocalization events compared with the NAFLD+ microcystin-LR ( $P < 0.01$ ) (fig.4 A and B). Furthermore, no significant change in colocalization events was found between Lean+ microcystin-LR and NAFLD only group. The above outcomes propose that microcystin induced p47phox expression in

NAFLD condition and assisted in the membrane association of p47phox and gp91phox that assumes significance in causing oxidative stress and mesangial cell activation in NAFLD. To demonstrate that mesangial cell NOX2 activation resulting in peroxynitrite generation, experiments were performed in the NAFLD mice model. Results showed that NAFLD+ microcystin had significant increase in mesangial cell proliferation compared with NAFLD only group, as assess in alpha smooth muscle actin reactivity ( $\alpha$ -SMA) ( $P < 0.01$ ) (fig.5 A and B). P47phox KO mice had significant decreased in  $\alpha$ -SMA activity compared with NAFLD+ microcystin ( $P < 0.01$ ) (fig.5 A and B). Our result also showed that 3-nitrotyrosine immunoreactivity was significantly increased in the DIO + BDCM group compared with the DIO group ( $P < 0.05$ ) (Fig. 5, C and D). P47phox KO mice had significant decreased in 3-nitrotyrosine immunoreactivity activity compared with NAFLD+ microcystin ( $P < 0.05$ ) (Fig. 5, C and D). The results suggested that microcystin was significantly associated with an increase in 3-nitrotyrosine immunoreactivity, and peroxynitrite might be a key performer in causing oxidative stress.

### **Microcystin administration upregulates Mesangial cell miR21 expression.**

Among all miRNAs have been identified, miR21 has been upregulated in different kidney diseases, such as chronic kidney disease and acute kidney disease. Although miR21 expression existed in health kidney condition, high level of miR21 expression was identified in kidney diseases, particularly in fibrosis (177). To prove that microcystin, through its activation of NOX2 in vitro increases miR21 expression, experiments were performed with mesangial cells (Fig. 6). Results showed that mesangial cell treated with 10  $\mu$ M microcystin-LR and 100ng leptin (MC+Leptin) had 2.5-fold increase in miR21 expression compared to mesangial cell control ( $P < 0.05$ ). Mesangial cells were

administrated to leptin and were treated with apocynin (MC+Leptin+Apo) or Phenyl Boronic Acid (MC+Leptin+FBA) had significant decrease in miR21 expression compared with MC+Leptin group ( $P < 0.05$ ). Results showed that mesangial cell treated with microcystin-LR had 1.8- fold increase in miR21 expression compared with mesangial cell control ( $P < 0.05$ ). To prove that microcystin, through high expression of miR21 activates mesangial cell, we performed experiments with NAFLD mice kidney tissues. Results showed that NAFLD+ microcystin had a significant increase in  $\alpha$ -SMA expression, as shown in immunofluorescent microscopy (2.7-fold increases) compared to NAFLD only group (Fig.7 A and B) ( $P < 0.05$ ). miR21 KO mice treated with microcystin (miR21 KO + MC) had a significant decrease in  $\alpha$ -SMA expression compared to NAFLD+MC mice group ( $P < 0.05$ ).

Next, we explored the role of microcystin mediated miR21 upregulate in mesangial cells by determined immunoreactivity of  $\alpha$ -SMA in mesangial cells. The results showed that mesangial cells treated with leptin and microcystin (leptin+MC) had a significant increase in  $\alpha$ -SMA compared to mesangial cell control (Fig. 7. C and D) ( $P < 0.05$ ). Furthermore, mesangial cells incubated with leptin and microcystin and treated with Apocynin (leptin+MC+Apo), FBA (leptin+MC+FBA), or miR21 inhibitor (leptin+MC+mir21 inh.) had a significant decrease in  $\alpha$ -SMA immunoreactivity compared to leptin+MC group (Fig. 7. C and D) ( $P < 0.05$ ). The above results show that mesangial cell proliferation is depends on miR21 upregulation. Inhibition of miR21 attenuates mesangial cell activation and reduce inflammation cytokines releasing.

### **Peroxynitrite- miR21 axis drives mesangial cell activation and death.**

Recent study from our laboratory has shown that NADPH oxidase activation consequence in peroxynitrite generation and resulting in cascade of events, such as NF- $\kappa$ B activation (16). To support that NOX2 mediates peroxynitrite generation resulting in mesangial cell activation and to find the link between peroxynitrite generation and miR21, we preformed experiment in mesangial cell line. Result showed that mesangial cell treated with leptin and microcystin (leptin+MC) had a significant increase in 3 nitro tyrosine (3NT) almost 1.8-fold increases compared to control mesangial cell group. (Fig. 8.A and B) ( $P < 0.05$ ). Mesangial cells were treated with leptin and microcystin and were incubated with Apocynin (Leptin+MC+Apo), FBA (Leptin+MC+FBA), or miR21 inhibitor (Leptin+MC+miR21 inh.) had a significant decrease in peroxynitrite formation compared with Leptin+MC mesangial cell group, as assess in 3NT immunoreactivity ( $P < 0.05$ ).

While ROS activation and peroxynitrite generation are consequence of microcystin-LR exposure, apoptosis is another consequence of MC-LR exposure in renal kidney cell line (178). One possible mechanistic pathway can be through endoplasmic reticular damages (179). To observe that microcystin caused cell death, experiments were performed in mesangial cell line. Results showed that leptin+MC group had a significant increase in number of apoptotic cells (1.5- fold increased) compared with mesnagial cells served as a control. (Fig. 8.C and D) ( $P < 0.05$ ). Leptin+MC+Apo, Leptin+MC+FBA, and Leptin+MC+miR21 inh had a significant decrease in apoptotic cell number compared with leptin+MC group (Fig. 8.C and D) ( $P < 0.05$ ). The results above suggest that microcystin-LR augmented NAFLD renal immunotoxicity through peroxynitrite – miR21 axis, as assess in the 3NT immunoreactivity which blocked by miR21 inhibitor. Additionally,

microcystin- LR causes cell death in mesangial cell in present of NAFLD, as observe in apoptotic cell percentage by using Tunel assay.

**Microcystin-LR mediated NOX2 activation and corresponding induction of miR21 in NAFLD are crucial for TGF- $\beta$  signaling pathway.**Our laboratory has been shown previously that NADPH oxidase activation and its subsequence of miR21 upregulation are necessary to TGF- $\beta$  signaling pathway which in turn response on fibrogenesis (74). To support that microcystin through NOX2- mir21 axis causes TGF- $\beta$  signaling pathway upregulation, experiments were performed in NAFLD mice model. Results showed that kidney tissue slices from NAFLD+MC group had a significant increase in TGF- $\beta$  immunoreactivity (as showed in immunohistochemistry) compared with NAFLD only group (Fig. 9.A and B) ( $P < 0.05$ ). On the other hand, miR21 KO mice (miR21KO + MC) had a significant decrease in TGF- $\beta$ . The morphometry analysis showed that miR21 KO+MC had a double fold decrease in TGF- $\beta$  immunoreactivity compared with NAFLD+MC, while no different in TGF- $\beta$  reactivity was found between miR21 KO+MC group and NAFLD only group. (Fig9. A and B) ( $P < 0.05$ ).

Post transcription of miR21 downregulates tumor suppressor PTEN both in vivo and in vitro. Repressing PETN and SMAD-7, play a key role in TGF- $\beta$  signaling pathway. To prove that NOX2-miR21 axis represses PTEN expression level, we performed experiments in mice model. Results showed that microcystin administration decreased the levels of PTEN, through upregulating of miR21 in the kidney, as shown by Western blot analysis compared with the NAFLD only (Fig. 10. A and B). The results showed also increase the levels of PTEN in P47phox KO +MC and miR21 KO +MC mice. The results

suggested that microcystin-LR might have a role in increasing NOX2-miR21 axis induced repression of PTEN, which in turn activates TGF- $\beta$ .

#### **4.4 DISCUSSION:**

The present study reports the first time that chronic exposure of microcystin-LR, a cyanobacteria heptapeptide toxin, has been shown heighten ectopic inflammation in the kidney. Microcystin enhances nonalcoholic fatty liver disease (NAFLD) caused renal immunotoxicity via mesangial cell activation, as indicated by an increase  $\alpha$ -SMA immunoreactivity (76). We also show that mesangial cell proliferation mediated by NOX2 activation and peroxynitrite generation leads to miR21 overexpression. Furthermore, using the rodent model of NAFLD, we observed miR21 activation caused TGF- $\beta$  activation and renal inflammation.

There is increasing evidence that a condition of NAFLD, which has high risks of progressing to NASH, cirrhosis, and hepatocellular carcinoma, can have comorbidities that may include kidney diseases and cardiovascular complications. The multiple hit theory is the most likely explanation for the progression of NAFLD to NASH. Oxidative stress, inflammatory adipokines, and environmental toxins are likely the second hit to the progression of the NAFLD condition (171). In addition, microcystin plays a critical role in ROS generation in the animal models and in the different cell lines (180). In the present study, we used microcystin-LR as an environmental toxin and a causative factor to lead to activation of NOX2 in renal NAFLD condition. Interestingly, our results showed that microcystin-LR altered the glomerular morphology by increasing wall thickness and increased immune cell filtration as indicated in the histopathology section of the kidney. The alteration of glomerular structure leads to mesangial cell activation and proliferation,



as assessed by  $\alpha$ -SMA immunoreactivity. Consequently, a significant increase in the levels of proinflammatory cytokines, like IL1 $\beta$ , MCP-1, F4/80, and CD68 has been shown (Fig.3). Mesangial cell proliferation is always associated with lipid peroxidation which triggers NOX2 upregulation and peroxynitrite generation (171,75). Mesangial cell activation is decreased in P47phox KO mice. NOX2 activation, as indicated by NOX2 subunits colocalization, is decreased in P47phox KO mice. Peroxynitrite formation also decreases in P47phox KO mice too, as assessed by 3 nitro tyrosine, a marker of peroxynitrite-mediated nitrative stress, indicating that mesangial cell activation is depended on the NOX2 pathway and peroxynitrite generation.

MicroRNAs (miRNAs) are small noncoding RNAs that reduce gene expression post-transcriptionally, thereby modulating the activity of signaling pathways, including stress responses in many physiologic and pathologic processes. Among all miRNAs, miR21 mediates damage to the kidney via reduction of several molecular targets (181). We found a high level of miR21 expression level in the mesangial cell exposed to microcystin-LR. We also found  $\alpha$ -SMA, a proliferative marker of mesangial cells repressed after the cell incubated with miR21 inhibitor. Mesangial cell proliferation also downregulated in 21 KO mice treated with microcystin-LR. These results support the conclusion that miR21 plays a dynamic role in microcystin induced mesangial cell activation. Microcystin-LR exposure triggered cell death (apoptosis) as a biochemical feature of microcystin toxicity. Several studies have shown that microcystin onset damages mitochondria via variant mechanisms that alters mitochondrial features resulting in ROS formation and pro-apoptotic cytokines releasing (55). In the present study, we identified that mesangial cells suffered from apoptosis after microcystin exposure, and that apoptotic event was less active

when mesangial cells were incubated with apocynin and FBA. This indicates the apoptotic probe of microcystin-induced mesangial cell death is NOX2 dependent, as assessed by the reduced number of positive apoptotic cells (Tunel assay) after administration of NADPH oxidase inhibitor and a specific scavenger and blocking agent of peroxynitrite. Activation of the TGF- $\beta$  pathway, which regulates different cell processes and functions, including cell proliferation and apoptosis, has been demonstrated in several pathological conditions, such as chronic kidney disease (182). TGF- $\beta$  mesangial extracellular matrix deposit is the most common component in fibrogenesis scheme. More recently, our team showed that NADPH oxidase-mediated miR21 activation significantly upregulated TGF- $\beta$  protein level in the condition of NAFLD (74). The result showed that miR21 inhibited SMAD-7 and PTEN, which target the SMAD2/3 pathway, is a critical step in TGF- $\beta$  activation. In this study, we affirm this model of the microcystin activated TGF- $\beta$  signaling pathway. NAFLD mice treated with microcystin-LR showed high immunoreactivity of TGF- $\beta$  compared with the NAFLD group (fig.9. A and B) which suggest that chronic exposure to microcystin activates the TGF- $\beta$  pathway and produces the extracellular matrix which is a vital sign of fibrosis. On the other hand, miR21 KO mice showed less TGF- $\beta$  immunoreactivity, which means the activation of TGF- $\beta$  pathway is miR21 dependent. Furthermore, PTEN protein levels were attenuated in mice exposed to microcystin, in parallel, mice with specific genes knocked out like P47phox and miR21 had a significant increase in PTEN protein level (fig. 10. A and B). The results above prove the existence of microcystin activated NOX2- miR21 axis, which attenuates PTEN expression resulting in the TGF- $\beta$  signaling pathway.

Taken together, our data describe a novel mechanistic role of microcystin-LR in augmenting NAFLD caused nephrotoxicity via NOX2- miR21 axis in mesangial cells resulting in the release of TGF- $\beta$  and tubular inflammation. Our results will help advance the current knowledge of the microcystin-LR mechanism and show the targeting of NOX2 by use apocynin, suggesting that apocynin might be a candidate for an interventional strategy to reduce ectopic inflammatory events in NAFLD with microcystin exposure.

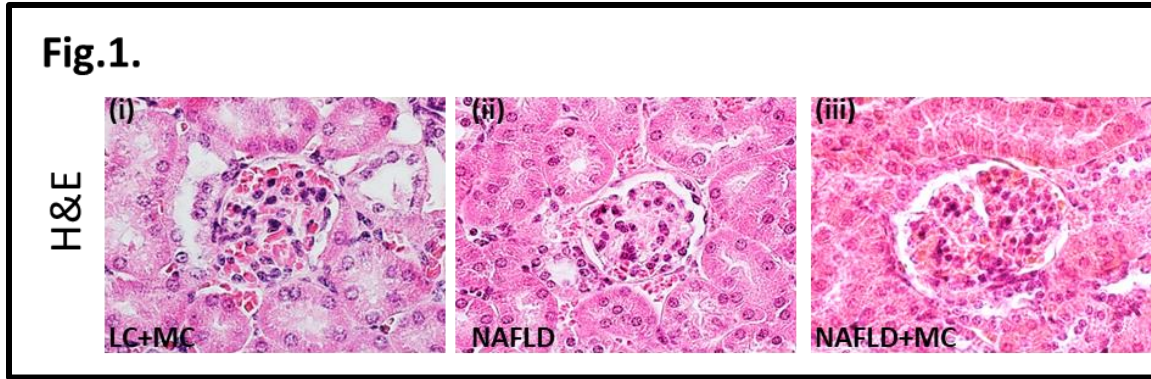


Figure 4. 1 Microcystin increases immune cell filtration in glomerulus:Microcystin-LR exposure heightened HAFLD causes immune cells infiltration in glomeruli and damage the glomerular structure. hematoxylin and eosin-stained paraffin-embedded kidney tissue sections (Lean+ MC; i) mice fed with normal chow diet and treated with microcystin-LR, (NAFLD; ii) mice were kept on MCD diet without microcystin treatment, and (NAFLD+MC; iii) NAFLD mice treated with microcystin-LR. Images were taken at 60X. (\*P<0.05).

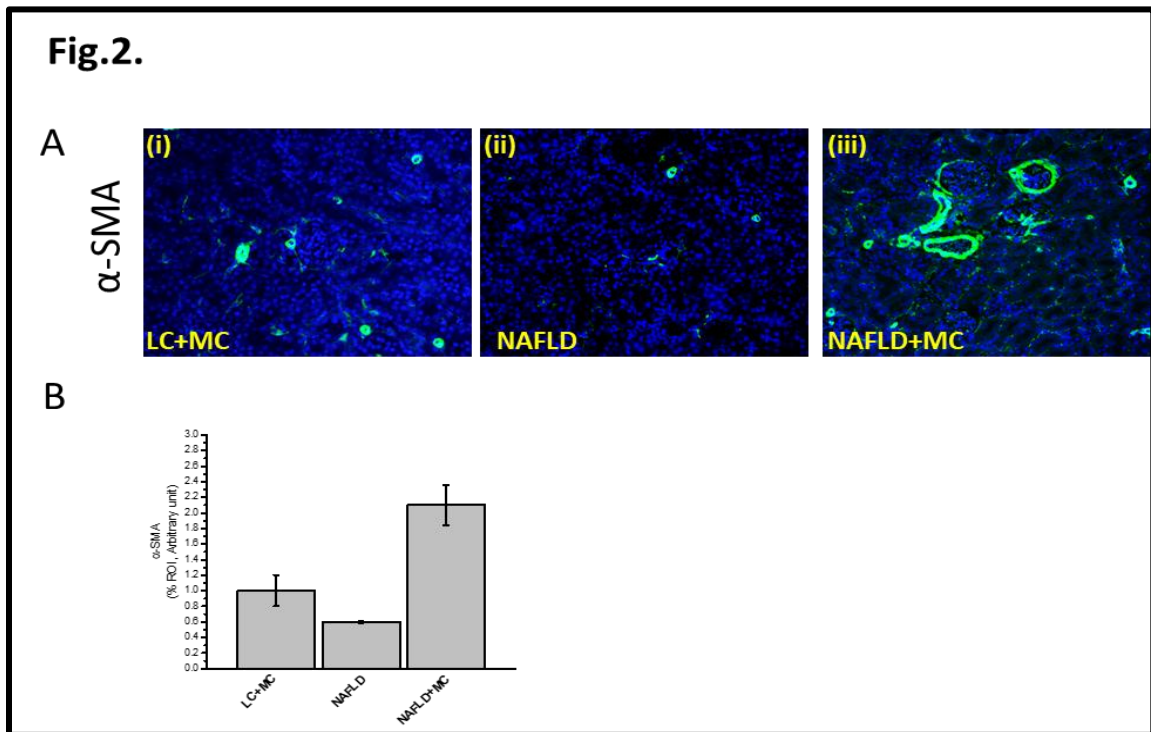


Figure 4.2 Microcystin exposure augment mesangial cell activation in NAFLD condition A, Immunoreactivity of alpha smooth muscle actin ( $\alpha$ -SMA, a marker for mesangial cell activation) as shown by immunofluorescent in kidney slices from mice fed with MCD diet (NAFLD) serve as a control, NAFLD mice exposed to microcystin-LR (NAFLD+MC),

microcystin administration to lean mice (lean+ MC), Images were taken at 20X. B, Morphometric analysis of  $\alpha$ - SMA immunoreactivity (mean data measured as arbitrary light units from three separate microscopic fields were plotted on y-axis) in NAFLD, NAFLD+MC, and lean+MC groups (\*P<0.05).

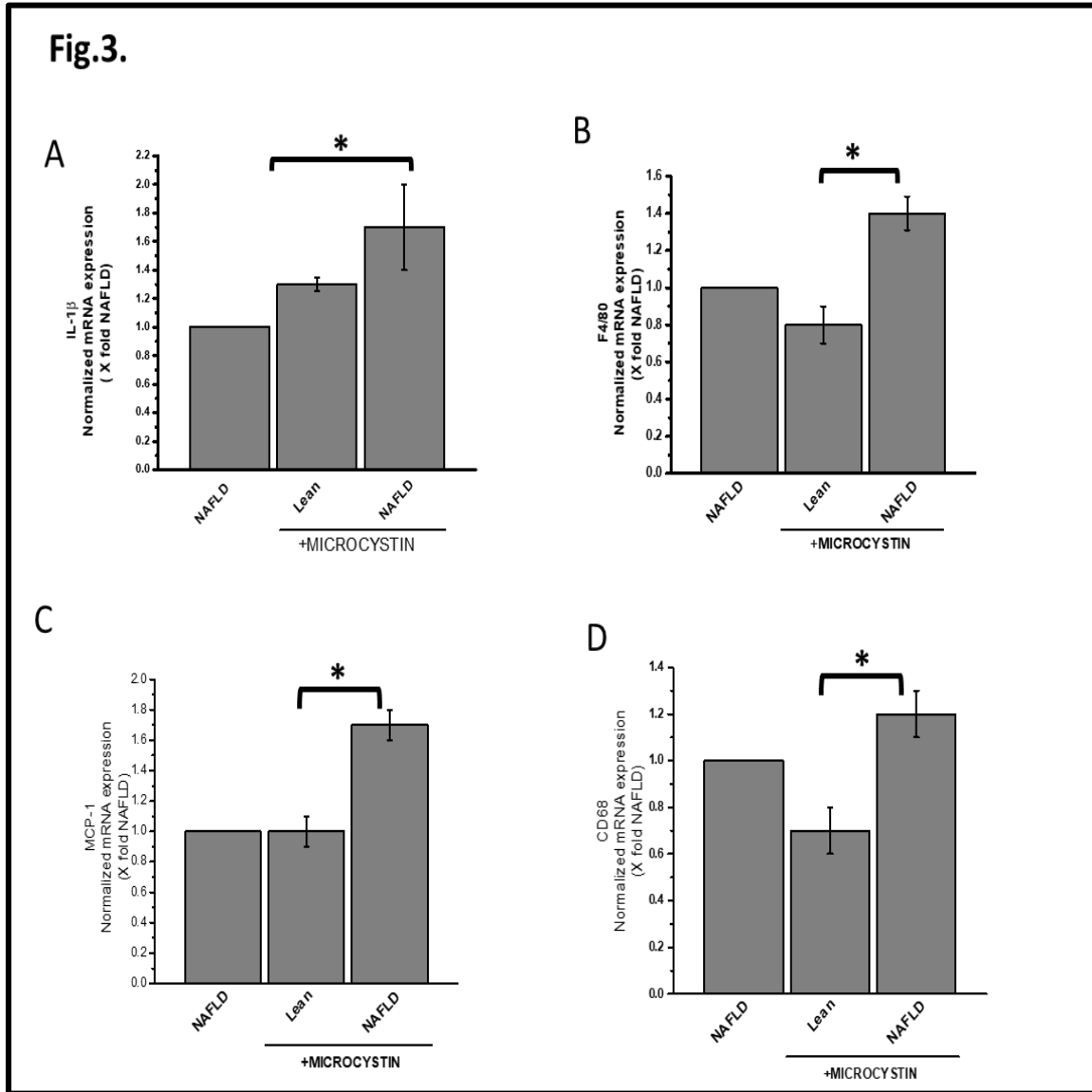


Figure 4.3 Microcystin exposure heighten glomerular inflammation in NAFLD exist. mRNA expression analysis of IL-1 $\beta$ , MCP-1, CD68, and F4/80 genes in kidney tissue of lean+MC, NAFLD, and NAFLD+MC. A, mRNA expressions of IL-1 $\beta$ . B, mRNA expressions of MCP-1. C, mRNA expressions of CD68. D, mRNA expressions of F4/80. All mRNA expression had been assessed by quantitative real-time PCR (qRTPCR) and expressions were normalized against NAFLD group (\*P<0.05).

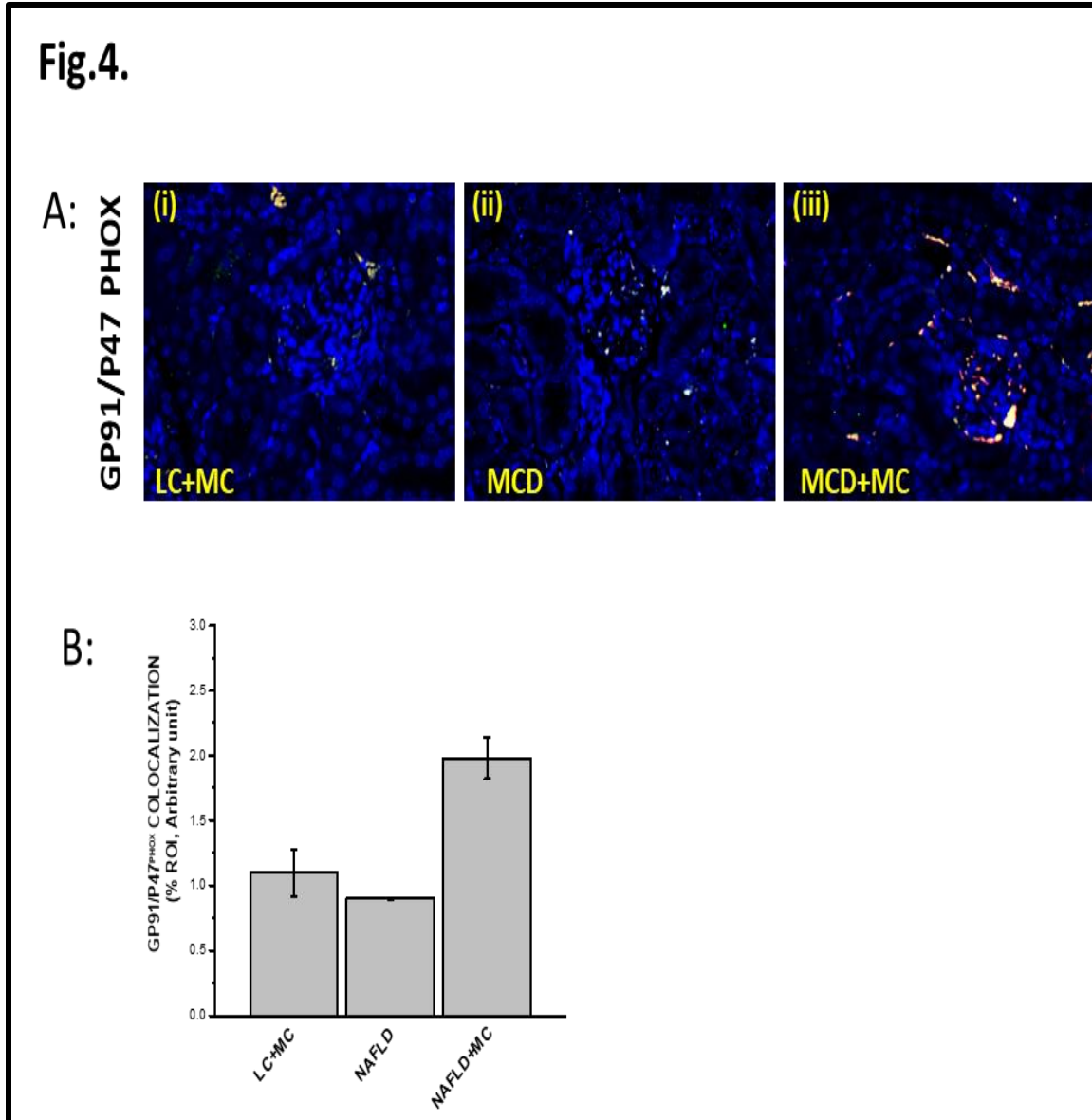


Figure 4.4 Microcystin exposure activate mesangial cell NOX2 Microcystin-LR activated NADPH oxidase (NOX2) via transported cytosolic subunit (P47phox) to membrane and colocalized with membranal subunit (GP91phox) A, Immunofluorescence for P47Phox (Green) and GP-91 Phox (Red) co-localization (Yellow)in kidney slices from mice fed MCD diet (NAFLD), NAFLD mice exposed to microcystin-LR (NAFLD+MC), and P47phox gene deficient mice fed with MCD diet and exposed to microcystin-LR (P47phox KO +MC). B, Morphometric analysis of GP91/P47phox colocalized in NAFLD, NAFLD+MC, P47phox KO+MC group of mice. All immunofluorescent Images were taken at 20X and mean colocalize measured as arbitrary light units from three separate microscopic fields were plotted on y-axis (\*P<0.05).

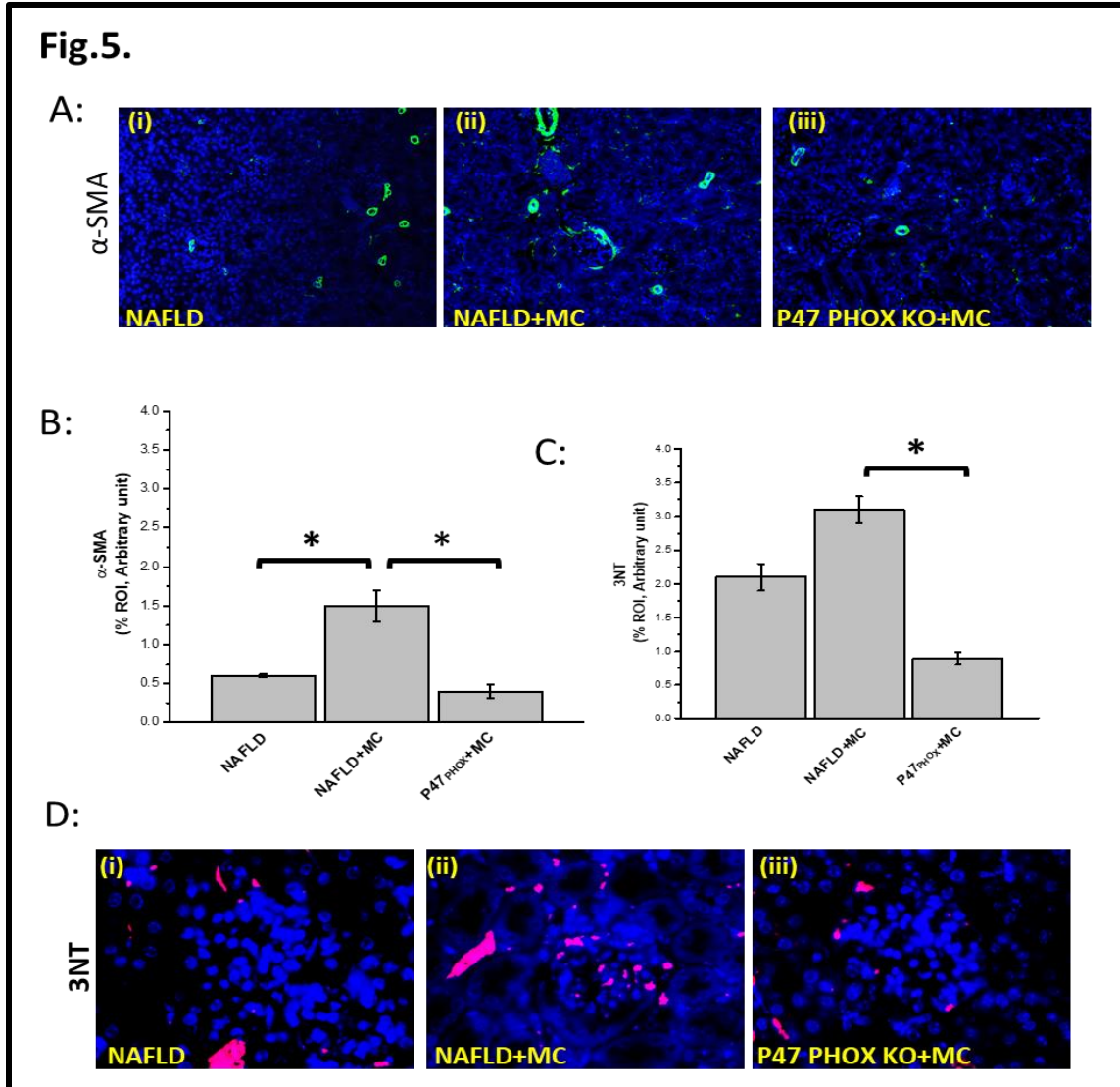


Figure 4.5 Microcystin mediates mesangial cell NOX2 generated peroxynitrite: Microcystin-LR generates peroxynitrite via NADPH oxidase (NOX2). A, Immunofluorescence for 3-Nitro-tyrosine (Red) reactivity in Kidney tissue from mice fed MCD diet (NAFLD), NAFLD mice exposed to microcystin-LR (NAFLD+MC), and P47phox gene deficient mice fed with MCD diet and exposed to microcystin-LR (P47phox KO + BDCM) images were taken in 20X. B, Morphometric analysis of GP91/P47phox colocalized in NAFLD, NAFLD+MC, P47phox KO+MC group of mice. All immunofluorescent Images were taken at 40X and mean colocalize measured as arbitrary light units from three separate microscopic fields were plotted on y-axis) (\*P<0.05).C, Immunoreactivity of ( $\alpha$ - SMA) as shown by immunofluorescent in kidney slices from (NAFLD) serve as a control, NAFLD+MC, and P47phox KO+ MC, Images were taken at 60X. D, Morphometric analysis of  $\alpha$ - SMA immunoreactivity (mean data from three separate microscopic fields were plotted on Y-axis) in NAFLD, NAFLD+MC and P47phox KO groups of mice (\*P<0.05).

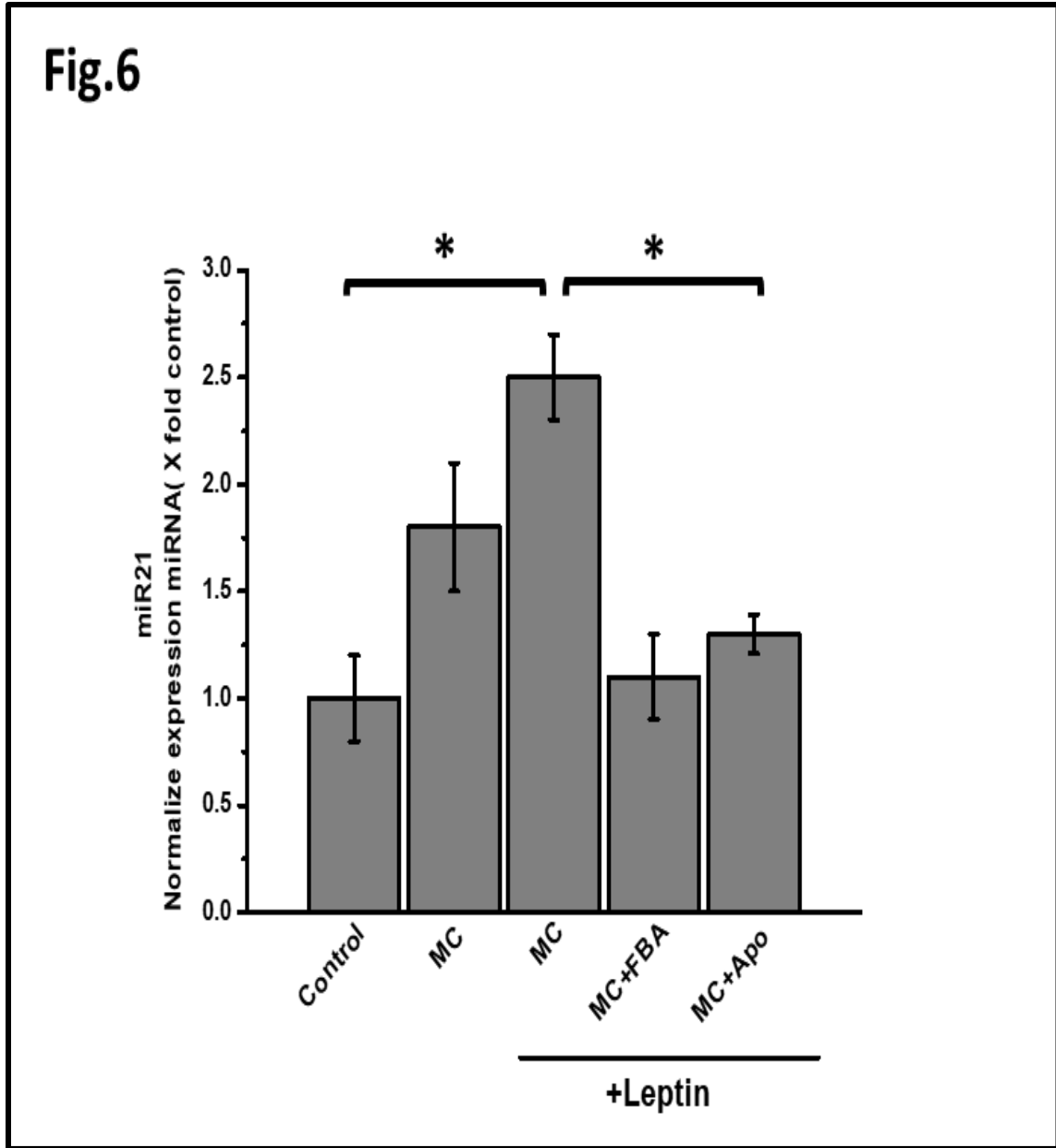


Figure 4.6 Microcystin administration upregulates Mesangial cell miR21 expression. Microcystin-LR-induced NADPH oxidase activation mediates upregulation of micro-RNA 21 (miR21). qRT-PCR analysis of miR21 expression of Mesangial cell (control), mesangial cell incubated with leptin and treated with microcystin (MC+MC+leptin), mesangial incubated with leptin and treated with both microcystin and apocynin (MC+Apo+leptin), and mesangial incubated with leptin and treated with both microcystin and FBA (MC+FBA+leptin). (\*P < 0.05).



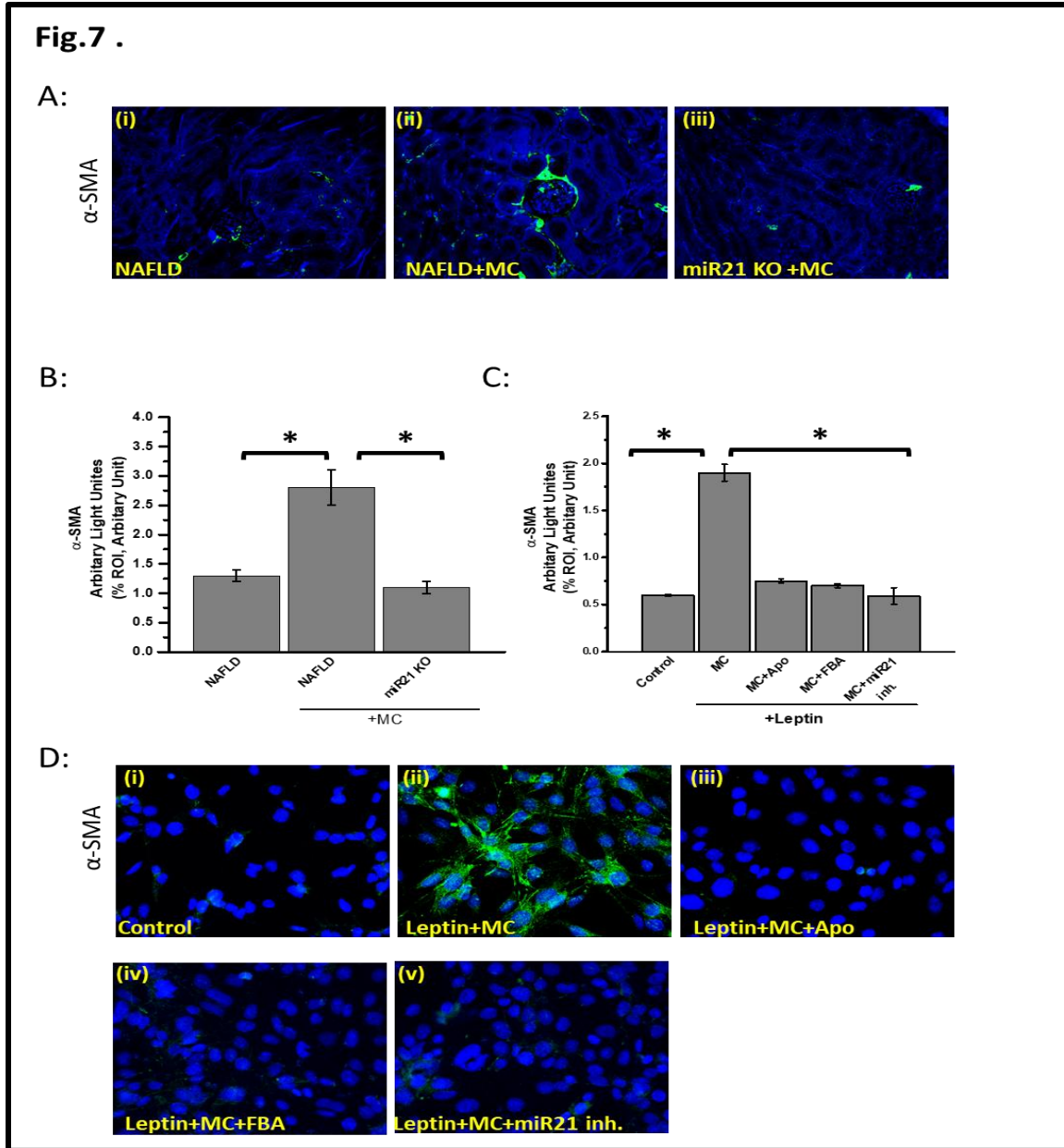


Figure 4.7 miR21 high expression causes mesangial cell activation:  $\alpha$ -SMA immunoreactivity as shown by immunofluorescent in kidney slices from NAFLD mice served as a control, NAFLD mice treated with microcystin-LR (NAFLD+MC), and miRNA-21 mice fed with MCD diet and exposed to microcystin (miR21 KO+MC), Images were taken at 20X. B, morphometric analysis of  $\alpha$ -SMA immunoreactivity (mean data from three separate microscopic fields were plotted on Y-axis) in NAFLD, NAFLD+MC and miR21 KO groups of mice. C, immunoreactivity of  $\alpha$ -SMA as shown by immunofluorescent in mesangial cells (control), mesangial cells exposed to both leptin and microcystin-LR (Leptin+MC), and cells treated leptin and microcystin-LR plus apocynin (leptin+MC+Apo), FBA (leptin+MC+ FBA), or miR21 inhibitor (leptin+MC+miR21 inh.), Images were taken at 40X. D, morphometric analysis of  $\alpha$ -SMA immunoreactivity (mean

data from three separate microscopic fields were plotted on Y-axis0 in cell control, leptin+MC, leptin+MC+Apo, leptin+MC+FBA, and leptin+MC+miR21 inh. (\*P < 0.05).

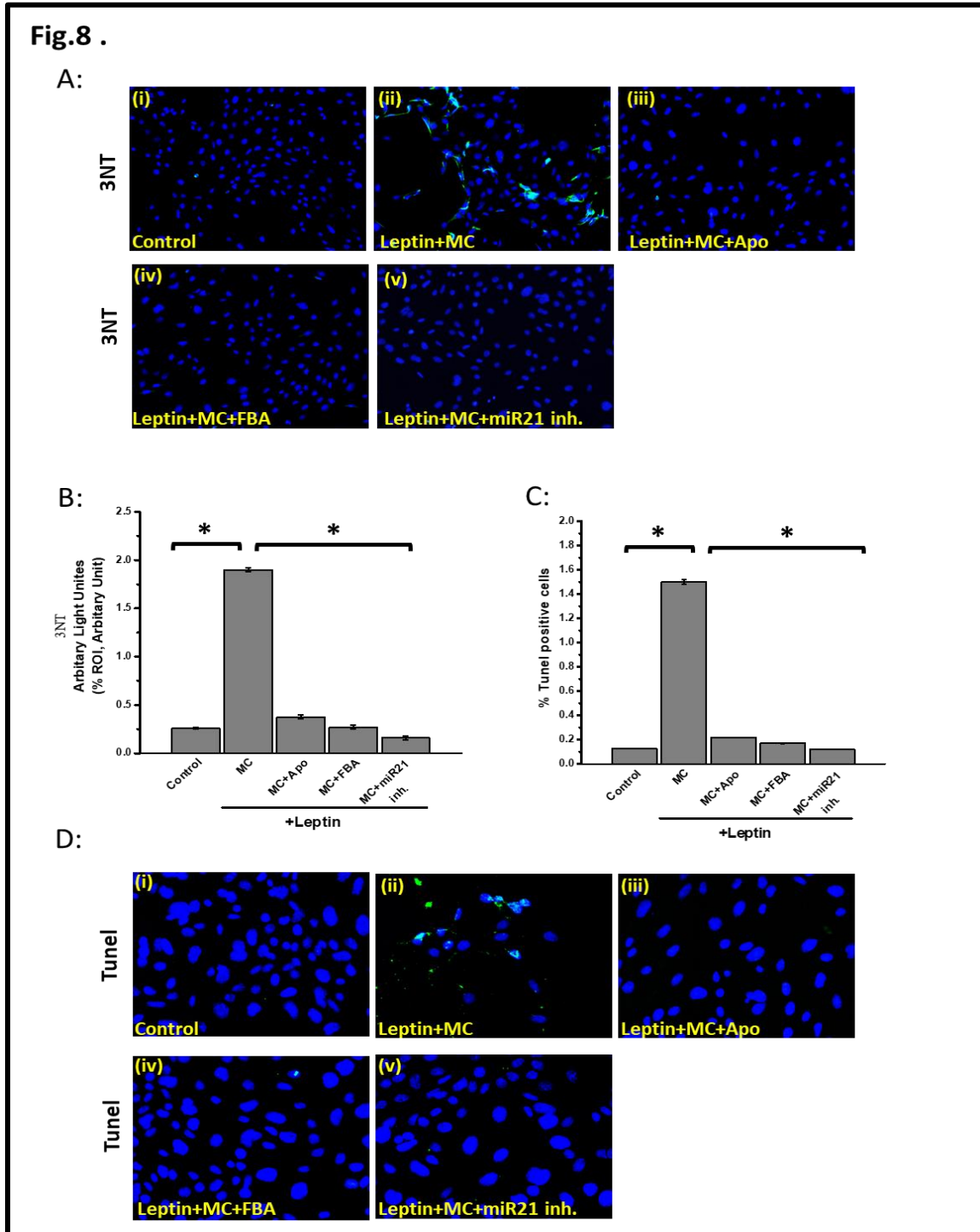


Figure 4.8 Peroxynitrite- miR21 axis drives mesangial cell activation and death: Microcystin-induced NOX2 generate peroxynitrite and mir21 activation increases mesangial cell activation and death. A, immunoreactivity of 3NT as shown by

immunofluorescent in mesangial cells (control), mesangial cells exposed to both leptin and microcystin-LR (Leptin+MC), and cells treated leptin and microcystin-LR plus apocynin (leptin+MC+Apo), FBA ( leptin+MC+ FBA), or miR21 inhibitor (leptin+MC+miR21 inh.), Images were taken at 20X. B, morphometric analysis of 3NT immunoreactivity (mean data from three separate microscopic fields were plotted on Y-axis) in cell control, leptin+MC, leptin+MC+Apo, leptin+MC+FBA, and leptin+MC+miR21 inh. (\*P < 0.05). C, number of apoptotic nuclei as shown by TUNEL immunofluorescence staining in leptin+MC, leptin+MC+Apo, leptin+MC+FBA, and leptin+MC+miR21 inh. The number of TUNEL-positive cells identified by their green-stained images were taken at 40X. D, percentage of TUNEL-positive cells (obtained by morphometric analysis done on images from three separate microscopic fields) in cell control, leptin+MC, leptin+MC+Apo, leptin+MC+FBA, and leptin+MC+miR21 inh. (\*P < 0.05).

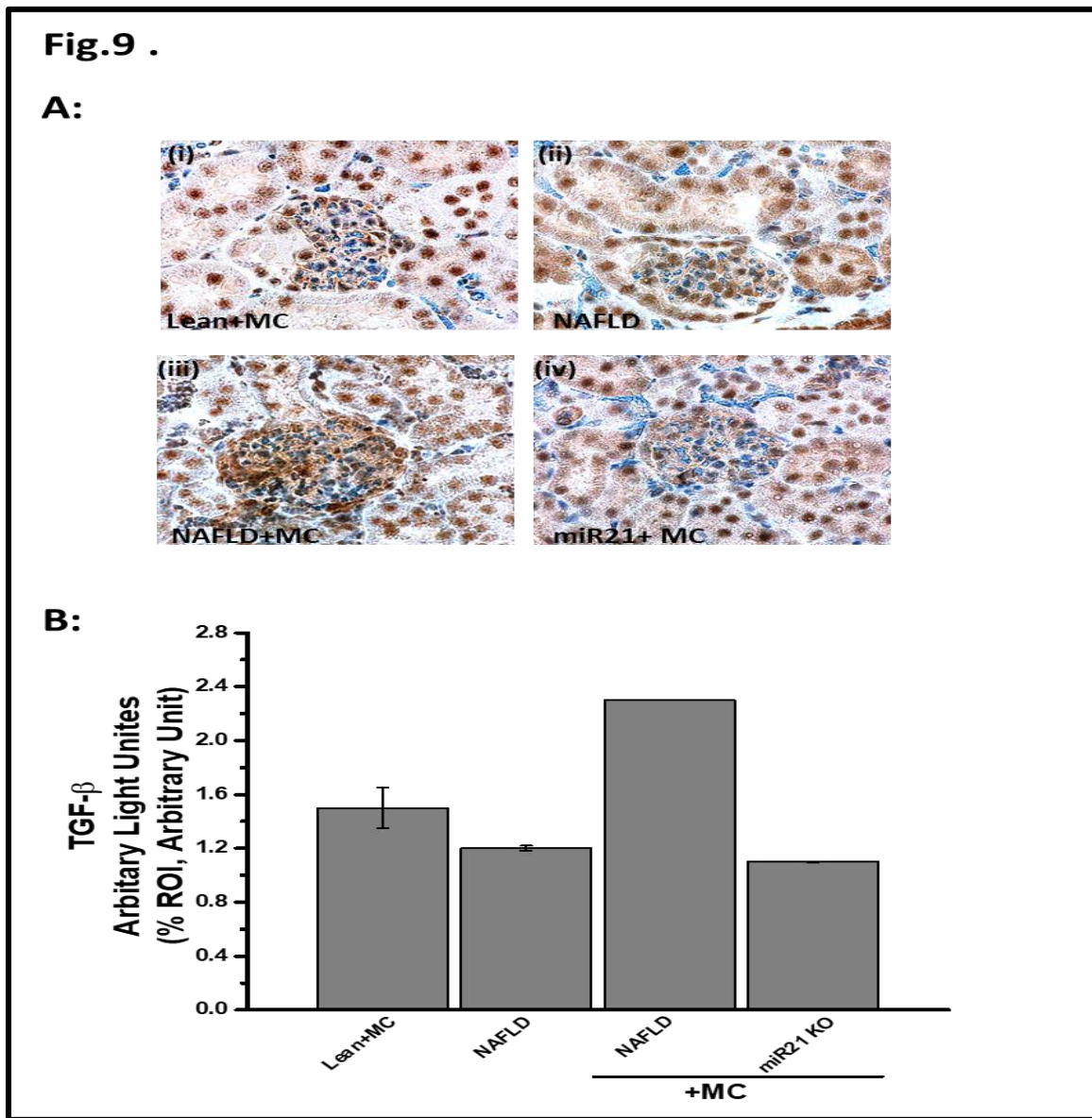


Figure 4.9 miR21 activates mesangial cell toxicity via increasing TGF- $\beta$ : A, immunoreactivity of transforming growth factor (TGF)- $\beta$ , as shown by immunohistochemistry in kidney slices from lean+MC (i), NAFLD (ii), NAFLD+MC (iii) and miR21 KO + MC (iv) groups of mice. All images were taken at 60X. B, morphometric analysis of TGF-  $\beta$  immunoreactivity (obtained by morphometric analysis done on images from three separate microscopic fields) in the lean+MC (i), NAFLD (ii), NAFLD+MC (iii) and miR21 KO + MC (iv) groups. \* $P < 0.05$ .

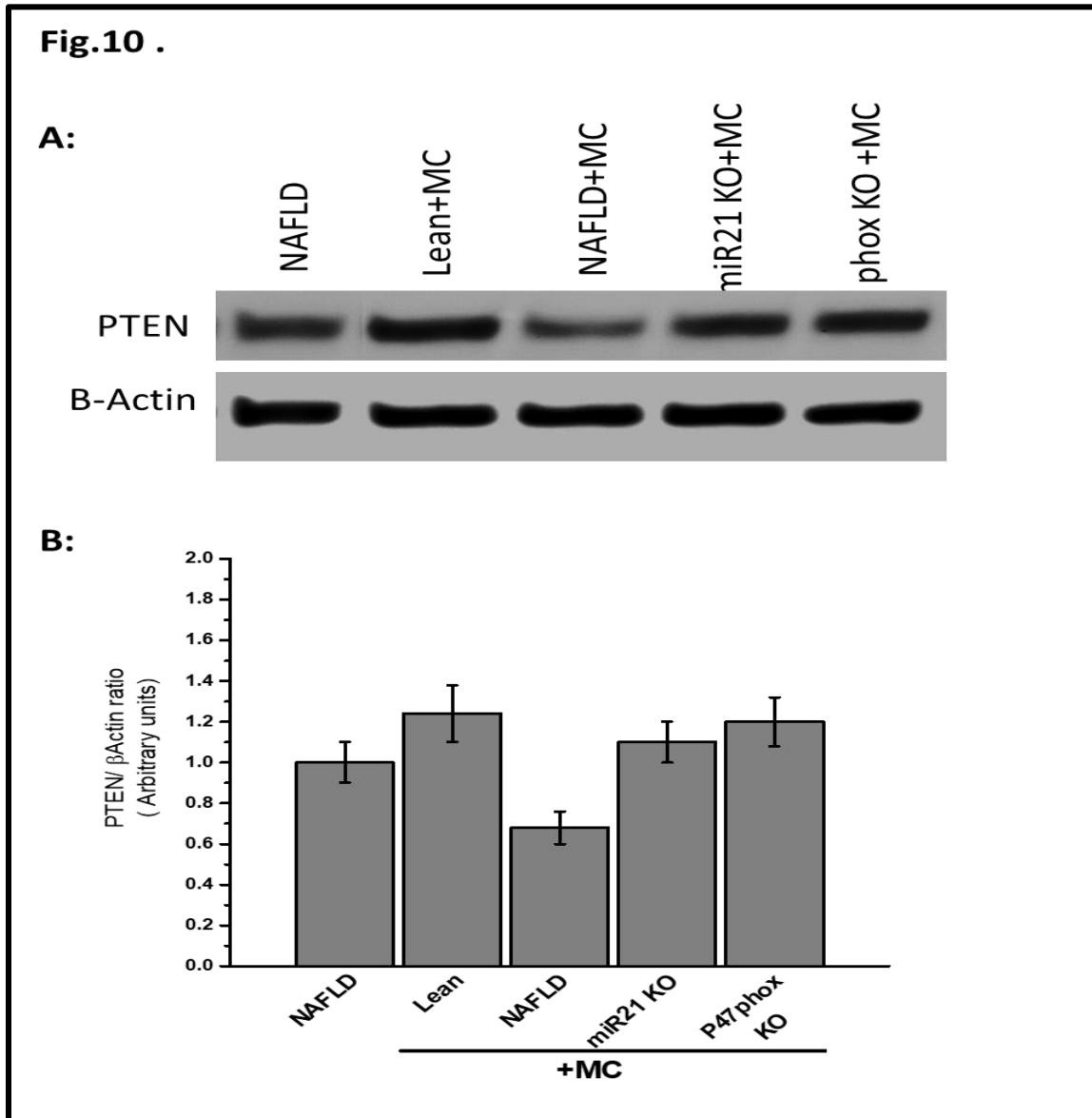


Figure 4.10 NOX2- miR21 axis heightens mesangial cells activation via PTEN decreasing:A, Western blot analysis of PTEN protein levels followed by normalizations against  $\beta$ -actin in lean+MC, NAFLD, NAFLD+MC, and miR21 KO + MC, and P47phox+MC groups. B, morphometric analysis of PTEN/  $\beta$ -Actin ratio.

## CHAPTER 5

### CONCLUSION

Obesity has become a public health problem. The prevalence of obesity has doubled in adults and children in the last two decades. Two thirds of Americans are overweight or obese. Obesity is a multifaceted disorder which reduces quality of life and dramatically increases of developing various physical diseases, which are the leading causes of death not only in the U.S. but also worldwide. Although genetic factors can contribute to the development of obesity, individual and societal behaviors, like education, food market, eating patterns, and physical activity are also important factor in increase obesity rates. People who have obesity are predisposed to have other diseases and health conditions, including, diabetes, heart disease, stroke, nonalcoholic fatty liver disease and some types of cancer. NAFLD, which is an umbrella term for numerous stages of disease, is a hepatic manifestation of metabolic syndrome which emerges due to abnormal fat (<5% of the liver weight) accumulation in the liver. The most acceptable theory for progressing nonalcoholic steatohepatitis (NASH), an advance stage of NAFLD, is a multi-hits theory. Accumulation of fat presents the first hit, which increases the vulnerability of the liver to various second hits, including oxidative stress, proinflammatory cytokines, adipokines and mitochondrial dysfunction that lead to fibrosis and cellular death and sometimes lead to hepatic cancer. Several studies in mice and human models showed that environmental toxins like environmental pollution including air, soil, and water pollutants, as well as chemical

materials could be considered risk factors for the onset of NAFLD and could increase the progression of NASH. Previous studies from our group have shown that chronic exposure to low doses of Bromo-dichloromethane (BDCM), a disinfectant byproduct when chlorine is used to control microbial contaminants in human water resources, is able to exacerbate liver injury causing Non-alcoholic steatohepatitis (NASH) where CYP2E1 mediated oxidative stress acts as the secondary hit in obese mice. Indeed, several studies link NAFLD with extrahepatic disorders, in the present study, I examined the molecular mechanisms by which the kidney is affected by an underlying condition of NASH induced by BDCM exposure. I also studied the role of microcystin-LR, a cyanobacteria heptapeptide toxin in the exacerbation of NAFLD caused kidney damage.

In the last two decades, several studies have focused on the communication and linkages between NAFLD and chronic kidney disease (CKD) (31,152), however the exact mechanism of the process is largely unclear. Here, I investigated the role of cytochrome P450 (CYP2E1) mediated NAFLD caused kidney immunotoxicity. High-fat (60% kcal) diet-fed BDCM induced mouse NASH models were used for this study along with mice deficient in genes for CD1D gene, PFP/Rag2 dual gene, and TLR4 gene deletion to show the molecular mechanistic role of different cells including NK and NKT cell in kidney inflammation. Mesangial cells and tubular cells were also used in this study in order to prove the function of these cells in our model. Our result showed that NAFLD mice produced BDCM, a CYP2E1 substrate, mediated lipid peroxidation in tubular cell. Lipid peroxidation increased proinflammatory markers like IL-1 $\beta$ , TNF- $\alpha$ , and IFN- $\gamma$  as well as mesangial cell activation, as indicated by the immunoreactivity of  $\alpha$ -SMA, a marker of mesangial cell proliferation. The increase in the expression of inflammatory markers was

remarkable lower in mice were treated with BDCM plus diallyl sulfate (DAS) a CYP2E1 blocker while all proinflammatory cytokines that were used in this study were highly expressed in mice that lack the CD1d gene. This indicate that CYP2E1 response to mesangial cell activation while NKT cells play a dynamic protective role in kidneys exposed to BDCM. In- vitro, mesangial cells were incubated with 4HNE, a lipid peroxidation marker.  $\alpha$ -SMA and TGF- $\beta$  expression was higher in mesangial cells treated with 4HNE compared with control cells. Then, tubular cells were treated with the mesangial cell supernatant. The results showed that tubular cells had significant immunoreactivity after being treated with mesangial cell supernatant, which suggests that mesangial cells play a key role in renal toxicity.

Leptin, a small peptide hormone mainly produce by adipocyte, has a direct effect on various cell types in the glomerulus including mesangial cells. In turn this leads to the release of proinflammatory cytokines, such as IL-1 $\beta$  and TGF- $\beta$  I and II (183, 184). Previous studies from our group showed that mice fed high fat diet and exposed to BDCM had increase leptin concentration which in turn led to NADPH oxidase (NOX2) activation and miR21 upregulation as a key regulator of fibrogenesis in the NASH (100, 119, 137). Here, I explored the role of leptin in renal toxicity in the condition of NAFLD. Wildtype mice fed a high fat diet (60% Kcal), along with mice with specific gene knock outs, like leptin KO, P47phox KO, and miR21 KO were used in this study. The results showed that the NAFLD group treated with BDCM had a significant increase in  $\alpha$ -SMA immunoreactivity as well as high levels of proinflammatory cytokine release. The glomerular immunoreactivity and tubular inflammation were decreased in the leptin KO and P47phox KO mice. NOX2 activation resulted in the release of free radicals and

Peroxynitrite generation (185), however, the role of peroxynitrite generation in ectopic glomerulonephritis is unclear. Here, I studied how peroxynitrite leads to renal damage. My results showed that NAFLD mice had a dramatic increase in tyrosine nitration, as assessed 3 nitro tyrosine immunoreactivity. Leptin KO and P47phox KO had a significant decrease in tyrosine nitration. Furthermore, miR21 KO mice showed significant decrease in proinflammatory mediators, suggesting that high circulatory leptin in NAFLD causes renal mesangial cell activation and tubular inflammation via a NOX2 dependent pathway that upregulates proinflammatory miR21. In-vitro, I used mesangial cells to explore this mechanistic pathway. Mesangial cells that were treated with leptin showed high immunoreactivity of  $\alpha$ -SMA while using apocynin or phenyl boronic acid (FBA) or DMPO or miR21 antagomir inhibited leptin induced-miR21-mediated mesangial cell activation in-vitro. This suggested the direct role of leptin-mediated NOX-2 in miR21-mediated mesangial cell activation. In addition, I showed that JAK-STAT inhibitor totally revoked the mesangial cell activation in leptin-primed cells, suggesting that leptin signaling in the mesangial cells depends on the JAK-STAT pathway.

The contamination of natural water resources by cyanotoxins produced by cyanobacterial blooms is a worldwide problem, causing serious water pollution to humans and livestock. Although the toxicity of microcystin-LR, a most potent cyanotoxin, primarily targets the liver, other organs can be targeted too, including the kidney (186) however the role of microcystin-LR in renal inflammation in NAFLD condition is not totally understood. Here, I investigated the microcystin mediated ectopic glomerulonephritis via NOX2- miR21 axis. Wildtype mice as well as mice that with disrupted P47phox gene and miR21 gene were used in this study. NAFLD mice treated



with microcystin-LR (10 $\mu$ g/Kg) showed increased  $\alpha$ -SMA marker as well as other proinflammatory cytokines, such as IL1 $\beta$ , MCP-1, CD68, and F4/80. NOX2 was also activated, as indicated by colocalization of NOX2 subunits (P47phox and GP91phox). Remarkably, the colocalization events along with tyrosine nitrations were decreased in P47phox KO mice suggesting that microcystin impacts NAFLD kidney through mesangial cell NOX2 activation. Since the TGF- $\beta$  signaling pathway is controlled by miR21-attenuated PETN and SMAD7, I looked for PTEN activity and I found that PTEN levels were significantly decreased in NAFLD mice treated with microcystin. miR21 KO mice had a remarkable increase in PTEN levels. TGF- $\beta$  signaling pathway also showed increased immunoreactivity in NAFLD+ microcystin group with less activation in miR21 KO mice. These results suggested that microcystin toxicity associated with kidney disruption occurs via mesangial cell NOX2 activation and miR21 upregulation. To investigate microcystin's role in apoptosis, mesangial cells were treated with microcystin-LR. The results showed that microcystin increased the number of apoptotic cells while this number decreased in cells incubated with apocynin or phenyl boronic acid (FBA) or miR21 antagomir suggesting that microcystin causes mesangial cell apoptosis via NOX2- miR21 axis. This thesis emphasizes that environmental toxins can damage the kidney and demonstrates the ectopic manifestation of NAFLD. Increased public consciousness about obesity and NAFLD, as well as encouraging people to adopt health eating and active lifestyles can help in reducing the mortality of NAFLD and slow its progression.

## REFERENCES

- 1- Bellentani S, Scaglioni F, Marino M, Bedogni G. Epidemiology of non-alcoholic fatty liver disease. *Digestive diseases*. 2010;28:155–61.
- 2- Loomba R., Sanyal A. J. The global NAFLD epidemic. *Nature Reviews Gastroenterology & Hepatology*. 2013;10(11):686–690. doi: 10.1038/nrgastro.2013.171.
- 3- Cimini FA, Barchetta I, Carotti S, et al. Relationship between adipose tissue dysfunction, vitamin D deficiency and the pathogenesis of non-alcoholic fatty liver disease. *World J Gastroenterol*. 2017;23:3407–3417.
- 4- Basaranoglu M, Ormeci N. Nonalcoholic fatty liver disease: diagnosis, pathogenesis, and management. *Turk J Gastroenterol*. 2014; 25(2): 127–132. doi: 10.5152/tjg.2014.7675.
- 5- Chatterjee S, Das S. P2X7 receptor as a key player in oxidative stress-driven cell fate in nonalcoholic steatohepatitis. *Oxidative medicine and cellular longevity*. 2015;2015:172493.
- 6- Zhou WC, Zhang QB, Qiao L. Pathogenesis of liver cirrhosis. *World J Gastroenterol*. 2014;20:7312–7324.
- 7- Angulo P, George J, Day CP, Vanni E, Russell L, De la Cruz AC, Liaquat H, et al. Serum ferritin levels lack diagnostic accuracy for liver fibrosis in patients with nonalcoholic fatty liver disease. *Clin Gastroenterol Hepatol*. 2014;12:1163–1169. e1161.
- 8- Ogden C.L., Yanovski S.Z., Carroll M.D., Flegal K.M. The epidemiology of obesity. *Gastroenterology*. 2007;132:2087–2102.
- 9- Andersen T, Christoffersen P, Gluud C. The liver in consecutive patients with morbid obesity: a clinical, morphological, and biochemical study. *Int J Obes*. 1984;8:107–115.
- 10- Verdelho Machado M, Cortez-Pinto H. Fatty liver in lean patients: is it a different disease? *Ann Gastroenterol*. 2012;25:1–2.
- 11- Divoux A, Clement K. Architecture and the extracellular matrix: the still unappreciated components of the adipose tissue. *Obes Rev*. 2011;12(5):e494–e503. doi: 10.1111/j.1467-789X.2010.00811.x.
- 12- Okorodudu D, Jumean M, Montori VM, Romero-Corral A, Somers V, Erwin P, et al. Diagnostic performance of body mass index to identify obesity as defined by body adiposity: a systematic review and meta-analysis. *Int J Obes* (2010) 34(5):791–9. doi:10.1038/ijo.2010.5

- 13- Mariman EC, Wang P. Adipocyte extracellular matrix composition, dynamics and role in obesity. *Cell Mol Life Sci.* 2010;67:1277–1292..
- 14- Szendroedi J, Roden M. Ectopic lipids and organ function. *Curr Opin Lipidol.* 2009;20:50–56.
- 15- Marchesini G, Bugianesi E, Forlani G, Cerrelli F, Lenzi M, Manini R, Natale S, Vanni E, Villanova N, Melchionda N, Rizzetto M. Nonalcoholic fatty liver, steatohepatitis, and the metabolic syndrome. *Hepatology (Baltimore, Md)* 2003;37:917–923.
- 16- McCullough AJ. Pathophysiology of nonalcoholic steatohepatitis. *J Clin Gastroenterol.* 2006;40(Suppl 1):S17–S29.
- 17- Targher G, Bertolini L, Rodella S, Tessari R, Zenari L, Lippi G et al. Nonalcoholic fatty liver disease is independently associated with an increased incidence of cardiovascular events in type 2 diabetic patients. *Diabetes Care.* 2007;30: 2119–2121. doi: 10.2337/dc07-0349
- 18- Targher G, Bertolini L, Rodella S, et al. Non-alcoholic fatty liver disease is independently associated with an increased prevalence of chronic kidney disease and proliferative/laser-treated retinopathy in type 2 diabetic patients. *Diabetologia* 2008;51:444–50.
- 19- McPherson S, Hardy T, Henderson E, Burt AD, Day CP, Anstee QM. Evidence of NAFLD progression from steatosis to fibrosing-steatohepatitis using paired biopsies: implications for prognosis and clinical management. *J Hepatol.* 2015;62:1148–1155.
- 20- Adams LA, Sanderson S, Lindor KD, Angulo P. The histological course of nonalcoholic fatty liver disease: a longitudinal study of 103 patients with sequential liver biopsies. *J Hepatol.* 2005;42:132–138. doi: 10.1016/j.jhep.2004.09.012.
- 21- Wang C., Wang X., Gong G., et al. Increased risk of hepatocellular carcinoma in patients with diabetes mellitus: a systematic review and meta-analysis of cohort studies. *International Journal of Cancer.* 2012;130(7):1639–1648. doi: 10.1002/ijc.26165.
- 22- Armstrong M. J., Adams L. A., Canbay A., Syn W.-K. Extrahepatic complications of nonalcoholic fatty liver disease. *Hepatology.* 2014;59(3):1174–1197. doi: 10.1002/hep.26717.
- 23- Fabbrini E, et al. Surgical removal of omental fat does not improve insulin sensitivity and cardiovascular risk factors in obese adults. *Gastroenterology.* 2010;139(2):448–455. doi: 10.1053/j.gastro.2010.04.056.
- 24- Villanova N, Moscatiello S, Ramilli S, et al. Endothelial dysfunction and cardiovascular risk profile in nonalcoholic fatty liver disease. *Hepatology* 2005;42:473–80.
- 25- Lee D. H., Ha M. H., Kim J. H., et al. Gamma-glutamyl transferase and diabetes - a 4-year follow-up study. *Diabetologia.* 2003;46:359–364. doi: 10.1007/s00125-003-1036-5.

- 26- Ford ES, Schulze MB, Bergmann MM, Thamer C, Joost HG, Boeing H. Liver enzymes and incident diabetes: findings from the European Prospective Investigation into Cancer and Nutrition (EPIC)-Potsdam Study. *Diabetes Care*. 2008;31:1138–1143
- 27- Goessling W, Massaro JM, Vasan RS, D'Agostino RB, Sr, Ellison RC, Fox CS. Aminotransferase levels and 20-year risk of metabolic syndrome, diabetes, and cardiovascular disease. *Gastroenterology*. 2008;135:1935-1944–1944.
- 28- Targher G, Bertolini L, Rodella S, Lippi G, Zoppini G, Chonchol M. Relationship between kidney function and liver histology in subjects with nonalcoholic steatohepatitis. *Clin J Am Soc Nephrol*. 2010;5:2166–2171.
- 29- Targher G, Bertolini L, Chonchol M, Rodella S, Zoppini G, Lippi G, et al. Non-alcoholic fatty liver disease is independently associated with an increased prevalence of chronic kidney disease and retinopathy in type 1 diabetic patients. *Diabetologia*. 2010;53: 1341–1348. doi: 10.1007/s00125-010-1720-1
- 30- Lafrance JP, Djurdjev O, Levin A. Incidence and outcomes of acute kidney injury in a referred chronic kidney disease cohort. *Nephrology, dialysis, transplantation: official publication of the European Dialysis and Transplant Association - European Renal Association*. 2010;25:2203–2209. doi: 10.1093/ndt/gfq011.
- 31- Ix JH, Sharma K. 2010. Mechanisms linking obesity, chronic kidney disease, and fatty liver disease: the roles of fetuin-A, adiponectin, and AMPK. *J. Am. Soc. Nephrol*. 21, 406–412. doi:10.1681/ASN.2009080820.
- 32- Georgescu EF. Angiotensin receptor blockers in the treatment of NASH/NAFLD: could they be a first-class option? *Adv Ther*. 2008;25(11):1141–74. doi:10.1007/s12325-008-0110-2.
- 33- Tardiff R. G., Carson M. L., Ginevan M. E. Updated weight of evidence for an association between adverse reproductive & developmental effects and exposure to disinfection by-products (DBPs) *Regulatory Toxicology and Pharmacology*. 2006;45(2):185–205.
- 34- Nieuwenhuijsen MJ, Toledano MB, Elliott P. Uptake of chlorination disinfection by-products; a review and a discussion of its implications for exposure assessment in epidemiological studies. *J Expo Sci Environ Epidemiol* 10:586–599.
- 35- Seth RK, Kumar A, Das S, Kadiiska MB, Michelotti G, Diehl AM, et al. Environmental toxin-linked nonalcoholic steatohepatitis and hepatic metabolic reprogramming in obese mice. *Toxicological sciences: an official journal of the Society of Toxicology*. 2013. Epub 2013/05/04.
- 36- Tomasi A, Albano E, Biasi F, Slater TF, Vannini V, Dianzani MU. Activation of chloroform and related trihalomethanes to free radical intermediates in isolated hepatocytes and in the rat in vivo as detected by the ESR-spin trapping technique. *Chem Biol Interact* 1985; 55:303-16; PMID:3000632; [http://dx.doi.org/10.1016/S0009-2797\(85\)80137-X](http://dx.doi.org/10.1016/S0009-2797(85)80137-X)
- 37- Das S., Seth R. K., Kumar A., et al. Purinergic receptor X7 is a key modulator of metabolic oxidative stress-mediated autophagy and inflammation in experimental

nonalcoholic steatohepatitis. *American Journal of Physiology Gastrointestinal and Liver Physiology*. 2013;305(12):G950–G963. doi: 10.1152/ajpgi.00235.2013.

38- Neafsey P, Ginsberg G, Hattis D, Johns DO, Guyton KZ, Sonawane B. Genetic polymorphism in CYP2E1: Population distribution of CYP2E1 activity. *J Toxicol Environ Health B Crit Rev*. 2009;12:362–388. doi: 10.1080/10937400903158359.

39- Chatterjee S., Rana R., Corbett J., Kadiiska M. B., Goldstein J., Mason R. P. P2X7 receptor-NADPH oxidase axis mediates protein radical formation and Kupffer cell activation in carbon tetrachloride-mediated steatohepatitis in obese mice. *Free Radical & Biology Medicine*. 2012;52(9):1666–1679. doi: 10.1016/j.freeradbiomed.2012.02.010.

40- Campos A., Vasconcelos V. Molecular mechanisms of microcystin toxicity in animal cells. *Int. J. Mol. Sci*. 2010;11:268–287. doi: 10.3390/ijms11010268.

41- Van Apeldoorn ME, van Egmond HP, Speijers GJ, Bakker. Toxins of cyanobacteria. *GJ MolNutr Food Res*. 2007 Jan; 51(1):7-60.

42- Puerto M, Pichardo S, Jos A, Cameán AM. Comparison of the toxicity induced by microcystin-RR and microcystin-YR in differentiated and undifferentiated Caco-2 cells. *Toxicol*. 2009 Aug; 54(2):161-9.

43- Klaassen CD, Lu H. Xenobiotic transporters: ascribing function from gene knockout and mutation studies. *Toxicol Sci*. 2008 Feb; 101(2):186-96.

44- Trauner M, Boyer JL. Bile salt transporters: molecular characterization, function, and regulation. *Physiol Rev*. 2003 Apr; 83(2):633-71.

45- Fischer WJ, Alheimer S, Cattori V, Meier PJ, Dietrich DR, Hagenbuch B. Organic anion transporting polypeptides expressed in liver and brain mediate uptake of microcystin. *Toxicol Appl Pharmacol*. 2005 Mar 15; 203(3):257-63.

46- Maynes JT, Luu HA, Cherney MM, Andersen RJ, Williams D, Holmes CF, James MN. Crystal structures of protein phosphatase-1 bound to motuporin and dihydromicrocystin-LA: elucidation of the mechanism of enzyme inhibition by cyanobacterial toxins. *J Mol Biol*. 2006 Feb 10; 356(1):111-20.

47- Yoshizawa S, Matsushima R, Watanabe MF, Harada K, Ichihara A, Carmichael WW, Fujiki H. Inhibition of protein phosphatases by microcystins and nodularin associated with hepatotoxicity. *J Cancer Res Clin Oncol*. 1990; 116(6):609-14.

48- Fladmark KE, Brustugun OT, Hovland R, Boe R, Gjertsen BT, Zhivotovsky B, Døskeland SO. Ultrarapid caspase-3 dependent apoptosis induction by serine/threonine phosphatase inhibitors. *Cell Death Differ*. 1999 Nov; 6(11):1099-108.

49- Ding WX, Shen HM, Ong CN. Critical role of reactive oxygen species and mitochondrial permeability transition in microcystin-induced rapid apoptosis in rat hepatocytes. *Hepatology*. 2000 Sep; 32(3):547-55.

50- Krakstad C, Herfindal L, Gjertsen BT, Bøe R, Vintermyr OK, Fladmark KE, Døskeland SO. CaM-kinaseII-dependent commitment to microcystin-induced apoptosis is coupled to

cell budding, but not to shrinkage or chromatin hypercondensation. *Cell Death Differ.* 2006 Jul; 13(7):1191-202.

51- Darley-Usmar V, Wiseman H, Halliwell B. Nitric oxide and oxygen radicals: a question of balance. *FEBS Lett.* 1995 Aug 7; 369(2-3):131-5.

52- Bieczynski F, Bianchi VA, Luquet CM. Accumulation and biochemical effects of microcystin-LR on the Patagonian pejerrey (*Odontesthes hatcheri*) fed with the toxic cyanobacteria *Microcystis aeruginosa*. *Fish Physiol Biochem.* 2013 Oct; 39(5):1309-21.

53- Xue L, Li J, Li Y, Chu C, Xie G, Qin J, Yang M, Zhuang D, Cui L, Zhang H, Fu X. N-acetylcysteine protects Chinese Hamster ovary cells from oxidative injury and apoptosis induced by microcystin-LR. *Int J Clin Exp Med.* 2015 Apr 15; 8(4):4911-21.

54- Crompton M. The mitochondrial permeability transition pore and its role in cell death. *Biochem J.* 1999 Jul 15; 341 ( Pt 2):233-49.

55- Lemasters JJ, Nieminen AL, Qian T, Trost LC, Elmore SP, Nishimura Y, Crowe RA, Cascio WE, Bradham CA, Brenner DA, Herman B. The mitochondrial permeability transition in cell death: a common mechanism in necrosis, apoptosis and autophagy. *Biochim Biophys Acta.* 1998 Aug 10; 1366(1-2):177-96.

56- Chen L, Chen J, Zhang X, Xie P. A review of reproductive toxicity of microcystins. *J Hazard Mater.* 2016 Jan 15; 301():381-99.

57- Zhang HZ, Zhang FQ, Li CF, Yi D, Fu XL, Cui LX. A cyanobacterial toxin, microcystin-LR, induces apoptosis of sertoli cells by changing the expression levels of apoptosis-related proteins. *Tohoku J Exp Med.* 2011; 224(3):235-42.

58- Chen Y, Zhou Y, Wang X, Qian W, Han X. Microcystin-LR induces autophagy and apoptosis in rat Sertoli cells in vitro. *Toxicol.* 2013 Dec 15; 76():84-93.

59- Pritmohinder S. Gill and Christopher S. Wilcox. *Antioxidants & Redox Signaling.* September 2006, 8(9-10): 1597-1607. doi:10.1089/ars.2006.8.1597.

60- Bedard K, Krause KH: The NOX family of ROS-generating NADPH oxidases: Physiology and pathophysiology. *Physiol Rev* 87: 245–313, 2007.

61- Nistala R, Whaley-Connell A, Sowers JR: Redox control of renal function and hypertension. *Antioxid Redox Signal* 10: 2047–2089, 2008.

62- You YH, Okada S, Ly S, Jandeleit-Dahm K, Barit D, Namikoshi T, Sharma K. Role of Nox2 in diabetic kidney disease. *Am J Physiol Renal Physiol.* 2013;304:F840–848.

63- Lakner AM, Bonkovsky HL, Schrum LW. microRNAs: Fad or future of liver disease. *World J Gastroenterol.* 2011;20:2536–2542.

64- Lai J. Y., Luo J., O'Connor C., et al. MicroRNA-21 in glomerular injury. *Journal of the American Society of Nephrology.* 2015;26(4):805–816. doi: 10.1681/ASN.2013121274.

65- Kölling M., Kaucsar T., Schauerte C. Therapeutic miR-21 silencing ameliorates diabetic kidney disease in mice. *Mol. Ther.* 2017;4(1):165–180. (25)

66. Abdelmegeed MA, Banerjee A, Yoo SH, Jang S, Gonzalez FJ, Song BJ. Critical role of cytochrome P450 2E1 (CYP2E1) in the development of high fat-induced non-alcoholic steatohepatitis. *J Hepatol* 57: 860–866, 2012.
67. Barnes MA, Roychowdhury S, Nagy LE. Innate immunity and cell death in alcoholic liver disease: role of cytochrome P4502E1. *Redox Biol* 2: 929–935, 2014.
68. Benigni A, Remuzzi G. How renal cytokines and growth factors contribute to renal disease progression. *Am J Kidney Dis* 37: S21–S24, 2001.
- 69 Bohinc BN, Diehl AM. Mechanisms of disease progression in NASH: new paradigms. *Clin Liver Dis* 16: 549–565, 2012.
70. Bonora E, Targher G. Increased risk of cardiovascular disease and chronic kidney disease in NAFLD. *Nat Rev Gastroenterol Hepatol* 9: 372–381, 2012.
71. Boor P, Ostendorf T, Floege J. PDGF and the progression of renal disease. *Nephrol Dial Transplant* 29, Suppl 1: i45–i54, 2014.
72. Byrne CD, Targher G. NAFLD: a multisystem disease. *J Hepatol* 62: S47–S64, 2015.
73. Chen R, Hou W, Zhang Q, Kang R, Fan XG, Tang D. Emerging role of high-mobility group box 1 (HMGB1) in liver diseases. *Mol Med* 19: 357–366, 2013.
74. Dattaroy D, Pourhoseini S, Das S, Alhasson F, Seth RK, Nagarkatti M, Michelotti GA, Diehl AM, Chatterjee S. Micro RNA 21 inhibition of SMAD 7 enhances fibrogenesis via leptin mediated NADPH oxidase in experimental and human nonalcoholic steatohepatitis. *Am J Physiol Gastrointest Liver Physiol* 308: G298–G312, 2015.
75. Fan J, Li Y, Levy RM, Fan JJ, Hackam DJ, Vodovotz Y, Yang H, Tracey KJ, Billiar TR, Wilson MA. Hemorrhagic shock induces NAD(P)H oxidase activation in neutrophils: role of HMGB1-TLR4 signaling. *J Immunol* 178: 6573–6580, 2007.
76. Floege J, Johnson RJ, Couser WG. Mesangial cells in the pathogenesis of progressive glomerular disease in animal models. *Clin Invest* 70: 857–864, 1992.
77. Fogo AB. Mechanisms of progression of chronic kidney disease. *Pediatr Nephrol* 22: 2011–2022, 2007.
78. Gallagher EJ, Leroith D, Karnieli E. Insulin resistance in obesity as the underlying cause for the metabolic syndrome. *Mt Sinai J Med* 77: 511–523, 2010.
79. Johnson RJ, Iida H, Alpers CE, Majesky MW, Schwartz SM, Pritzi P, Gordon K, Gown AM. Expression of smooth muscle cell phenotype by rat mesangial cells in immune complex nephritis. Alpha-smooth muscle actin is a marker of mesangial cell proliferation. *J Clin Invest* 87: 847–858, 1991.
80. Kinsey GR, Okusa MD. Expanding role of T cells in acute kidney injury. *Curr Opin Nephrol Hypertens* 23: 9–16, 2014.
81. Klahr S. Progression of chronic renal disease. *Heart Dis* 3: 205–209, 2001.

82. Klune JR, Dhupar R, Cardinal J, Billiar TR, Tsung A. HMGB1: endogenous danger signaling. *Mol Med* 14: 476–484, 2008.
83. Lee HS, Song CY. Differential role of mesangial cells and podocytes in TGF- $\beta$ -induced mesangial matrix synthesis in chronic glomerular disease. *Histol Histopathol* 24: 901–908, 2009.
84. Leung TM, Nieto N. CYP2E1 and oxidant stress in alcoholic and non-alcoholic fatty liver disease. *J Hepatol* 58: 395–398, 2013.
85. Lieber CS. CYP2E1: from ASH to NASH. *Hepatol Res* 28: 1–11, 2004. [PubMed]
86. Lopez-Hernandez FJ, Lopez-Novoa JM. Role of TGF- $\beta$  in chronic kidney disease: an integration of tubular, glomerular and vascular effects. *Cell Tissue Res* 347: 141–154, 2012.
87. Martinez-Salgado C, Eleno N, Tavares P, Rodriguez-Barbero A, Garcia-Criado J, Bolanos JP, Lopez-Novoa JM. Involvement of reactive oxygen species on gentamicin-induced mesangial cell activation. *Kidney Int* 62: 1682–1692, 2002.
88. Mendelson KG, Contois LR, Tevosian SG, Davis RJ, Paulson KE. Independent regulation of JNK/p38 mitogen-activated protein kinases by metabolic oxidative stress in the liver. *Proc Natl Acad Sci USA* 93: 12908–12913, 1996.
89. Meng XM, Nikolic-Paterson DJ, Lan HY. Inflammatory processes in renal fibrosis. *Nat Rev Nephrol* 10: 493–503, 2014.
90. Musso G, Tabibian JH, Charlton M. Chronic kidney disease (CKD) and NAFLD: time for awareness and screening. *J Hepatol* 62: 983–984, 2015.
91. Nakhoul N, Batuman V. Role of proximal tubules in the pathogenesis of kidney disease. *Contrib Nephrol* 169: 37–50, 2011.
92. Naruse K, Ito H, Moriki T, Miyazaki E, Hayashi Y, Nakayama H, Kiyoku H, Hiroi M, Kurashige T, Enzan H. Mesangial cell activation in the collagenofibrotic glomerulonephropathy. Case report and review of the literature. *Virchows Arch* 433: 183–188, 1998.
93. Nieto N, Friedman SL, Cederbaum AI. Cytochrome P450 2E1-derived reactive oxygen species mediate paracrine stimulation of collagen I protein synthesis by hepatic stellate cells. *J Biol Chem* 277: 9853–9864, 2002.
94. Orlic L, Mikolasevic I, Bagic Z, Racki S, Stimac D, Milic S. Chronic kidney disease and nonalcoholic Fatty liver disease-is there a link? *Gastroenterol Res Pract* 2014: 847539, 2014.
95. Park JS, Kim GH, Jo CH, Kim S, Lee CH, Kim YS, Kang CM. Effect of mycophenolic acid on cyclosporin A-induced fibronectin expression in rat mesangial cells. *Pharmacology* 91: 20–28, 2013.
96. Riedel JH, Paust HJ, Turner JE, Tittel AP, Krebs C, Disteldorf E, Wegscheid C, Tiegs G, Velden J, Mittrucker HW, Garbi N, Stahl RA, Steinmetz OM, Kurts C, Panzer U.



Immature renal dendritic cells recruit regulatory CXCR6(+) invariant natural killer T cells to attenuate crescentic GN. *J Am Soc Nephrol* 23: 1987–2000, 2012.

97. Ruef C, Kashgarian M, Coleman DL. Mesangial cell-matrix interactions. Effects on mesangial cell growth and cytokine secretion. *Am J Pathol* 141: 429–439, 1992.

98. Sasso AF, Schlosser PM, Kedderis GL, Genter MB, Snawder JE, Li Z, Rieth S, Lipscomb JC. Application of an updated physiologically based pharmacokinetic model for chloroform to evaluate CYP2E1-mediated renal toxicity in rats and mice. *Toxicol Sci* 131: 360–374, 2013.

99. Satou R, Miyata K, Gonzalez-Villalobos RA, Ingelfinger JR, Navar LG, Kobori H. Interferon- $\gamma$  biphasically regulates angiotensinogen expression via a JAK-STAT pathway and suppressor of cytokine signaling 1 (SOCS1) in renal proximal tubular cells. *FASEB J* 26: 1821–1830, 2012.

100. Seth RK, Das S, Kumar A, Chanda A, Kadiiska MB, Michelotti G, Manautou J, Diehl AM, Chatterjee S. CYP2E1-dependent and leptin-mediated hepatic CD57 expression on CD8+ T cells aid progression of environment-linked nonalcoholic steatohepatitis. *Toxicol Appl Pharmacol* 274: 42–54, 2014.

101. Sterzel RB, Schulze-Lohoff E, Marx M. Cytokines and mesangial cells. *Kidney Int Suppl* 39: S26–S31, 1993.

102. Sunden-Cullberg J, Norrby-Teglund A, Treutiger CJ. The role of high mobility group box-1 protein in severe sepsis. *Curr Opin Infect Dis* 19: 231–236, 2006.

103. Targher G, Chonchol M, Zoppini G, Abaterusso C, Bonora E. Risk of chronic kidney disease in patients with non-alcoholic fatty liver disease: is there a link? *J Hepatol* 54: 1020–1029, 2011.

104. Uesugi T, Froh M, Arteel GE, Bradford BU, Thurman RG. Toll-like receptor 4 is involved in the mechanism of early alcohol-induced liver injury in mice. *Hepatology* 34: 101–108, 2001.

105. Wang J, Liang M, Xu J, Cao W, Wang GB, Zhou ZM, Tian JW, Jia N, Zhang Z, Nie J, Liu Y, Hou FF. Renal expression of advanced oxidative protein products predicts progression of renal fibrosis in patients with IgA nephropathy. *Lab Invest* 94: 966–977, 2014.

106. Wu H, Ma J, Wang P, Corpuz TM, Panchapakesan U, Wyburn KR, Chadban SJ. HMGB1 contributes to kidney ischemia reperfusion injury. *J Am Soc Nephrol* 21: 1878–1890, 2010.

107. Yang SH, Kim SJ, Kim N, Oh JE, Lee JG, Chung NH, Kim S, Kim YS. NKT cells inhibit the development of experimental crescentic glomerulonephritis. *J Am Soc Nephrol* 19: 1663–1671, 2008.

108. Yasui K, Sumida Y, Mori Y, Mitsuyoshi H, Minami M, Itoh Y, Kanemasa K, Matsubara H, Okanoue T, Yoshikawa T. Nonalcoholic steatohepatitis and increased risk of chronic kidney disease. *Metab Clin Exp* 60: 735–739, 2011.

109. Yilmaz Y, Younossi ZM. Obesity-associated nonalcoholic fatty liver disease. *Clin Liver Dis* 18: 19–31, 2014.
110. Zhang L, Pang S, Deng B, Qian L, Chen J, Zou J, Zheng J, Yang L, Zhang C, Chen X, Liu Z, Le Y. High glucose induces renal mesangial cell proliferation and fibronectin expression through JNK/NF- $\kappa$ B/NADPH oxidase/ROS pathway, which is inhibited by resveratrol. *Int J Biochem Cell Biol* 44: 629–638, 2012.
111. Paschos P, Paletas K. Non alcoholic fatty liver disease and metabolic syndrome. *Hippokratia*. 2009;13:9-19.
112. Sundaram SS, Zeitler P, Nadeau K. The metabolic syndrome and nonalcoholic fatty liver disease in children. *Current opinion in pediatrics*. 2009;21:529-35.
113. Kneeman JM, Misraji J, Corey KE. Secondary causes of nonalcoholic fatty liver disease. *Therapeutic advances in gastroenterology*. 2012;5:199-207.
114. Bhatia LS, Curzen NP, Calder PC, Byrne CD. Non-alcoholic fatty liver disease: a new and important cardiovascular risk factor? *European heart journal*. 2012;33:1190-200.
115. Chalasani N, Younossi Z, Lavine JE, Diehl AM, Brunt EM, Cusi K, et al. The diagnosis and management of non-alcoholic fatty liver disease: practice guideline by the American Gastroenterological Association, American Association for the Study of Liver Diseases, and American College of Gastroenterology. *Gastroenterology*. 2012;142:1592-609.
116. Marcuccilli M, Chonchol M. NAFLD and Chronic Kidney Disease. *International journal of molecular sciences*. 2016;17:562.
117. Alhasson F, Dattaroy D, Das S, Chandrashekar V, Seth RK, Schnellmann RG, et al. NKT cell modulates NAFLD potentiation of metabolic oxidative stress-induced mesangial cell activation and proximal tubular toxicity. *American journal of physiology Renal physiology*. 2016;310:F85-F101.
118. McCullough K, Sharma P, Ali T, Khan I, Smith WC, MacLeod A, et al. Measuring the population burden of chronic kidney disease: a systematic literature review of the estimated prevalence of impaired kidney function. *Nephrology, dialysis, transplantation : official publication of the European Dialysis and Transplant Association - European Renal Association*. 2012;27:1812-21.
119. Chatterjee S, Ganini D, Tokar EJ, Kumar A, Das S, Corbett J, et al. Leptin is key to peroxynitrite-mediated oxidative stress and Kupffer cell activation in experimental nonalcoholic steatohepatitis. *J Hepatol*. 2012.
120. Das S, Kumar A, Seth RK, Tokar EJ, Kadiiska MB, Waalkes MP, et al. Proinflammatory adipokine leptin mediates disinfection byproduct bromodichloromethane-induced early steatohepatitic injury in obesity. *Toxicology and applied pharmacology*. 2013;269:297-306.
121. Munzberg H. Leptin-signaling pathways and leptin resistance. *Forum of nutrition*. 2010;63:123-32.

122. Marra F, Aleffi S, Bertolani C, Petrai I, Vizzutti F. Adipokines and liver fibrosis. *European review for medical and pharmacological sciences*. 2005;9:279-84.
123. Tilg H, Diehl AM. NAFLD and extrahepatic cancers: have a look at the colon. *Gut*. 2011;60:745-6.
124. Das S, Alhasson F, Dattaroy D, Pourhoseini S, Seth RK, Nagarkatti M, et al. NADPH Oxidase-Derived Peroxynitrite Drives Inflammation in Mice and Human Nonalcoholic Steatohepatitis via TLR4-Lipid Raft Recruitment. *The American journal of pathology*. 2015;185:1944-57.
125. Day CP, James OF. Steatohepatitis: a tale of two "hits"? *Gastroenterology*. 1998;114:842-5.
126. Tilg H, Moschen AR. Evolution of inflammation in nonalcoholic fatty liver disease: the multiple parallel hits hypothesis. *Hepatology*. 2010;52:1836-46.
127. Sumida Y, Niki E, Naito Y, Yoshikawa T. Involvement of free radicals and oxidative stress in NAFLD/NASH. *Free radical research*. 2013;47:869-80.
128. Seth RK, Das S, Dattaroy D, Chandrashekar V, Alhasson F, Michelotti G, et al. TRPV4 activation of endothelial nitric oxide synthase resists nonalcoholic fatty liver disease by blocking CYP2E1-mediated redox toxicity. *Free Radic Biol Med*. 2016;102:260-73.
129. Chandrashekar V, Seth RK, Dattaroy D, Alhasson F, Ziolenka J, Carson J, et al. HMGB1-RAGE pathway drives peroxynitrite signaling-induced IBD-like inflammation in murine nonalcoholic fatty liver disease. *Redox biology*. 2017;13:8-19.
130. Lambeth JD, Kawahara T, Diebold B. Regulation of Nox and Duox enzymatic activity and expression. *Free Radic Biol Med*. 2007;43:319-31.
131. Gill PS, Wilcox CS. NADPH oxidases in the kidney. *Antioxid Redox Signal*. 2006;8:1597-607.
132. Sedeek M, Nasrallah R, Touyz RM, Hebert RL. NADPH oxidases, reactive oxygen species, and the kidney: friend and foe. *Journal of the American Society of Nephrology : JASN*. 2013;24:1512-8.
133. Chatterjee S, Lardinois O, Bonini MG, Bhattacharjee S, Stadler K, Corbett J, et al. Site-specific carboxypeptidase B1 tyrosine nitration and pathophysiological implications following its physical association with nitric oxide synthase-3 in experimental sepsis. *J Immunol*. 2009;183:4055-66.
134. Hotamisligil GS, Shargill NS, Spiegelman BM. Adipose expression of tumor necrosis factor- $\alpha$ : direct role in obesity-linked insulin resistance. *Science (New York, NY)*. 1993;259:87-91.
135. Li J, Baud O, Vartanian T, Volpe JJ, Rosenberg PA. Peroxynitrite generated by inducible nitric oxide synthase and NADPH oxidase mediates microglial toxicity to oligodendrocytes. *Proceedings of the National Academy of Sciences of the United States of America*. 2005;102:9936-41.

136. Wang H, Li Y, Liu H, Liu S, Liu Q, Wang XM, et al. Peroxynitrite mediates glomerular lesion of diabetic rat via JAK/STAT signaling pathway. *Journal of endocrinological investigation*. 2009;32:844-51.
137. Pourhoseini S, Seth RK, Das S, Dattaroy D, Kadiiska MB, Xie G, et al. Upregulation of miR21 and repression of Grhl3 by leptin mediates sinusoidal endothelial injury in experimental nonalcoholic steatohepatitis. *PloS one*. 2015;10:e0116780.
138. Sheedy FJ. Turning 21: Induction of miR-21 as a Key Switch in the Inflammatory Response. *Frontiers in immunology*. 2015;6:19.
139. Sawant DV, Yao W, Wright Z, Sawyers C, Tepper RS, Gupta SK, et al. Serum MicroRNA-21 as a Biomarker for Allergic Inflammatory Disease in Children. *MicroRNA*. 2015;4:36-40.
140. Hennino MF, Buob D, Van der Hauwaert C, Gnemmi V, Jomaa Z, Pottier N, et al. miR-21-5p renal expression is associated with fibrosis and renal survival in patients with IgA nephropathy. *Scientific reports*. 2016;6:27209.
141. Glowacki F, Savary G, Gnemmi V, Buob D, Van der Hauwaert C, Lo-Guidice JM, et al. Increased
142. Blanca AJ, Ruiz-Armenta MV, Zambrano S, Salsoso R, Miguel-Carrasco JL, Fortuno A, et al. Leptin Induces Oxidative Stress Through Activation of NADPH Oxidase in Renal Tubular Cells: Antioxidant Effect of L-Carnitine. *Journal of cellular biochemistry*. 2016;117:2281-8.
143. Braunersreuther V, Montecucco F, Asrih M, Pelli G, Galan K, Frias M, et al. Role of NADPH oxidase isoforms NOX1, NOX2 and NOX4 in myocardial ischemia/reperfusion injury. *Journal of molecular and cellular cardiology*. 2013;64:99-107.
144. Wan C, Su H, Zhang C. Role of NADPH Oxidase in Metabolic Disease-Related Renal Injury: An Update. *Oxidative medicine and cellular longevity*. 2016;2016:7813072.
145. Yi F, Xia M, Li N, Zhang C, Tang L, Li PL. Contribution of guanine nucleotide exchange factor Vav2 to hyperhomocysteinemic glomerulosclerosis in rats. *Hypertension*. 2009;53:90-6.
146. Radeke HH, Resch K. The inflammatory function of renal glomerular mesangial cells and their interaction with the cellular immune system. *The Clinical investigator*. 1992;70:825-42.
147. Murata M, Kawanishi S. Oxidative DNA damage induced by nitrotyrosine, a biomarker of inflammation. *Biochem Biophys Res Commun*. 2004;316:123-8.
148. Kaur H, Halliwell B. Evidence for nitric oxide-mediated oxidative damage in chronic inflammation. Nitrotyrosine in serum and synovial fluid from rheumatoid patients. *FEBS letters*. 1994;350:9-12.
149. Quinn SR, O'Neill LA. A trio of microRNAs that control Toll-like receptor signalling. *International immunology*. 2011;23:421-5.

150. Jajoo S, Mukherjea D, Kaur T, Sheehan KE, Sheth S, Borse V, et al. Essential role of NADPH oxidase-dependent reactive oxygen species generation in regulating microRNA-21 expression and function in prostate cancer. *Antioxid Redox Signal*. 2013;19:1863-76.
151. Loboda A, Sobczak M, Jozkowicz A, Dulak J. TGF-beta1/Smads and miR-21 in Renal Fibrosis and Inflammation. *Mediators of inflammation*. 2016;2016:8319283.
152. Musso G, Cassader M, Cohny S, De Michieli F, Pinach S, Saba F, et al. Fatty Liver and Chronic Kidney Disease: Novel Mechanistic Insights and Therapeutic Opportunities. *Diabetes care*. 2016;39:1830-45.
153. Schnaper HW, Hayashida T, Hubchak SC, Poncelet A-C. TGF-beta signal transduction and mesangial cell fibrogenesis. *American journal of physiology Renal physiology*. 2003;284:F243-52.
154. Li YF, Jing Y, Hao J, Frankfort NC, Zhou X, Shen B, et al. MicroRNA-21 in the pathogenesis of acute kidney injury. *Protein & cell*. 2013;4:813-9.
155. Bellém F., Nunes S., Morais M. Cyanobacteria toxicity: Potential public health impact in south Portugal populations. *J. Toxicol. Environ. Health Part A*. 2013;76:263–271. doi: 10.1080/15287394.2013.757204.
156. Zhang JG, Wang JJ, Zhao F, Liu Q, Jiang K, Yang GH. MicroRNA-21 (miR-21) represses tumor suppressor PTEN and promotes growth and invasion in non-small cell lung cancer (NSCLC) *Clin Chim Acta*. 2010;411(11–12):846–852. doi: 10.1016/j.cca.2010.02.074.
157. Liu J., Sun Y. The role of PP2A-associated proteins and signal pathways in microcystin-LR toxicity. *Toxicol. Lett*. 2015;236:1–7. doi: 10.1016/j.toxlet.2015.04.010.
158. Luukainen R., Namikoshi M., Sivonen K., Rinehart K.L., Niemela S.I. Isolation and identification of 12 microcystins from 4 strains and 2 bloom samples of *Microcystis* spp: structure of a new hepatotoxin. *Toxicon*. 1994;32:133–139.
159. Botha N., van de Venter M., Downing T.G., Shephard E.G., Gehringer M.M., Gehringer The effect of intraperitoneally administered microcystin-LR on the gastrointestinal tract of Balb/c mice. *Toxicon*, 43 (2004), pp. 251-254.
160. Humpage A.R., Hardy S.J., Moore E.J., Froscio S.M., Falconer I.R. Microcystins (Cyanobacterial toxins) in drinking water enhance the growth of aberrant crypt foci in the mouse colon. *J. Toxicol. Environ. Health A*. 2000;61:155–165.
161. Herfindal L., Selheim F. Microcystin produces disparate effects on liver cells in a dose dependent manner. *Mini-Rev. Med. Chem*. 2006;6:109–120. doi: 10.2174/138955706775197794.
162. Ueno Y, Nagata S, Tsutsumi T, Hasegawa A, Watanabe MF, Park HD, Chen GC, Chen G, Yu SZ. Detection of microcystins, a blue-green algal hepatotoxin, in drinking water sampled in Haimen and Fusui, endemic areas of primary liver cancer in China, by highly sensitive immunoassay. *Carcinogen*. 1996;17:1317–1321. doi: 10.1093/carcin/17.6.1317.

163. Svirčev Z., Krstić S., Miladinov-Mikov M., Baltić V., Vidović M. Freshwater cyanobacterial blooms and primary liver cancer epidemiological studies in Serbia. *J. Environ. Sci. Health Part C*. 2009;27:36–55. doi: 10.1080/10590500802668016.
164. Ohta T., Nishiwaki R., Yatsunami J., Komori A., Suganuma M., Fujiki H. Hyperphosphorylation of cytokeratins 8 and 18 by microcystin-LR, a new liver tumor promoter, in primary cultured rat hepatocytes. *Carcinogenesis*. 1992;13:2443–2447. doi: 10.1093/carcin/13.12.2443.
165. Falconer IR, Yeung DS. Cytoskeletal changes in hepatocytes induced by Microcystis toxins and their relation to hyperphosphorylation of cell proteins. *Chem Biol Interact*. 1992;81:181–196. doi: 10.1016/0009-2797(92)90033-H.
166. Nong Q, Komatsu M, Izumo K, Indo HP, Xu B, Aoyama K, Majima HJ, Horiuchi M, Morimoto K, Takeuchi T. Involvement of reactive oxygen species in Microcystin-LR-induced cytogenotoxicity. *Free radical research*. 2007;41:1326–1337. doi: 10.1080/10715760701704599.
167. Calle EE, Thun MJ, Petrelli JM, Rodriguez C, Heath CW., Jr. Body-mass index and mortality in a prospective cohort of U.S. adults. *N. Engl. J. Med*. 1999;341:1097–1105. doi: 10.1056/NEJM199910073411501
168. Fabbrini E, Sullivan S, Klein S. Obesity and nonalcoholic fatty liver disease: biochemical, metabolic, and clinical implications. *Hepatology* 2010. 51 679–689. (10.1002/hep.23280).
169. Brunt EM, Wong VW, Nobili V, Day CP, Sookoian S, Maher JJ, Bugianesi E, Sirlin CB, Neuschwander-Tetri BA, Rinella ME. Nonalcoholic fatty liver disease. *Nat Rev Dis Primers*. 2015;1:15080. doi: 10.1038/nrdp.2015.80.
170. Seth RK, Kumar A, Das S, Kadiiska MB, Michelotti G, Diehl AM, Chatterjee S. Environmental toxin-linked nonalcoholic steatohepatitis and hepatic metabolic reprogramming in obese mice. *Toxicological sciences: an official journal of the Society of Toxicology*. 2013. Epub 2013/05/04.
171. Alhasson F, Dattaroy D, Das S, Chandrashekar V, Seth RK, Schnellmann RG, Chatterjee S. NKT cell modulates NAFLD potentiation of metabolic oxidative stress-induced mesangial cell activation and proximal tubular toxicity. *American journal of physiology Renal physiology*. 2016;310(1):F85–F101. Epub 2015/10/09. PubMed Central PMCID: PMC4675804. doi:
172. Karim AS, Reese SR, Wilson NA, Jacobson LM, Zhong W, Djamali A. Nox2 is a mediator of ischemia reperfusion injury. *Am J Transplant*. 2015;15:2888–2899.
173. Djamali A., Vidyasagar A., Adulla M., Hullett D., Reese S. Nox-2 is a modulator of fibrogenesis in kidney allografts. *Am. J. Transplant*. 2009;9:74–82. doi: 10.1111/j.1600-6143.2008.02463.x.
174. Djamali A, Reese S, Hafez O, Vidyasagar A, Jacobson L, Swain W, Kolehmainen C, Huang L, Wilson NA, Torrealba JR. Nox2 is a mediator of chronic CsA nephrotoxicity. *Am J Transplant*. 2012;12:1997–2007.

175. Milutinović A, Živin M, Zorc-Pleskovič R, Sedmak B, Šuput D. Nephrotoxic effects of chronic administration of microcystins -LR and -YR. *Toxicol off J Int Soc Toxicol.* 2003;42:281–288.
176. Li MS, Adesina SE, Ellis CL, Gooch JL, Hoover RS, Williams CR. NADPH oxidase-2 mediates zinc deficiency-induced oxidative stress and kidney damage. *Am J Physiol Cell Physiol.* 2017 Jan 1;312(1):C47-C55. doi: 10.1152/ajpcell.00208.2016.
177. Gomez IG, Gomez IG, MacKenna DA, Johnson BG, Kaimal V, Roach AM, Ren S, Nakagawa N, Xin C, Newitt R, Pandya S, Xia TH, Liu X, Borza DB, Grafals M, Shankland SJ, Himmelfarb J, Portilla D, Liu S, Chau BN, Duffield JS. Anti-microRNA-21 oligonucleotides prevent Alport nephropathy progression by stimulating metabolic pathways. *J. Clin. Invest.* 2015;125:141–156. doi: 10.1172/JCI75852.
178. Alverca E, Andrade M, Dias E, Sam Bento F, Batoréu MC, Jordan P, Silva MJ, Pereira P. Morphological and ultrastructural effects of microcystin-LR from *Microcystis aeruginosa* extract on a kidney cell line. *Toxicol.* 2009;54:283–294. doi: 10.1016/j.toxicol.2009.04.014.
179. Qi M., Dang Y., Xu Q., Yu L., Liu C., Yuan Y., Wang J. Microcystin-LR induced developmental toxicity and apoptosis in zebrafish (*Danio rerio*) larvae by activation of ER stress response. *Chemosphere.* 2016;157:166–173. doi: 10.1016/j.chemosphere.2016.05.038.
180. Wei Y, Weng D, Li F, Zou X, Young DO, Ji J, Shen P. Involvement of JNK regulation in oxidative stress-mediated murine liver injury by microcystin-LR. *Apoptosis.* 2008;13:1031–1042.
181. Chau BN, Xin C, Hartner J, Ren S, Castano AP, Linn G, Li J, Tran PT, Kaimal V, Huang X, Chang AN, Li S, Kalra A, Grafals M, Portilla D, MacKenna DA, Orkin SH, Duffield JS. MicroRNA-21 promotes fibrosis of the kidney by silencing metabolic pathways. *SciTransl Med* (2012) 121:121ra18.10.1126/scitranslmed.3003205.
182. Massagué J, Wotton D. Transcriptional control by the TGF-beta/Smad signaling system. *EMBO J.* 2000;19(8):1745–1754.
183. Zhang J, Wang N. Leptin in chronic kidney disease: a link between hematopoiesis, bone metabolism, and nutrition. *Int Urol Nephrol* 2013; 46: 1169–1174.
184. Wolf G, Chen S, Han DC, Ziyadeh FN. Leptin and renal disease. *Am J K Dis.* 2002;39:1–11.
185. Kawano T, Kunz A, Abe T, Girouard H, Anrather J, Zhou P, Iadecola C. iNOS-derived NO and nox2-derived superoxide confer tolerance to excitotoxic brain injury through peroxynitrite. *J Cereb Blood Flow Metab.* 2007;27:1453–62.
186. Piyathilaka MA, Pathmalal MM, Tennekoon KH, De Silva BG, Samarakoon SR, Chanthirika S. Microcystin-LR-induced cytotoxicity and apoptosis in human embryonic kidney and human kidney adenocarcinoma cell lines. *Microbiology.* 2015 Apr;161(Pt 4):819-28. doi: 10.1099/mic.0.000046.

## APPENDIX A

### PERMISSION OF AMERICAN JOURNAL OF PHYSIOLOGY FOR REPRINTING MANUSCRIPT USED IN CHAPTER 2.

2/26/2018 RE: Permission of copyright

RE: Permission of copyright

AP APS Permissions <permissions@the-aps.org> Today, 12:05 PM ALHASSON, FIRAS A

Inbox


Dear Dr Al-Hasson,

APS grants permission for you to use your paper in your thesis as described below.

Kind Regards, Delete Junk | ...

Stephani

Stephani Rozier  
Circulation Department  
The American Physiological Society  
9650 Rockville Pike  
Bethesda, MD 20814  
[www.the-aps.org](http://www.the-aps.org)  
phone: (301) 634-7796  
fax: (301) 634-7418

 ... Empowering discovery to improve health.

Confidentiality Notice: This e-mail message, including any attachments, is for the sole use of the intended recipient(s) and may contain confidential and privileged information. Any unauthorized review, copy, use,